SYSTEMATIC PROCESS DEVELOPMENT BY SIMULTANEOUS MODELING AND OPTIMIZATION OF SIMULATED MOVING BED CHROMATOGRAPHY

A Thesis
Presented to
The Academic Faculty

by

Jason A. Bentley

In Partial Fulfillment
of the Requirements for the Degree
Doctor of Philosophy in the
School of Chemical & Biomolecular Engineering

Georgia Institute of Technology
May 2013

SYSTEMATIC PROCESS DEVELOPMENT BY SIMULTANEOUS MODELING AND OPTIMIZATION OF SIMULATED MOVING BED CHROMATOGRAPHY

Approved by:

Dr. Yoshiaki Kawajiri, Advisor
School of Chemical & Biomolecular Engineering
Georgia Institute of Technology

Dr. Panagiotis Tsiotras
School of Aerospace Engineering
Georgia Institute of Technology

Dr. William Koros
School of Chemical & Biomolecular Engineering
Georgia Institute of Technology

Dr. Krista Walton
School of Chemical & Biomolecular Engineering
Georgia Institute of Technology

Dr. Matthew Mealff
School of Chemical & Biomolecular Engineering
Georgia Institute of Technology

Date Approved: 8 January 2013

This thesis is dedicated to my Lord and Savior, Jesus Christ.
I am convinced that without him I could not have entered graduate school at Georgia Tech, and could not have completed this work.

ACKNOWLEDGEMENTS

There are many people to thank who have helped me along the way in doing this work. First, I want to thank God, the Maker of all people, who has been a faithful Father to me and given me help far beyond what I deserve. I am grateful for his mercy. Without Him I certainly would have failed this graduate school program and not completed this thesis. I am grateful that through graduate school I was able to trust in the Lord and receive help from him when things became too difficult for me. I will always remember that apart from Jesus Christ I can do nothing, yet nothing is too difficult for Him.

I want to thank my adviser, Dr. Yoshiaki Kawajiri, who was a consistent source of wisdom, direction, and encouragement throughout graduate school. I learned much about numerical optimization and continuous chromatography from him. He also helped me to grow as a technical writer and speaker. I am honored to be his student, and I am grateful to God that he was my adviser.

I'm grateful to my Ph.D. reading committee, who reviewed and approved this thesis, and gave me many insightful comments and questions from their expertise. They reviewed my Ph.D. proposal and checked my progress along the way to help me stay on course.

I want to thank my research collaborators: Dr. Qinglin Huang, Dr. Mladen Eic, Dr. Seidel-Morgenstern, Dr. Suzhou Li, and Charlotte Sloan. Dr. Seidel-Morgenstern in particular invited me to Magdeburg, Germany, to meet with him, tour the Max Planck Institute there, and discuss collaborations. We also had fruitful discussions about this work at technical conferences over the last few years.

I'm grateful to my colleagues, Dr. Balamurali Sreedhar and Gaurav Agrawal, who

helped me with laboratory and class work, and we had many fruitful discussion about this research. I'm also thankful to all the members of the Kawajiri Research Group for being friendly co-workers, and helping me to prepare for some tough presentations. I'm also thankful to the ChBE 2008 entering class, many of whom have been friends to me in graduate school. I especially thank Sung Gu Kang, Wun-Gwi Kim, Kai Chang and Nae Chul Shin for their close friendship and loyalty since we met at Georgia Tech. I'm grateful to God for giving me such wonderful friends.

I'm very thankful for my undergraduate lab assistants: Charlotte Sloan, Andrew Tatum, Tung Vu, Joshua Nagy, and Taylor McClung. It was a joy to work with them in the lab, and they all did excellent work. I'm grateful to God for giving me such talented assistants for the lab work.

The financial support from Semba Biosciences is gratefully acknowledged. The technical support from Asahi Kasei Technikrom, Daiso, and YMC America is also gratefully acknowledged.

I'm thankful to all the faculty and staff at the School of Chemical & Biomolecular Engineering at the Georgia Institute of Technology for working together to create a vibrant academic community. I'm grateful to the Lord that I was able go to graduate school at Georgia Tech.

I also want to thank those people who have supported me spiritually and emotionally through these years of graduate school. I'm grateful to Nathanael and Emmy L'Heureux for their prayers, counseling, and support through everything. I'm thankful for the love and prayers of my family: Johan and Nancy Bentley, my parents, and David Bentley, my brother. I'm grateful to God for giving me such a wonderful family and wise counselors.

TABLE OF CONTENTS

LIST OF TABLES

LIST OF FIGURES

SUMMARY

Adsorption separation processes are extremely important to the chemical industry, especially in the manufacturing of food, pharmaceutical, and fine chemical products. This work addresses three main topics: first, systematic decision-making between rival gas phase adsorption processes for the same separation problem; second, process development for liquid phase simulated moving bed chromatography (SMB); third, accelerated startup for SMB units. All of the work in this thesis uses model-based optimization to answer complicated questions about process selection, process development, and control of transient operation.

It is shown in this thesis that there is a trade-off between productivity and product recovery in the gaseous separation of enantiomers using SMB and pressure swing adsorption (PSA). These processes are considered as rivals for the same separation problem and it is found that each process has a particular advantage that may be exploited depending on the production goals and economics. The processes are compared on a fair basis of equal capitol investment and the same multi-objective optimization problem is solved with equal constraints on the operating parameters.

Secondly, this thesis demonstrates by experiment a systematic algorithm for SMB process development that utilizes dynamic optimization, transient experimental data, and parameter estimation to arrive at optimal operating conditions for a new separation problem in a matter of hours. Comparatively, the conventional process development for SMB relies on careful system characterization using single-column experiments, and manual tuning of operating parameters, that may take days and weeks. The optimal operating conditions that are found by this new method ensure both

high purity constraints and optimal productivity are satisfied. The proposed algorithm proceeds until the SMB process is optimized without manual tuning. In some case studies, it is shown with both linear and nonlinear isotherm systems that the optimal performance can be reached in only two changes of operating conditions following the proposed algorithm.

Finally, it is shown experimentally that the startup time for a real SMB unit is significantly reduced by solving model-based startup optimization problems using the SMB model developed from the proposed algorithm. The startup acceleration with purity constraints is shown to be successful at reducing the startup time by about 44%, and it is confirmed that the product purities are maintained during the operation. Significant cost savings in terms of decreased processing time and increased average product concentration can be attained using a relatively simple startup acceleration strategy.

CHAPTER 1

INTRODUCTION

The chemical industry has been developing many fine chemical, pharmaceutical, and food products over the last forty years, and the trend has been to push high-purity chemicals for specialized uses. With the increase of regulation of chemical products, especially in the pharmaceutical industry, there is a great need for versatile separations that can generate needed fractions of high purity components to test physical properties and efficacy. Some regulatory agencies require that the toxicological properties of each major component of a product be tested before it will be allowed on the market. Separations that are based on adsorption principles have been found to be more versatile, with the many types of adsorbent materials that are now available, than other industrial separation techniques. Preparative chromatography in particular is capable to separate components of a mixture that only differ slightly in their affinity for an adsorbent, granting significant power for purifications [36].

The present use of adsorption principles in separation processes is rooted in the development of liquid chromatography. At the turn of the 20^{th} century, chromatography first began to be used as a preparative separation technique where fractions of eluent from a single column were collected sequentially and each fraction was analyzed offline [81]. At that point it was found that the components of a complex chemical mixture may move through a column with various speeds and these fractions could be collected at different times. It was not until the 1930s that chromatography became more widely recognized as a powerful tool for purifying single components from complex mixtures and in various phases [36]. In the 1950s there were advances made in gas chromatography for the separation and analysis of volatile fatty acids among

other applications [42].

1.1 Principle of Chromatography

Modern chromatography equipment consists of four basic parts: column, mobile phase, pump, and detector [71]. The column is a packed bed of solid particles. The mobile phase is a fluid that is pumped through the packed bed of a column. The detector is an analytical instrument that is designed to transform changes in some physical property of the fluid eluting from the column into a signal that can be measured over time. Although the detector is not necessary for chromatographic separation to occur, it allows the operator to observe the performance of the process.

The important aspect of chromatography is that various components of a fluid mixture have different interactions with the packed bed, or stationary phase, in a chromatographic column. If a particular component has weak interactions with the stationary phase, then it moves through the column with the mobile phase and has a relatively short residence time. On the other hand, if a component has strong interactions with the stationary phase, it adsorbs to the solid significantly and has a relatively long residence time. Even if there is only a slight difference in the strength of interaction for two or more components, this can be exploited to achieve very high purity of one or more products.

In Figure 1.1 there is an illustration of how chromatography can be used for bulk separation. A mixture of fluid components A and B is shown where A is less-retained, and B is more-retained. In a batch operation, a sample volume of the mixture is injected to the column, and the mobile phase is pumped through the packed bed. Over time, the less-retained component moves with greater concentration ahead of the more-retained. With a suitable detector attached in-line with the eluent from the column, it is obvious when component A elutes from the column, and the fraction is collected in a product tank. After the appropriate time, component B is also collected

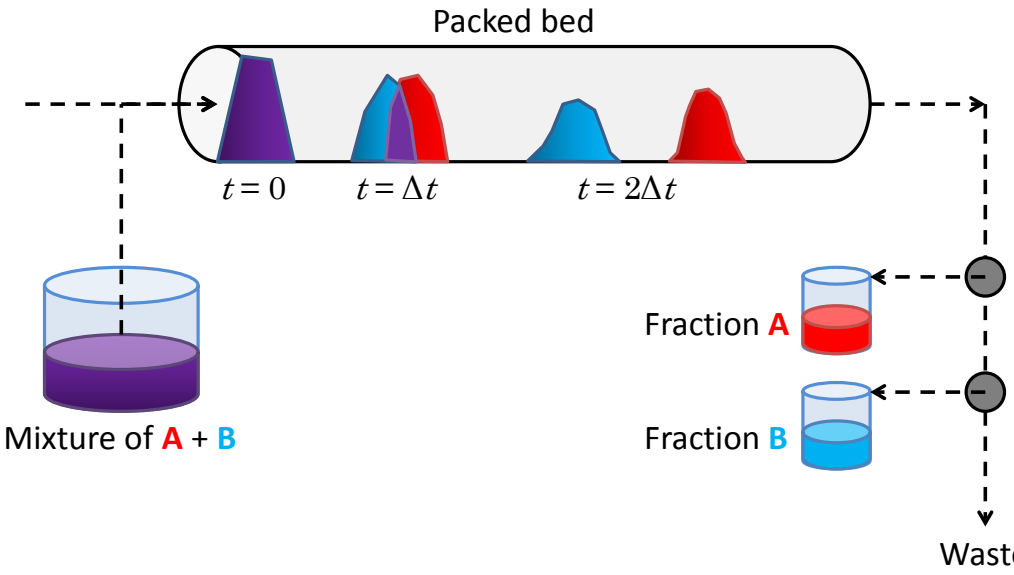

Figure 1.1: Illustration of chromatographic separation. Fractions of A and B are collected at different times when the components elute from the column

as a separate fraction. Complete separation can be achieved readily using this scheme, although the operating costs may be high considering solvent consumption and long production times.

Chromatographic columns have been made with various kinds of stationary phases which make use of different physico-chemical mechanisms to achieve separation. These separation mechanisms can be classified into general modes of chromatographic operation. One popular mode for the separation of small organic molecules is called reversed-phase chromatography (RP), which makes use of a non-polar stationary phase and some amount of water in the mobile phase to drive preferential phase partitioning of fluid components based on polarity [40]. In RP mode, the more non-polar components have increased retention on the stationary phase provided that the mobile phase is sufficiently polar. Another useful mode in the pharmaceutical industry uses a chiral stationary phase (CSP), which is an enantioselective material, such as poly-saccharides and cyclodextrins, to preferentially adsorb components with the corresponding orientation of chiral centers [86]. The separation mechanism using CSP

is similar to hand-shaking, where the right-hand binds with another right-hand more easily than a left-hand bonds with a right-hand. There are other useful modes of operation such as ion-exchange, size-exclusion, and super-critical fluid chromatography that are out of scope of this thesis.

1.2 Cyclic Adsorption Processes

In recent years, the chemical industry has made use of adsorption processes for separations with ever-increasing complexity. After further development of chromatography as a preparative separation technique in the 1950s, the principles of semi-continuous gas adsorption and continuous chromatographic processes were invented. Continuous adsorption separations are usually preferred to batch processes, because in general they can have better performance [66, 68]. The pressure swing adsorption process (PSA) was in rapid development for preferential adsorption of gasses in industrial mixtures around the late 1960s and 70s [67, 83]. The simulated moving bed process (SMB) was invented by Universal Oil Products in the 1960s for the preparative separation of petrochemicals and this process is gaining more and more popularity as a liquid phase separation process for fine chemicals, especially for chiral separations [18, 68, 71]. SMB units have been constructed with production rates ranging from a few kilograms per year to more than a million tons per year [36]. Over the last decade there have been hundreds of research articles published with "simulated moving bed" as a keyword indicating the technological advantages of this process [64].

1.2.1 Simulated Moving Bed

A SMB process exploits multiple chromatographic columns connected in series where inlet/outlet port switching occurs between columns to simulate the counter-current flow of the stationary phase. An important observation in chemical engineering is that counter-current processes, where the two phases in contact move in opposite directions, achieve greater transport efficiency of heat, mass, momentum, etc. [66]. It

may be desirable to have a counter-current operation of chromatography, such as the true moving bed (TMB) process, which is described later, but transport of the solid phase is often impractical. SMB technology makes it possible to reach the separation performance of a TMB unit, without having to move or pump the solid phase.

The SMB is controlled by switching the desorbent, extract, feed and raffinate positions and/or flow rates over time. The typical SMB configuration for binary separation has four zones where the most-retained component is desorbed in Zone 1, and adsorbed in Zone 2, and the least-retained component is desorbed in Zone 3, and adsorbed in Zone 4. A classical SMB configuration consists of four-columns and four-zones denoted (1,1,1,1) with recycle where all of the fluid flowing out of the last column in the series passes through a pump and is recycled to the beginning of the loop. A schematic of the SMB process is shown in Figure 1.2. This represents a base-case design of the SMB process.

In Figure 1.2 two steps of the cyclic SMB operation are shown to illustrate the concept of port switching and continuous binary separation. In Step 1, shown in part (a), the feed is supplied with flow rate F_{feed} between Columns 2 and 3 consisting of a mixture of components A and B, usually dissolved in the desorbent D. The mixture of the two components is indicated by the mixture of colors red and blue for components A and B respectively. The extract product is withdrawn with flow rate F_{ext} between Columns 1 and 2 where the purity of B is high, as seen in part (c), and the raffinate product is withdrawn with flow rate F_{raf} between Columns 3 and 4 where the purity of A is high, shown in part (c). Desorbent is supplied with flow rate F_{des} between Columns 4 and 1 to regenerate the adsorbent of the stationary phase. At the determined step time the positions of the inlet/outlet ports switch ahead one column in the direction of fluid flow. The switch is shown in parts (b) and (d) of the figure. This motion maintains the product purities in the extract and raffinate streams throughout the process, following the internal concentration profiles

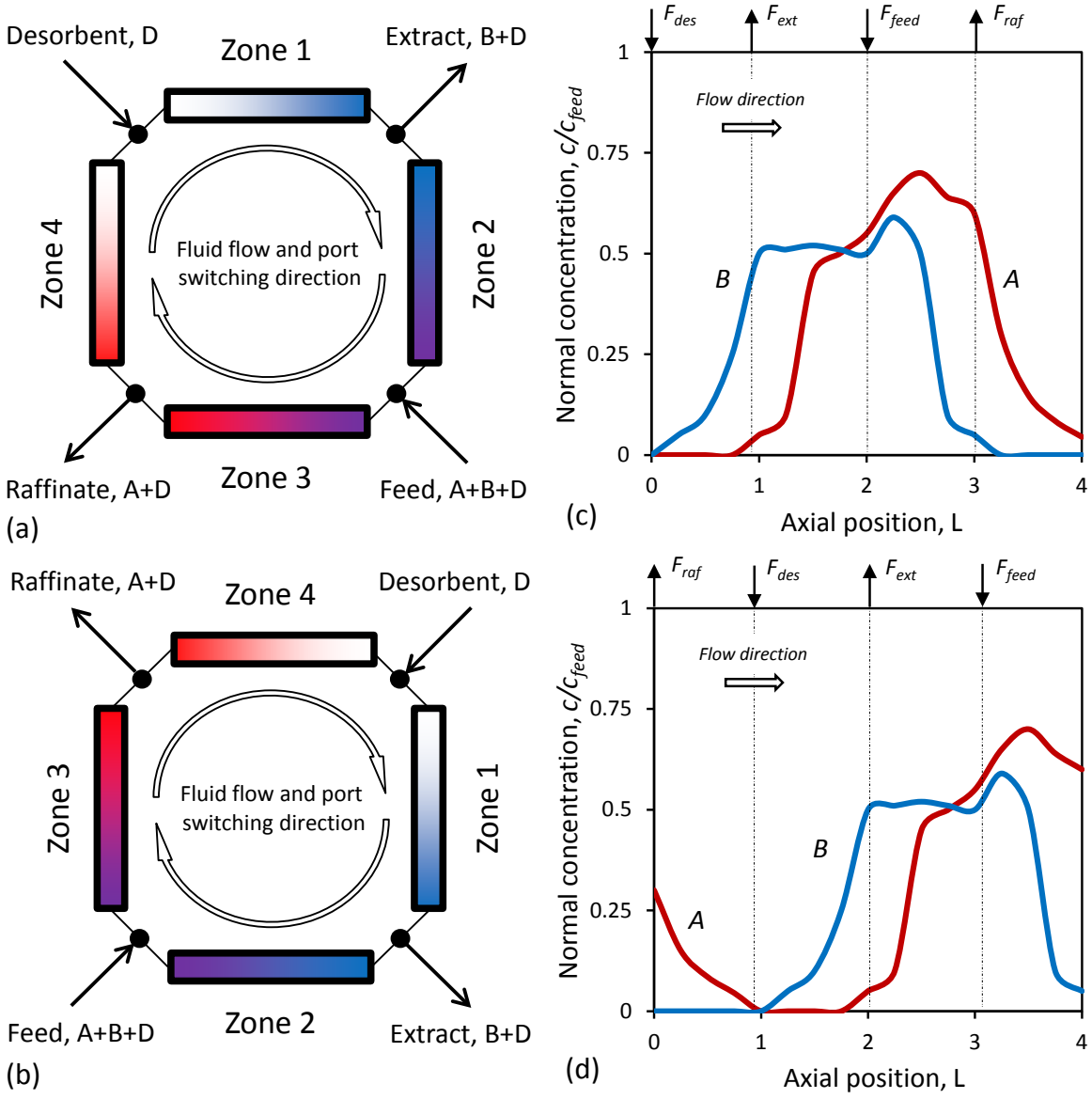

Figure 1.2: Schematic of SMB process showing two steps of cyclic operation. Four-zone configuration for (a) Step 1 and (b) Step 2, with normalized internal concentration profiles at cyclic steady state operation for (c) Step 1 and (d) Step 2

of components A and B through the column series. The ports are switched in a cycle so that the feed is continuously supplied and the purified products are continuously collected only from different positions in the column series over time. The internal concentration profiles illustrated in Figure 1.2 can be predicted by a detailed SMB model, which is discussed in Chapter 3.

There are basically two modeling approaches for SMB: a detailed mathematical model, accounting for dispersion and mass transfer effects, which requires a numerical solution, and a TMB model that is based on equilibrium theory, which can be solved for an explicit steady-state performance. The former modeling approach is discussed later in Chapter 3, and the latter approach is elaborated in the next section.

1.2.2 True Moving Bed Model and Design of SMB

The true moving bed (TMB) model considers both the fluid and solid phases moving in opposite directions as indicated in Figure 1.3. Perhaps the greatest advantage of this continuous process over batch chromatography (shown in Figure 1.1) is that there is no need of complete resolution, or total separation of the internal concentrations of components, to achieve high-purity products. In other words, there is still a significant mixture of components A and B in Zones 2 and 3 of the unit, and yet the extract and raffinate products can have pure B and pure A respectively.

In previous works of others the TMB model was used to determine optimal operating conditions for the theoretical process [74, 76]. The important operating parameters are the ratios of the fluid flow rate and the solid flow rate in each zone of the TMB given by:

$$m_j = \frac{F_j^{TMB}}{F_{sol}}, \quad j = 1, 2, \ldots, 4 \tag{1.1}$$

where F_j^{TMB} is the fluid flow rate in Zone j, and F_{sol} is the solid flow rate. In a special case of linear adsorption isotherms, that is where the adsorbed concentration of component i at thermodynamic equilibrium is directly proportional only to the

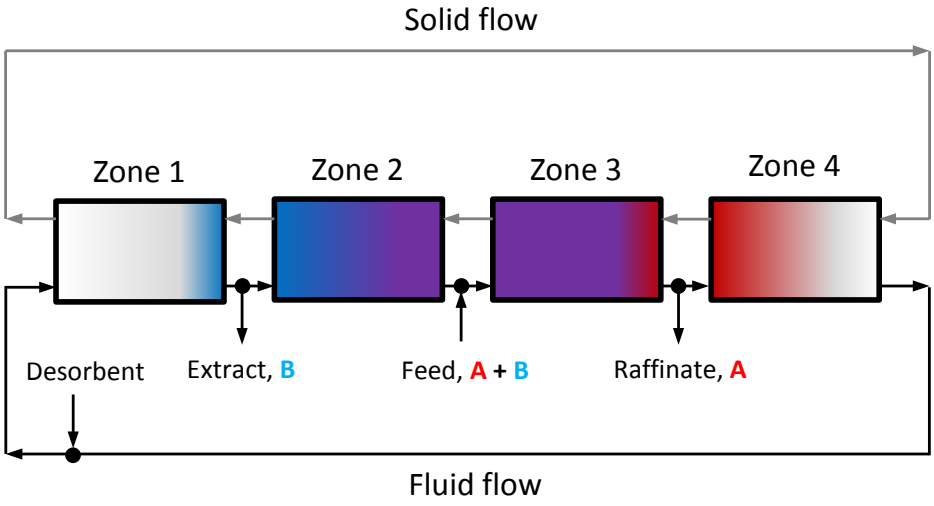

Figure 1.3: Schematic of TMB process with four-zone configuration

fluid phase concentration of component i, then the TMB model has a simple analytical solution. The linear adsorption isotherm is:

$$q_i^{eq} = H_i c_i \tag{1.2}$$

where q_i^{eq} is the adsorbed phase concentration of component i in equilibrium with the fluid phase, H_i is the Henry's constant, and c_i is the fluid phase concentration of component i. As a result, a region of operating parameter values can be defined where complete separation of components A and B is achieved. For the linear adsorption case, the complete separation region is defined as:

$$\begin{aligned} H_B &\leq m_1 \\ H_A \leq m_2 &\leq H_B \\ H_A \leq m_3 &\leq H_B \\ m_4 &\leq H_A \end{aligned} \tag{1.3}$$

where component A is less-retained, and B is more-retained on the stationary phase. The definition of this complete separation region is known as triangle theory, and

similar regions have been defined for various systems, including multi-component, and nonlinear isotherm systems [58, 76].

There are equivalent m-values that can be defined for the SMB process, and the same complete separation region given by Equation 1.3 holds in the linear isotherm case. In SMB the ratio of fluid-to-solid flow rates is:

$$m_j = \frac{F_j^{SMB} t_{step} - V_{col}\epsilon_b}{V_{col}(1-\epsilon_b)}, \quad j = 1, 2, \ldots, 4 \tag{1.4}$$

where t_{step} is the symmetric step time for SMB process, V_{col} is the column volume, ϵ_b is the overall porosity of a column. Therefore, using m-values defined for complete separation performance, corresponding t_{step} and F_j^{SMB} values can be found for robust SMB operating conditions.

The triangle theory is a heuristic approach to SMB design that is the most commonly used in industry, although it is based on a modeling approach that only approximates real SMB dynamics [64].

CHAPTER 2

SCOPE OF THESIS

The work presented in this thesis is based on available mathematical modeling and optimization methods for cyclic adsorption separations. There are three main objectives:

1. Provide framework for systematic decision-making between rival gas phase adsorption processes for the same separation problem

2. Streamline process development methodology for SMB chromatography through simultaneous modeling and optimization

3. Demonstrate optimization of transient operation of SMB processes for significant cost savings

The first objective is the topic of Chapter 4, where optimizing the gaseous separation of enantiomers is presented. There is valuable information that can be derived from the results of multi-objective optimization of each process, and this information is used to choose between two rival processes. The processes selected are SMB and PSA, which are both cyclic adsorption processes for gas phase systems, and there has not been any work showing a systematic comparison of these processes for the same separation problem until now. The comparison is based on classical processes with a fair basis of equal capital investment and equal constraints on the optimization problems.

The second objective is the topic of Chapters 5 and and 6, which are focused on SMB processes for liquid phase separations. In these chapters a systematic algorithm is proposed to optimize the SMB operation starting from a new mixture and ending

with optimal operating conditions that maximize productivity and maintain high purity products. It is assumed that there is not prior knowledge of the SMB model parameters for the new mixture. In the procedure, the SMB unit with columns, mobile phase, and operating temperature are already decided. Following the proposed algorithm, the SMB process is modeled and optimized simultaneously in an iterative scheme where model parameters are estimated from SMB startup data, and the SMB operating conditions are re-optimized based on refined model parameters. This new method is capable to optimize SMB separations in a matter of hours, whereas the conventional process development methods can take days or even weeks to arrive at optimal operating conditions.

The final objective is the topic of Chapter 7, and solves the problem of optimizing transient SMB operation. In particular, the problem of SMB startup acceleration is solved and demonstrated experimentally which provides substantial cost savings in terms of reducing overall processing time, increasing the average product concentration by increasing the average throughput, and decreasing the average desorbent consumption of the process. This is the first example of model-based SMB startup optimization shown experimentally.

Altogether this work makes use of various modeling and optimization tools, including differential algebraic equation solvers and nonlinear programming solvers, to solve various optimization problems for cyclic steady state operating conditions, parameter estimation, and optimal control of transient operation. These optimization problems offer systematic solutions to achieve the objectives of the thesis outlined above. An interesting and important aspect of this model-based optimization approach is that it eliminates the need for trial-and-error methods which rely on human intuition and experience. Also, solving model-based optimization problems may provide solutions to complicated questions that were previously untried by human research.

CHAPTER 3

SMB MODELING AND OPTIMIZATION

This chapter is devoted to the detailed mathematical modeling of the SMB process, which is based on first principles, and model-based optimization methods. A detailed SMB model, which takes into account axial dispersion and mass transport kinetics, is needed to simulate real SMB dynamics that can also be used for process design with model-based optimization [78]. This approach is necessary for applications in the pharmaceutical industry, such as chiral separations, where the purity requirements are stringent [77].

3.1 SMB Model

In this section, the typical 4-zone SMB model is described for a multi-component mixture with multiple columns. Various types of SMB models with different levels of complexity were compared for dynamic simulation of the SMB process by Dunnebier and Klatt [22]. It was shown that the kinetic model, which is used largely in this thesis, is capable to predict experimental data rather well, even for nonlinear isotherm systems. The following assumptions are used in this modeling approach [64]:

1. Isothermal operation, i.e. no energy balances
2. All columns have the same overall porosity
3. No concentration gradients in the radial direction of the column
4. Constant fluid velocity in the axial direction of the column
5. No concentration gradients within the stationary phase particle, the adsorbed concentration is an average surface concentration

6. Only the overall column porosity is considered, no intra-pore volume or pore-diffusion kinetics

7. The linear driving force (LDF) model is used to describe mass transfer phenomena between fluid and adsorbed phases

8. The axial-dispersion effect is accounted for by a lumped parameter in the LDF model, the overall mass-transfer coefficient

Some researchers use SMB models where some of these assumptions are relaxed, and other approaches to SMB modeling may be found in the literature [32, 36, 66, 71]. However, in most of this thesis dealing with liquid phase separations, the same modeling assumptions listed above are used. Additional models and assumptions are used for gas phase systems, and these are discussed only in Chapter 4.

For each column the component mass balance in the fluid phase is stated as:

$$\frac{\partial c_i^j(z,t)}{\partial t} + \frac{1-\epsilon_b}{\epsilon_b}\frac{\partial q_i^j(z,t)}{\partial t} = -v^j(t)\frac{\partial c_i^j(z,t)}{\partial z} \tag{3.1}$$

$$i = A, B, \ldots, n_{comp} \quad j = 1, 2, \ldots, n_{col}$$

where c_i^j is the fluid phase concentration of component i in column j, ϵ_b is the overall bed porosity, q_i^j is the adsorbed phase concentration of component i in column j, v^j is the linear mobile phase velocity in column j, z is the axial coordinate, t is the time, alphabetic characters are used according to the number of adsorbable components in the system ($i = A, B$ for binary separation), n_{comp} is the number of components, and n_{col} is the number of columns.

The component mass balance in the adsorbed phase is described by the linear driving force (LDF) mass transfer model:

$$\frac{\partial q_i^j(z,t)}{\partial t} = k_i(q_i^{eq,j}(z,t) - q_i^j(z,t)) \tag{3.2}$$

$$i = A, B, \ldots, n_{comp} \quad j = 1, 2, \ldots, n_{col}$$

where k_i is the overall mass transfer coefficient for component i, and $q_i^{eq,j}$ is the adsorbed phase concentration of component i in equilibrium with the fluid phase in column j. This model assumes that the primary resistance to mass transfer exists in the adsorbed phase. In the LDF model, k_i is a lumped parameter used to describe band broadening effects, and it has been shown that such a simplified model can still predict experimental behavior provided that a reliable value for k_i can be obtained [30, 36].

In general, the adsorption isotherm equation is written as:

$$q_i^{eq,j}(z,t) = f(c_A^j(z,t), c_B^j(z,t), \ldots, c_{n_{comp}}^j(z,t)) \tag{3.3}$$

$$i = A, B, \ldots, n_{comp} \quad j = 1, 2, \ldots, n_{col}$$

There are many useful adsorption isotherm models. Yet in this work, and in most industrial applications, the linear isotherm model is used most frequently. The linear isotherm is described by Equation (1.2) in Section 1.2.2. Some other frequently used adsorption isotherm models are detailed by Do [20], and a common model used in this work for nonlinear adsorption is the single-component Langmuir isotherm:

$$q_i^{eq}(z,t) = \frac{H_i c_i(z,t)}{1 + b_i c_i(z,t)} \tag{3.4}$$

where H_i is the Henry's constant for component i, b_i is the equilibrium affinity of component i. This model assumes that there are a finite number of adsorption sites and the saturation capacity for component i, q_i^{sat}, is the quotient of the Henry's constant and the equilibrium affinity. Another common model used in this work for competitive adsorption is the competitive Langmuir isotherm:

$$q_i^{eq}(z,t) = \frac{H_i c_i(z,t)}{1 + \sum_{i=A,B,\ldots,n_{comp}} b_i c_i(z,t)} \tag{3.5}$$

where the concentration of each component with the associated affinity constant is added to the denominator to model the competition for the same adsorption sites.

The isotherm model is probably the single most important part of the SMB model in describing phase equilibrium in the column to predict real process performance.

The boundary conditions for Equation (3.1) are:

$$c_i^j(0,t)v^j(t) = c_{i,in}^j(t)v_{in}^j(t) + \gamma_{feed}^j(t)c_{i,feed}v_{feed} \tag{3.6}$$

$$i = A, B, \ldots, n_{comp} \quad j = 1, 2, \ldots, n_{col}$$

where $c_i^j(0,t)$ is the concentration of component i in column j at position $z = 0$, the column entrance, $c_{i,in}^j$ is the concentration of component i in the inlet connection to column j, v_{in}^j is the velocity in the inlet connection to column j, γ_{feed}^j is a binary variable equal to 1 if column j is at the feed location and 0 otherwise, $c_{i,feed}$ is the concentration of component i in the feed, and v_{feed} is the feed velocity. Since only one column is at the feed location at a time, $\gamma_{feed}^j = 0$ for all columns except one during a given step of the SMB process.

To model the inlet/outlet ports, overall mass balances are written as:

$$\begin{aligned} v^j(t) &= v_{in}^j(t) + \gamma_{des}^j(t)v_{des} + \gamma_{feed}^j(t)v_{feed} \\ v_{out}^j(t) &= v^j(t) - \gamma_{ext}^j(t)v_{ext} - \gamma_{raf}^j(t)v_{raf} \end{aligned} \tag{3.7}$$

$$j = 1, 2, \ldots, n_{col}$$

where γ_{des}^j is a binary variable for the desorbent location, v_{des} is the desorbent velocity, v_{out}^j is the velocity in the outlet connection of column j, γ_{ext}^j is a binary variable for the extract location, v_{ext} is the extract velocity, γ_{raf}^j is a binary variable for the raffinate location, and v_{raf} is the raffinate velocity. The binary variables equal 1 if column j is at the inlet/outlet location and 0 otherwise. These equations assume constant cross-sectional areas in the columns and connections so that conversions from volumetric flow rates to velocities in the tubing are not necessary.

To model column connections the following equations are used:

$$\begin{aligned} c_{i,out}^{j-1}(t) &= c_{i,in}^{j}(t), \quad j = 2, 3, \ldots, n_{col} \\ c_{i,out}^{n_{col}}(t) &= c_{i,in}^{1}(t) \\ v_{i,out}^{j-1}(t) &= v_{i,in}^{j}(t), \quad j = 2, 3, \ldots, n_{col} \\ v_{i,out}^{n_{col}}(t) &= v_{i,in}^{1}(t) \end{aligned} \tag{3.8}$$

where $c_{i,out}^{j}$ is the concentration of component i in the outlet connection of column j. The following simple relation is also used to describe the outlet concentration from column j:

$$c_{i,out}^{j}(t) = c_{i}^{j}(L_c, t) \tag{3.9}$$

$$j = 1, 2, \ldots, n_{col}$$

where $c_{i}^{j}(L, t)$ is the concentration of component i in column j at position $z = L$, and L is the column length.

In order for the SMB model to be useful for dynamic simulation and optimization, there must be found a reliable set of model parameters. The methods for parameter estimation will be discussed in detail in the appropriate chapters in this thesis.

3.2 SMB Optimization

There are a variety of model-based optimization techniques that have been proposed to find optimal design and operating parameters for chemical processes. In the literature there are examples of optimization problems which are solved following either stochastic or deterministic optimization algorithms. Numerical methods for solving optimization problems of these types has been the topic of considerable research in recent decades [15].

A popular form of the stochastic method is called non-dominated sorting genetic algorithm (NSGA), and has been applied to some complex engineering problems with multiple objectives to be optimized simultaneously [13]. This method has been used

to investigate the optimal performance of reactive SMB, or SMBR, and SMB for chiral separation in a few references [79, 87, 88]. One of the claims of the genetic algorithm (GA) is that the global optimal solution can be found even if there are multiple local minima in the feasible search space, because it does not rely on derivatives of the objective function or constraints to converge. However, the results of this optimization approach are heuristic, and cannot be relied upon to provide systematic optimal solutions because the search algorithm is based on random mutation of the decision variables.

Another useful optimization approach follows the deterministic method, which is based nonlinear programming with a systematic search using first- and second-derivative information of the objective function and constraints to find a local minimum. This method has been used by others to optimize operating conditions for both SMB and PSA processes in various references [21, 49, 62]. There are also various ways to set-up the optimization problem using a discretized model which are compared by Kawajiri and Biegler [46] for SMB optimization, and are discussed later in this chapter. The advantage of deterministic optimization is that a local optimum can be efficiently obtained given a decent initial guess of the decision variables.

Significant optimization work has been performed by others to find optimal SMB configurations, that is the column configuration and operating strategy, for both gas and liquid phase separations [7, 47, 61, 87]. Although, in this thesis, only the optimal operating conditions are investigated for an existing separation unit.

Furthermore, significant research efforts have been made by others to use model-based optimization for on-line control of chromatographic separations in both batch and SMB modes [24]. The goal of these works on control have been to maintain the process performance on-line by rejecting disturbances and overcoming the problem of model-mismatch [4]. The popular approach has been to use deterministic optimization with a simplified and linearized SMB model to obtain optimal operating conditions

using feedback control principles.

Clearly, from the above discussion there are various aspects of the SMB process that can be considered in an optimization problem. In this work, the main focus is on process development and the investigation of optimal operating conditions to achieve certain performance criteria.

3.2.1 Problem Formulation

The SMB optimization problem used primarily in this work is described in this section. The typical 4-zone SMB model, described in Section 3.1, is used to solve a nonlinear programming problem and determine optimal operating conditions for the SMB. The following optimization problem is written for a binary separation with multiple columns in the unit, and this problem formulation was first proposed for periodic adsorption processes by Nilchan and Pantelides [62], and was implemented for SMB optimization by Kawajiri and Biegler [46].

The SMB optimization objective function, $\phi_{SMB}(u)$, is stated as maximization of the feed flow rate, F_{feed}, which is a measure of productivity. The optimization problem is formulated as:

$$\begin{aligned}
\max \quad \phi_{SMB}(u) &= F_{feed} && (3.10)\\
\text{s.t.} \quad \text{Purity}_A^{raf} &\geq \text{Purity}_{A,min}^{raf} && (3.11)\\
\text{Purity}_B^{ext} &\geq \text{Purity}_{B,min}^{ext} \\
c_i^j(z,0) &= c_i^{j+1}(z,t_{step}), \quad j=1,2,\ldots,n_{col}-1 && (3.12)\\
c_i^{n_{col}}(z,0) &= c_i^1(z,t_{step}) \\
q_i^j(z,0) &= q_i^{j+1}(z,t_{step}), \quad j=1,2,\ldots,n_{col}-1 \\
q_i^{n_{col}}(z,0) &= q_i^1(z,t_{step}) \\
F_x &\leq F_{max}, \quad x=1,2,3,4 && (3.13)
\end{aligned}$$

Equations (3.1) - (3.3), (3.6), (3.7), (3.8)

where u is the vector of SMB operating conditions

$u^T = [t_{step}, m_1, m_2, m_3, m_4,]$, t_{step} is the step time, m_x is the fluid-to-solid flow rate ratio in zone x, which is determined by the equation:

$$m_x = \frac{F_x t_{step} - V_{col}\epsilon_b}{V_{col}(1-\epsilon_b)} \tag{3.14}$$

where F_x is the volumetric flow rate in zone x, and V_{col} is the total column volume. With these m-values specified, the flow rates in each zone of the SMB unit can be calculated given the column volume and overall porosity. The purity constraints in Equation (3.11) require that the purity of component A in the raffinate must be at least the minimum required and the purity of component B in the extract must be at least the minimum required. Components A and B are the less- and more-retained components respectively. The purity of component A in the raffinate is defined as:

$$\text{Purity}_A^{raf} = \sum_{j=1}^{n_{col}} \gamma_{raf}^j(t) \frac{\int_0^{t_{step}} v_{raf} c_{A,out}^j(t)\, dt}{\sum_{i=A,B} \int_0^{t_{step}} v_{raf} c_{i,out}^j(t)\, dt} \tag{3.15}$$

and the purity of component B in the extract is defined as:

$$\text{Purity}_B^{ext} = \sum_{j=1}^{n_{col}} \gamma_{ext}^j(t) \frac{\int_0^{t_{step}} v_{ext} c_{B,out}^j(t)\, dt}{\sum_{i=A,B} \int_0^{t_{step}} v_{ext} c_{i,out}^j(t)\, dt} \tag{3.16}$$

The cyclic steady state (CSS) constraints in Equation (3.12) are defined for a single step of the SMB process. The CSS constraints mean that the fluid and adsorbed phase concentration profiles are the same at the beginning and end of a step only shifted one column in the direction of fluid flow. The maximum flow rate constraints in Equation (3.13) are based on the total pressure drop limits for the SMB pumps with a safety factor.

This is an interesting nonlinear programming problem because of the partial differential equation (PDE) constraints from the SMB model. In order to solve the

problem there needs to be a numerical method for discretizing the PDEs into a system of differential algebraic equations (DAEs) or a large system of algebraic equations to evaluate the constraints. Some useful numerical solution strategies are discussed in the next section.

3.2.2 Numerical Solution

Due to the PDE constraints in the optimization problem, the solution is not yet straightforward to solve using traditional nonlinear programming. In order to solve the dynamic optimization problem, there must be some amount of discretization of the PDEs included in the process model. There are three main types of methods that have been proposed to solve such dynamic optimization problems for SMB and PSA, which are described by [43, 46, 80]. The methods are known as:

1. Nested, single-discretization
2. Simultaneous, single-discretization
3. Simultaneous, full-discretization

In the nested, single-discretization approach a Newton-based solver is used to search for optimal operating conditions and the PDE model is discretized and integrated to obtain the CSS performance. The PDEs are only discretized in the axial domain, generating a DAE system that is integrated in time by the method of lines [70]. The process model is solved for the entire startup process until the CSS conditions are satisfied, and then the objective function and constraints are checked. The partial derivatives of the objective function and constraints with respect to the decision variables can be obtained by finite differences.

In the simultaneous, single-discretization approach a Newton-based solver is used to search for both optimal operating conditions and the CSS concentration profiles

simultaneously. This problem formulation includes a large number of decision variables that describe the CSS profiles. The single-discretization refers to the PDEs of the process model, which are only discretized in the axial domain, generating a DAE system that is integrated in time by the method of lines [70]. The process model is solved for a single-step or cycle and then the objective function and constraints are checked. Sensitivity equations, which are another DAE system, are integrated together with the discretized model integration to approximate the partial derivatives of the objective function and constraints with respect to the many decision variables.

In the simultaneous, full-discretization approach a Newton-based solver is used to search for both optimal operating conditions and the full CSS concentration profiles for the entire step or cycle time horizon, simultaneously. This method requires that the PDE system given by Equations (3.1) - (3.3) in Section 3.1 be fully discretized in time and space yielding a large-scale optimization problem with only algebraic constraints. This problem has a very large number of decision variables, but does not require any time integration of a DAE system, as in the other methods described above. The size of the optimization problem scales with the number of columns in the SMB model and the number of discretization points in time and the axis of the columns. If many discretization nodes are required, for example in case of high efficiency chromatographic columns, then the number of decision variables becomes huge, and the problem may take a long time to solve. Therefore, it is crucial to choose an efficient optimization solver in this approach.

CHAPTER 4

COMPARISON OF GAS PHASE ADSORPTION PROCESSES FOR ENANTIOMER SEPARATION BY MULTI-OBJECTIVE OPTIMIZATION

4.1 Motivation

This chapter is focused on the separation of gaseous enantiomers with an emphasis on the systematic comparison of two rival adsorption processes: SMB and PSA. The comparison of these processes is carried out, assuming a fair basis of capital investment, by multi-objective optimization with the same constraints on common operating conditions [12].[1]

The resolution of racemates, one-to-one mixtures of molecules that have the same chemical formula and covalent bonds but whose atoms have different spatial orientations, is a particularly interesting problem. About one-third of all synthetic drugs are marketed as racemates, despite the fact that drug receptors in the body may differentiate between stereoisomers in various ways, such that binding likely favors one orientation over another [84]. Some of these stereoisomers are more specifically called enantiomers if their three-dimensional projections are non-superimposable. In the past decade, there have been numerous studies that indicate the enantiomers of biologically active molecules have measurable differences in their toxicity and metabolism in the human body [6]. More specifically, the mechanism of anesthetic action for fluorinated volatile anesthetics needs to be investigated further in order to design safer general anesthetics with pure enantiomers [5]. Enabling such research is the primary

[1] This chapter is published in Bentley *et al.* [12]

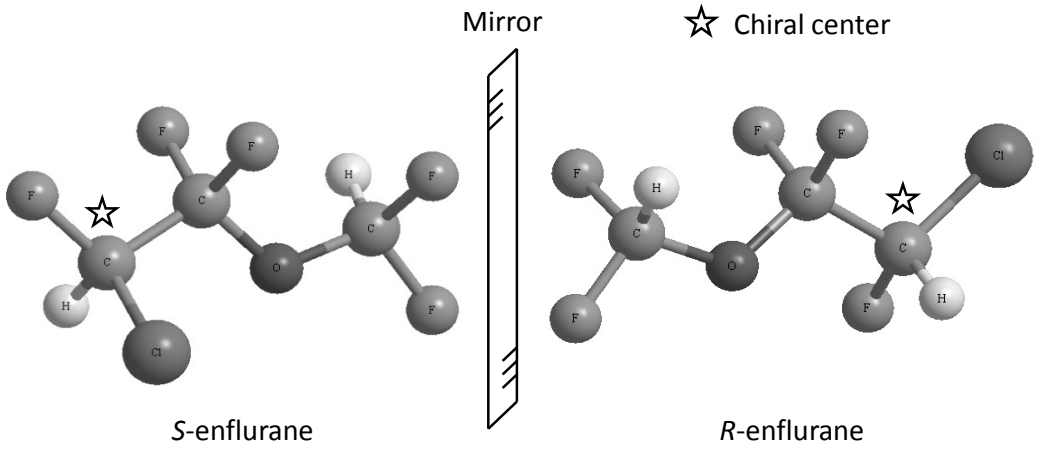

Figure 4.1: Sturctures of the enantiomers of enflurane

motivation for the work presented here.

Some investigations of volatile anesthetic compounds have shown that purified enantiomers may have better pharmacological properties compared to the racemate. For example, isoflurane enantiomers have been studied [37, 38]. However, the results of such studies are inconclusive because the pure enantiomers are so scarce that only a few animal tests could be performed [23, 84]. Hence, there is a need for increased production of pure enantiomers of volatile anesthetics to substantiate these claims. Enflurane, a structural isomer of isoflurane, is another volatile anesthetic with a chiral center that requires further investigation. The structures of enflurane are shown in Figure 4.1. One study showed that the metabolism of *R*-enflurane was twice that of *S*-enflurane in the liver, indicating that *R*-enflurane is less toxic than the racemate [29]. Thus, it may be possible to improve the safety of general anesthesia by using an enantiomerically purified anesthetic.

The chiral separation of enflurane and other inhalation anesthetics has been demonstrated experimentally using capillary chromatography [59], and the productivity was improved by using a gas chromatographic simulated moving bed (SMB)

process [16, 17, 44]. Small particles of octakis(3-*O*-butanoyl-2,6-di-*O*-*n*-pentyl)-γ-cyclodextrin (γ-CD) were used as the adsorbent, first analyzed by König *et al.* [50], which requires a careful synthesis and is rather expensive. *R*- and *S*-enflurane have a slight but exploitable difference in affinity using this chiral adsorbent. The separation factor is about 1.5 at 33 °C.

For the purification of pharmaceutical molecules most SMB processes have been developed applying liquid mobile phases [71]. In comparison, there are less applications of SMB technology for gas phase separations [69, 75]. There are also a few applications of SMB in supercritical fluid separations where typically CO_2 is utilized as a solvent [63]. In the case considered here, i.e., the separation of the enantiomers of enflurane (or other volatile anesthetics), the chiral separation has been performed in the gas phase where the racemate is diluted in nitrogen. This may be the only proven continuous process for achieving enantiomerically pure enfluranes. In addition, pressure swing adsorption (PSA) may be a viable alternative because it also operates continuously (or semi-continuously) and is capable of purifying gas components with differing affinity for the adsorbent. Although, to date enantiomer separation has not been investigated using PSA alone, it has been reported that SMB may be operated at variable pressure conditions in the adsorption bed [65], or when assisted by a pressure swing could achieve complete enantiomer separation with a noticeable reduction in desorbent consumption over the SMB system by itself [51]. In general, there are a number of combinations of gas adsorption processes that merit further research. Indeed, there exist other configurations of adsorption columns with dedicated port switching and pressure swing steps that have not yet been investigated systematically [19, 53].

In this chapter, the PSA operation is investigated by dynamic simulation and optimization based on the same system parameters used in the experimental SMB work of Juza *et al.* [44] and Biressi *et al.* [16, 17]. PSA involves changing the total

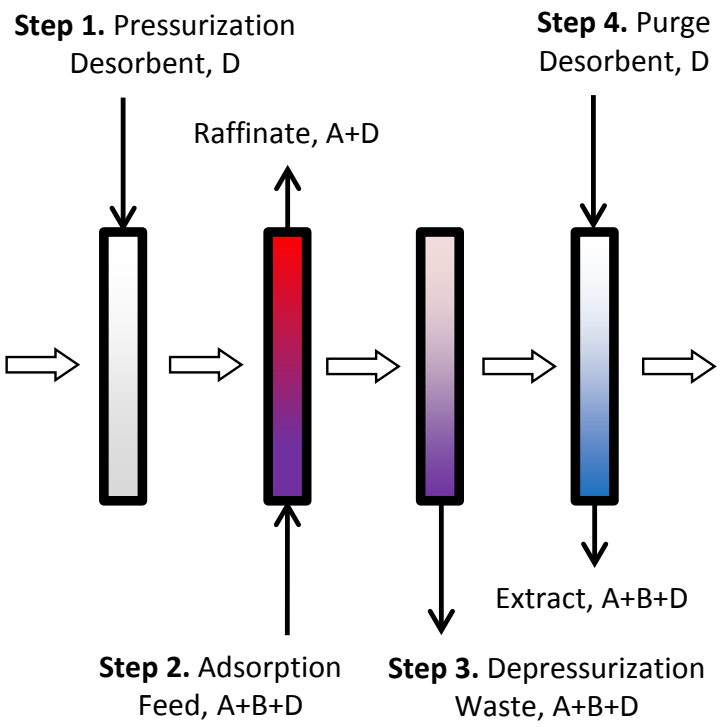

Figure 4.2: 4-step PSA cycle: Step 1: pressurization with desorbent supplied until high pressure for duration of t_{press}; Step 2: adsorption at high pressure with feed supplied and raffinate collected for duration of t_{ads}; Step 3: depressurization until atmospheric pressure with extract wasted for duration of $t_{depress}$; Step 4: purge with desorbent supplied at atmospheric pressure and extract collected for duration of t_{purge}. A is the less-retained component, B is the more-retained component, and D is the desorbent gas

pressure in an adsorption column in order to manipulate the elution of the gas phase components. It may be operated with multiple columns in parallel, as well as with numerous operation steps in a cycle. A more detailed description of PSA is given by [67]. In this work, a base-case design of a single column with four elementary steps was considered, and each step is defined in Figure 4.2. A single PSA cycle consists of these four steps.

The dynamic simulation and optimization of gas phase SMB and PSA processes have been performed by various researchers previously. Ko *et al.* [49] worked on the optimization of PSA for CO_2 sequestration from flue gas. Mota *et al.* [61] reported

optimal SMB configurations and operating conditions for the separation of CH_4 and CO_2. Huang *et al.* [41] showed that PSA could be optimized to separate H_2 from CH_4. Likewise, Gomes *et al.* [69] investigated the feasibility of using SMB for the separation of propane from propylene using a numerical optimization scheme. Kostroski and Wankat [51] demonstrated the enantiomer separation of enflurane with a hybrid SMB/PSA system along with numerical simulation results. This research provides insight about how to choose operating conditions for the process in question.

The work presented in this chapter is one of the first systematic studies based on dynamic optimization addressing concepts to select a gas phase adsorption process out of rivaling options [12]. Dynamic simulations and optimizations of SMB and PSA processes are performed to find the optimal operating conditions for the enantiomer separation of enflurane. The operating parameters to be optimized include step times, pressures, and flow rates at which SMB and PSA are the most productive while achieving an enantiomerically pure product. From these solutions, the two processes are compared regarding productivity and desorbent consumption.

4.2 Modeling

4.2.1 Adsorption Column Model

The modeling of gas phase SMB and PSA processes is described in this section. The modeling assumptions applied for the adsorption column model are the same as those described in Section 3.1. Isothermal operation is assumed because the feed is diluted by a carrier gas and the heat of adsorption can be neglected. These assumptions are typically made for trace gas phase systems [67, 69]. The main difference in the gas phase system is the fluid compressibility, and the ideal gas law is used to describe concentrations.

Both a component mass balance and an overall mass balance are used to capture

the dynamics of convection and adsorption in the column. The ideal gas law is justified because the total pressure and feed concentrations are relatively low. Furthermore, a negligible pressure drop is assumed in the columns at the selected operating conditions. This assumption is frequently used in modeling gas phase chromatography [41, 67]. Hence, the component mass balance in the gas phase is:

$$\epsilon_b \frac{\partial y_i^j(z,t)}{\partial t} + (1-\epsilon_b)\frac{RT}{P^j(t)}\frac{\partial q_i^j(z,t)}{\partial t} = -v_s^j(z,t)\frac{\partial y_i^j(z,t)}{\partial z} - y_i^j(z,t)\frac{\partial v_s^j(z,t)}{\partial z} \qquad (4.1)$$

$$i = A, B \quad j = 1, 2, \ldots, n_{col}$$

where ϵ_b is the overall porosity, y_i^j is the gas phase mole fraction of component i in column j, R is the gas constant, T is the temperature, P^j is the pressure in column j, q_i^j is the adsorbed phase concentration of component i in column j, v_s^j is the superficial fluid velocity in column j, z is the axial coordinate, and t is the time. Alphabetic characters are used according to the number of adsorbable components in the system where A is the less-retained component and B is the more-retained component, and n_{col} is the number of columns.

The constant column pressure model was used for the overall mass balance in the SMB process and in the adsorption and purge steps of PSA (see Figure 4.2, Step 2 and Step 4):

$$(1-\epsilon_b)\frac{RT}{P^j(t)}\sum_{i=A,B}\frac{\partial q_i^j(z,t)}{\partial t} = -\frac{\partial v_s^j(z,t)}{\partial z} \qquad (4.2)$$

$$j = 1, 2, \ldots, n_{col}$$

The variable column pressure model was used for the overall mass balance in the pressurization and depressurization steps of PSA (see Figure 4.2, Step 1 and Step 3):

$$(1-\epsilon_b)\frac{RT}{P^j(t)}\sum_{i=A,B}\frac{\partial q_i^j(z,t)}{\partial t} + \epsilon_b\frac{1}{P^j(t)}\frac{\partial P^j(t)}{\partial t} = -\frac{\partial v_s^j(z,t)}{\partial z} \qquad (4.3)$$

$$j = 1, 2, \ldots, n_{col}$$

where the total pressure in a column is assumed to change linearly with time. The inclusion of overall mass balances is necessary for gas phase systems to account for the compressibility of the fluid during the adsorption/desorption process.

For the component mass balance in the adsorbed phase, the linear driving force (LDF) model was used assuming a finite mass transfer resistance in the boundary layer of the adsorbent particles. The LDF model is given by Equation (3.2) in Section 3.1.

A linear isotherm model was used for each adsorbing component because the enantiomers are diluted by a carrier gas in the feed stream. In the gas phase, the linear isotherm model is:

$$q_i^{eq,j}(z,t) = H_i \frac{P(t) y_i^j(z,t)}{RT} \tag{4.4}$$

$$i = A, B \quad j = 1, 2, \ldots, n_{col}$$

where H_i is the Henry's constant for component i.

4.2.2 SMB Model

In this section, the specific model equations are shown for the SMB model, which was already described in Section 3.1. A schematic of SMB was shown in Figure 1.2 along with a discussion of the operating principles in Section 1.2.1. The boundary conditions for Equation (4.1) are:

$$\begin{aligned} y_i^j(0,t) v_s^j(0,t) &= y_{i,in}^j(t) v_{s,in}^j(t) + \gamma_{feed}^j(t) y_{i,feed} v_{s,feed} \\ v_s^j(0,t) &= v_{s,in}^j(t) + \gamma_{des}^j(t) v_{s,des} + \gamma_{feed}^j(t) v_{s,feed} \end{aligned} \tag{4.5}$$

$$i = A, B \quad j = 1, 2, \ldots, n_{col}$$

where $y_i^j(0,t)$ is the mole fraction of component i in column j at position $z = 0$, the column entrance, $v_s^j(0,t)$ is the superficial velocity in column j at position $z = 0$, $y_{i,in}^j$ is the mole fraction of component i in the inlet connection to column j, $v_{s,in}^j$ is the superficial velocity in the inlet connection to column j, γ_{feed}^j is a binary variable equal

to 1 if column j is at the feed location and 0 otherwise, $y_{i,feed}$ is the mole fraction of component i in the feed, and $v_{s,feed}$ is the feed velocity. Also γ^j_{des} is a binary variable for the desorbent location, $v_{s,des}$ is the desorbent velocity. Since only one column is at the feed location at a time, $\gamma^j_{feed} = 0$ for all columns except one during a given step of the SMB process. There is no pressure term in Equation (4.5) because the operating pressure is kept constant during the SMB process.

Note that the outlet variables from the previous column are equal to the inlet variables of the next column according to the equations:

$$\begin{aligned}
P^{j-1}_{out}(t) &= P^j(t), \quad j = 2, 3, \ldots, n_{col} \\
P^{n_{col}}_{out}(t) &= P^1(t) \\
y^{j-1}_{i,out}(t) &= y^j_{i,in}(t), \quad j = 2, 3, \ldots, n_{col} \\
y^{n_{col}}_{i,out}(t) &= y^1_{i,in}(t) \\
v^{j-1}_{s,out}(t) &= v^j_{s,in}(t), \quad j = 2, 3, \ldots, n_{col} \\
v^{n_{col}}_{s,out}(t) &= v^1_{s,in}(t)
\end{aligned} \tag{4.6}$$

where P^j_{out} is the pressure in the outlet connection of column j, $y^j_{i,out}$ is the mole fraction of component i in the outlet connection of column j, and $v^j_{s,out}$ is the superficial velocity in the outlet connection of column j. These equations describe the column connections.

The inlet port model is a boundary condition on v^j_s shown in Equation (4.5). To model the outlet port, an overall mass balance is used:

$$P^j_{out}(t)v^j_{s,out}(t) = P^j(t)(v^j_s(L,t) - \gamma^j_{ext}(t)v_{s,ext} - \gamma^j_{raf}(t)v_{s,raf}) \tag{4.7}$$

$$j = 1, 2, \ldots, n_{col}$$

where $v^j_s(L,t)$ is the superficial velocity in column j at position $z = L$, L is the column length, γ^j_{ext} is a binary variable for the extract location, $v_{s,ext}$ is the extract velocity, γ^j_{raf} is a binary variable for the raffinate location, and $v_{s,raf}$ is the raffinate

velocity. The binary variables equal 1 if column j is at the inlet/outlet location and 0 otherwise. These equations assume constant cross-sectional areas in the columns and connections so that conversions from molar flow rates to velocities in the tubing are not necessary.

4.2.3 PSA Model

In this section, the specific model equations are shown for the PSA process model. The 4-step PSA process was already described in Section 4.1 (see Figure 4.2). This approach to PSA modeling was shown by Ko *et al.* [49] and Huang *et al.* [41]. The boundary conditions for Equation (4.1) are different in each step of the PSA process.

Step 1: Pressurization

$$\begin{aligned} y_i(L,t) &= 0, \quad i = A, B \\ v_s(0,t) &= 0 \end{aligned} \tag{4.8}$$

where $y_i(L,t)$ is the mole fraction of component i at position $z = L$, the end of the column. Desorbent is supplied at the end of the column, and there is no flow out of the other end of the column during pressurization.

Step 2: Adsorption

$$\begin{aligned} y_i(0,t) &= y_{i,feed}, \quad i = A, B \\ v_s(0,t) &= v_{s,feed} \end{aligned} \tag{4.9}$$

Feed is supplied at the entrance of the column, and the feed velocity is supplied by a pump.

Step 3: Depressurization

$$\begin{aligned} \frac{\partial y_i(0,t)}{\partial z} &= 0, \quad i = A, B \\ v_s(L,t) &= 0 \end{aligned} \tag{4.10}$$

The column entrance is open to the atmosphere so that gas escapes from the column until atmospheric pressure is reached. There is no gas velocity at the end of the column.

Step 4: Purge

$$\begin{aligned} y_i(L,t) &= 0, \quad i = A, B \\ v_s(L,t) &= v_{s,purge} \end{aligned} \tag{4.11}$$

Desorbent is supplied at the end of the column, and the purge velocity, $v_{s,purge}$ is supplied by a pump.

The 4-step PSA process in this work is modeled as a single adsorption column, and Equations (4.1)-(4.3) and (3.2) are solved by changing the boundary conditions in each step using binary variables. In a real PSA system, there may be multiple columns following the 4-step process in parallel to each other.

4.2.4 Numerical Simulation

For dynamic simulation using the SMB and PSA models, Equations (4.1)-(4.3) and (3.2) are discretized in the axial domain into a system of DAEs, which are integrated in time by the method of lines [70]. In this work, the discretization is done in gPROMS using a second-order central finite difference method [1]. The initial conditions are specified for the mole fraction of each component at each axial position in both liquid and adsorbed phases. For simulation starting from a clean bed, the initial conditions are $y_i^j(z,0) = 0$ and $q_i^j(z,0) = 0$ for all $i = A, B$ and all $j = 1, 2, \ldots, n_{col}$ and all $z = (0, L]$.

4.2.5 System Parameters

Based on the experimental studies of Juza *et al.* [44] and Biressi *et al.* [17], the system parameters used for the simulation and optimization of SMB and PSA for the enantiomer separation of enflurane are shown in Table 4.1. Unless otherwise stated, it is

understood that the given values were used in both SMB and PSA models. The particle size of the chiral γ-CD adsorbent was 250 to 350 μm, and the overall porosity was measured to be 0.75, and the Darcys law constant was measured to be 6 bar sec m^{-2}. The pressure drop observed in the experimental work was about 1 bar over 8 columns with a total length of 6.4 m [17], and it was assumed that the pressure drop would be negligible in the systems for this study. This assumption is frequently used for modeling gas phase systems [41, 67]. The Henrys constants for R- and S-enflurane were measured at 306 K and are given in Table 4.1. The target molecule, R-enflurane, is the less adsorbed component in this separation and is therefore collected in both SMB and PSA as the raffinate product. The separation factor for the enantiomers at this temperature is about 1.5. At a temperature of 306 K the vapor pressure of enflurane is about 0.4 bar. The mass transfer coefficients were not directly available for this system; however, the column efficiency was reported [17]. A reasonable value for the mass transfer coefficient was chosen based on its consistency with the reported column efficiency, which corresponds to a plate number of approximately 500 (i.e. $k_i = 1$ sec^{-1}). A pulse experiment was done in simulation, and it was found that the chromatograms were relatively insensitive to the value of k_i.

The adsorption columns have an internal diameter of 0.015 m. The SMB unit has 4 columns, which is the classical 4-zone column configuration. The length of each SMB column was set at 0.4 m and the total length of the system is 1.6 m, while the PSA process may be operated with a single column of length 0.4 m, and only a single column is modeled for simulation and optimization purposes.

The feed mole fractions are 0.018 for both R- and S-enflurane, and these are diluted in nitrogen, an inert (non-adsorbed) carrier gas, and the total mole fraction of enflurane in the feed was 0.036. This value is small enough to avoid condensation and to justify the application of linear isotherms. This concentration is also consistent with the range of feed concentrations used in the experiments [17].

Table 4.1: System parameters for separation of enflurane enantiomers

Parameter	Value
Average adsorbent particle size[a], d_p [μm]	300
Overall porosity[a], ϵ_b	0.75
Henry's constant for R-enflurane[b], H_A	118
Henry's constant for S-enflurane[b], H_B	175
Mass transfer coefficients, $k_A = k_B$ [sec^{-1}]	1
Column diameter[a], d_c [m]	0.015
Single column length, L [m]	0.4
Number of columns, n_{col}	SMB: 4, PSA: 1
Operating temperature, T [K]	306
Feed mole fractions, $y_{A,feed} = y_{B,feed}$	0.018

[a] from Biressi *et al.* [17], [b] from Juza *et al.* [44]

Nitrogen is employed as desorbent in both SMB and PSA systems at the system pressure, and the only components in the gas phase for each system are R-enflurane, S-enflurane and nitrogen. Nitrogen acts as an inert carrier gas, therefore its Henrys constant is zero, and there is no consideration of competition between nitrogen and the enfluranes for adsorption sites.

4.3 Optimization

4.3.1 Problem Formulation

For both SMB and PSA processes, a multi-objective optimization problem is considered. The objectives are to maximize both the feed throughput and target recovery. The trade-off of these two objectives is investigated by dynamic optimization using the ϵ-constraint method for multi-objective optimization [82]. For SMB, the objective function is to maximize feed throughput and this function is constrained by a minimum raffinate recovery. The problem is formulated as:

$$\begin{aligned} &\max \quad \text{Throughput}_{SMB} \\ &\text{s.t.} \quad \text{Recovery}^{raf}_{A,SMB} \geq \epsilon_{Rec} \end{aligned} \tag{4.12}$$

where A is the target molecule in the raffinate stream, and ϵ_{Rec} is a minimum raffinate recovery that is varied to generate a Pareto curve. Throughput in the SMB unit is defined as:

$$\text{Throughput}_{SMB} = Pv_{s,feed} \tag{4.13}$$

and recovery of component A in the SMB is defined as:

$$\text{Recovery}^{raf}_{A,SMB} = \sum_{j=1}^{n_{col}} \gamma^{j}_{raf}(t) \frac{\int_0^{t_{step}} v_{s,raf} y^{j}_{A}(L,t)\, dt}{\int_0^{t_{step}} v_{s,feed} y_{A,feed}\, dt} \tag{4.14}$$

where t_{step} is the symmetric step time.

On the other hand, for PSA the objective function is reformulated to maximize the recovery of component A in the raffinate and this function is constrained by a minimum throughput. If the previous objective function in Equation (4.12) is used for PSA, at high values of ϵ_{Rec} the optimization becomes infeasible. Therefore, the problem is reformulated as:

$$\begin{aligned} &\max \quad \text{Recovery}^{raf}_{A,PSA} \\ &\text{s.t.} \quad \text{Throughput}_{PSA} \geq \epsilon_{Thr} \end{aligned} \tag{4.15}$$

where ϵ_{Thr} is a minimum throughput that is varied to generate a Pareto curve. Recovery of component A in PSA is defined as:

$$\text{Recovery}^{raf}_{A,PSA} = \frac{\int_0^{t_{ads}} v_s(L,t) y_A(L,t)\, dt}{\int_0^{t_{ads}} v_{s,feed} y_{A,feed}\, dt} \tag{4.16}$$

where t_{ads} is the time of the adsorption step. Throughput in the PSA unit is defined as:

$$\text{Throughput}_{PSA} = P_H v_{s,feed} \rho_{ads} \tag{4.17}$$

where P_H is the high pressure of the PSA system during the adsorption step, and ρ_{ads} is the ratio of t_{ads} to the cycle time, t_{cycle}.

The SMB process has six degrees of freedom in the optimization problem. The decision variables are the step time, t_s, the inlet and outlet velocities, $v_{s,des}$, $v_{s,ext}$, $v_{s,feed}$, $v_{s,raf}$, and the operating pressure, P. On the other hand, the PSA process has five degrees of freedom in the optimization problem. The decision variables are the adsorption time, t_{ads}, the purge time, t_{purge}, the inlet velocities, $v_{s,feed}$, $v_{s,purge}$, and the high pressure during adsorption, P_H. Some of the operating conditions in PSA are decided *a priori*. The low pressure during desorption, P_L, is set to atmospheric pressure, and the duration of pressurization and depressurization steps are both 30 sec.

The separation performance of SMB and PSA was evaluated based on the purity and recovery of component A in the raffinate. The recovery was defined for SMB and PSA in Equations (4.14) and (4.16) respectively. For the SMB process, purity of component A in the raffinate is defined as:

$$\text{Purity}_{A,SMB}^{raf} = \sum_{j=1}^{n_{col}} \gamma_{raf}^{j}(t) \frac{\int_0^{t_{step}} v_{s,raf} y_A^j(L,t)\,dt}{\sum_{i=A,B} \int_0^{t_{step}} v_{s,raf} y_i^j(L,t)\,dt} \tag{4.18}$$

For the PSA process, purity of component A in the raffinate is defined as:

$$\text{Purity}_{A,PSA}^{raf} = \frac{\int_0^{t_{ads}} v_s(L,t) y_A(L,t)\,dt}{\sum_{i=A,B} \int_0^{t_{ads}} v_s(L,t) y_i(L,t)\,dt} \tag{4.19}$$

In both SMB and PSA the purity of component A in the raffinate stream was constrained to be greater than or equal to 99% according to pharmaceutical industry regulations.

The optimization problems for SMB and PSA also include cyclic steady state (CSS) constraints, as described previously by Equation (3.12) in Section 3.1. For gas

phase SMB a single-step formulation is again used to describe the CSS condition:

$$\begin{aligned} y_i^j(z,0) &= y_i^{j+1}(z,t_{step}), \quad j = 1,2,\ldots,n_{col}-1 \\ y_i^{n_{col}}(z,0) &= y_i^1(z,t_{step}) \\ q_i^j(z,0) &= q_i^{j+1}(z,t_{step}), \quad j = 1,2,\ldots,n_{col}-1 \\ q_i^{n_{col}}(z,0) &= q_i^1(z,t_{step}) \end{aligned} \tag{4.20}$$

In Equation (4.20) the CSS condition means that the internal profiles in the gas and adsorbed phases must be equal at every discretized point at the beginning and end of a step only shifted forward one column in the direction of fluid flow. For PSA a single-cycle formulation is used to describe the CSS condition:

$$\begin{aligned} y_i(z,0) &= y_i(z,t_{cycle}) \\ q_i(z,0) &= q_i(z,t_{cycle}) \end{aligned} \tag{4.21}$$

In Equation (4.21) the CSS condition means that the internal profiles in the gas and adsorbed phases must be equal at every discretized point at the beginning and end of a cycle. In this work, the PSA cycle consists of four steps shown in Figure 4.2.

The superficial velocities, pressures, and step/cycle times were constrained by upper and lower bounds. These constraints were selected to match the experimental conditions used by Biressi *et al.* [16, 17], and are shown in Table 4.2. The bounds are the same for both SMB and PSA as applicable. Identical upper bounds are chosen assuming the same operating equipment is used, such as gas compressors. The lower bounds were set to reasonable values that can be easily realized, and later confirmed that these lower bounds are always inactive at the optimal solutions. The upper bounds on the step and cycle times are always inactive at the optimal solutions.

4.3.2 Numerical Solution

The optimization problems for SMB and PSA are constrained by the mass balances described by the adsorption column model in Equations (4.1)-(4.3). To solve these

Table 4.2: Constraints on the decision variables for SMB and PSA

Decision variable	Lower bound	Upper bound
Superficial velocity, v_s [cm sec^{-1}]	0	10.7
Pressure, P [bar]	1	4.5
Step time, t_{step} [sec]	10	10000
Cycle time, t_{cycle} [sec]	10	10000

dynamic optimization problems numerically, in this work the simultaneous, single-discretization method, described in Section 3.2.2, is used. These optimization problems for SMB and PSA were written in gPROMS and the SRQPD solver is used, which follows a modified sequential quadratic programming (SQP) algorithm [3, 15]. The optimization algorithm on average converged in two hours depending on the number of discretization points used in the axial domain. More details on the optimization strategy are described by others who used the same program [41, 46, 49]. Each optimization problem was initialized with feasible operating conditions which were obtained by simulation of the process models in gPROMS to find reasonably good performance. For SMB there is a triangle theory that can be used as an initial guess of optimal conditions given by [44].

4.4 Results

4.4.1 Comparison of SMB and PSA Separation Performance

The separation performance of SMB and PSA in enflurane separation is compared by observing the simulated internal profiles at their respective optimal operating conditions. The SMB and PSA optimization problems are given by Equations (4.12) and (4.15) and their respective optimal solutions are shown in Tables 4.3 and 4.4, and the optimal internal profiles are shown in Figures 4.3 and 4.5. The molecules R-enflurane and S-enflurane are represented by A and B respectively. The model parameters used for the enflurane system are shown previously in Table 4.1.

Table 4.3: SMB optimal operating conditions with 99% raffinate purity, 99% raffinate recovery, and 5.0 g_{feed} day^{-1} cm^{-3} adsorbent

Operating parameter	Value
Step time, t_{step} [sec]	181.6
Pressure, P [bar]	4.5*
Velocity in Zone 1, v_s^1	10.7*
Velocity in Zone 2, v_s^2	7.1
Velocity in Zone 3, v_s^3	9.1
Velocity in Zone 4, v_s^4	6.1

* indicates active upper bound

In Table 4.3 the optimal solution for the SMB process has some remarkable features. The maximized throughput is 5.0 g_{feed} day^{-1} cm^{-3} adsorbent with 99% raffinate purity and 99% raffinate recovery, which means both enantiomers of enflurane can be produced at 99% purity with a throughput of about 800 g_{feed} processed per day with the lab scale unit. The pressure and velocity in Zone 1 are both active at the upper bounds. These operating parameters facilitate the regeneration of the stationary phase in Zone 1, and thus they allow maximum throughput.

In Figure 4.3 the internal profiles of the SMB have a nearly symmetrical shape, which is a characteristic of the linear isotherm system. A clear separation of the mole fraction profiles for components A and B is clearly established in the SMB at the CSS condition. Figure 4.4 shows the raffinate profiles for components A and B during a single step. These raffinate profiles correspond to those time-varying mole fractions shown in Figure 4.3 at the axial position $z = 0.12$, which is the end of Column 3. The unwanted component B pollutes the raffinate product just before the switch, and therefore 99% raffinate purity is achieved. The average concentration of A in the raffinate product can be estimated by integrating the mole fraction profile and dividing by the step time. This value is about 0.012, which is two-thirds of the feed concentration.

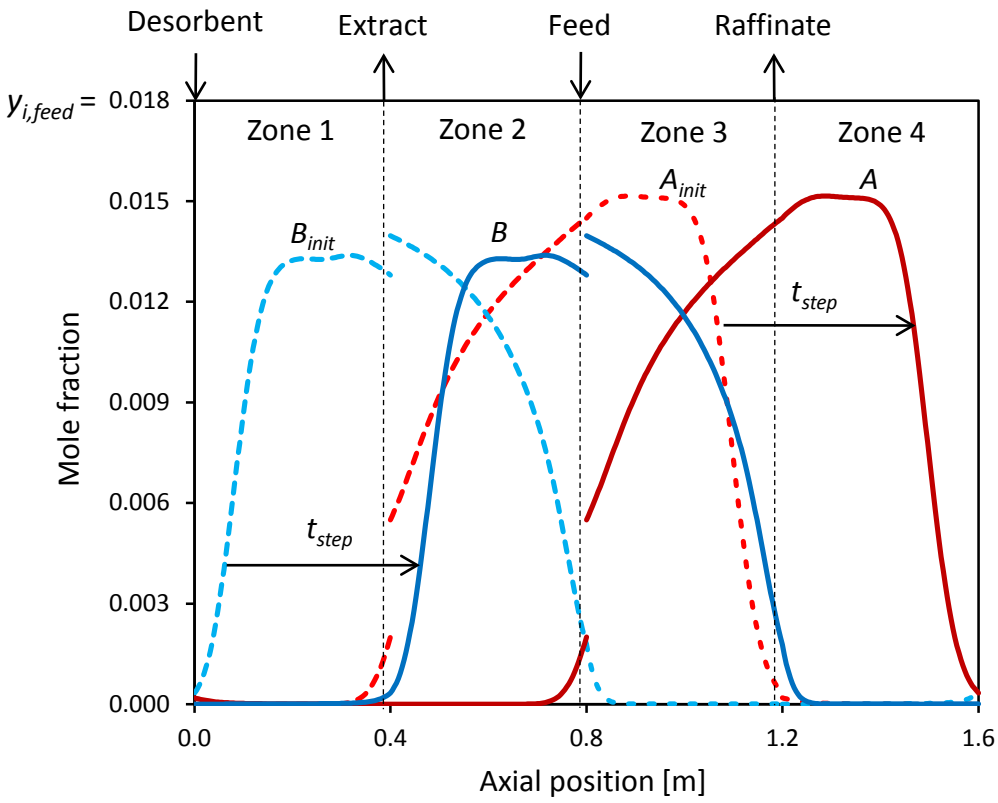

Figure 4.3: SMB internal profiles at beginning and end of a step at CSS condition. Operating conditions shown in Table 4.3

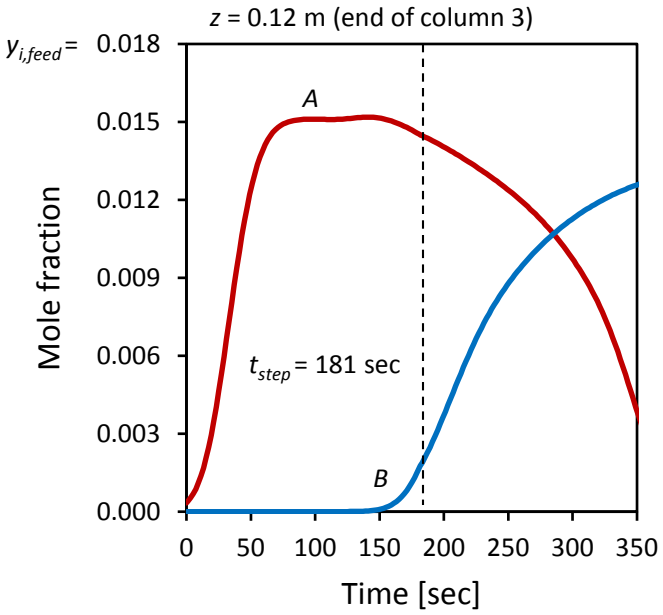

Figure 4.4: SMB raffinate profiles during a step at CSS condition. Operating conditions shown in Table 4.3

In Table 4.4 the optimal solution for the PSA process also has some remarkable features. The maximized raffinate recovery is 27.3% and the throughput is 16.6 g_{feed} day^{-1} cm^{-3} adsorbent with 99% raffinate purity. This means one enantiomer of enflurane can be produced at 99% purity with a throughput of about 2650 g_{feed} processed per day with a lab scale unit equivalent in volume to the SMB unit. From this result, it is concluded that at the sacrifice of recovery, the PSA process can produce pure R-enflurane at a relatively high throughput. The upper bound on pressure is active during the adsorption step when it is critical to force the less-retained component through the column. Also, the velocity during the purge step is active at the upper bound to minimize the purge time.

Table 4.4: PSA optimal operating conditions with 99% raffinate purity, 16.6 g_{feed} day^{-1} cm^{-3} adsorbent, and 27.3% raffinate recovery

Operating parameter	Value
Feed velocity, $v_{s,feed}$ [cm sec^{-1}]	2.2
Purge velocity, $v_{s,purge}$ [cm sec^{-1}]	10.7*
High pressure, P_H [bar]	4.5*
Low pressure, P_L [bar]	1.0^o
Pressurization time, t_{press} [sec]	30^o
Adsorption time, t_{ads} [sec]	760
Depressurization time, $t_{depress}$ [sec]	30^o
Purge time, t_{purge} [sec]	210
Cycle time, t_{cycle} [sec]	1030

* indicates active upper bound, ^{o} indicates fixed quantity in optimization

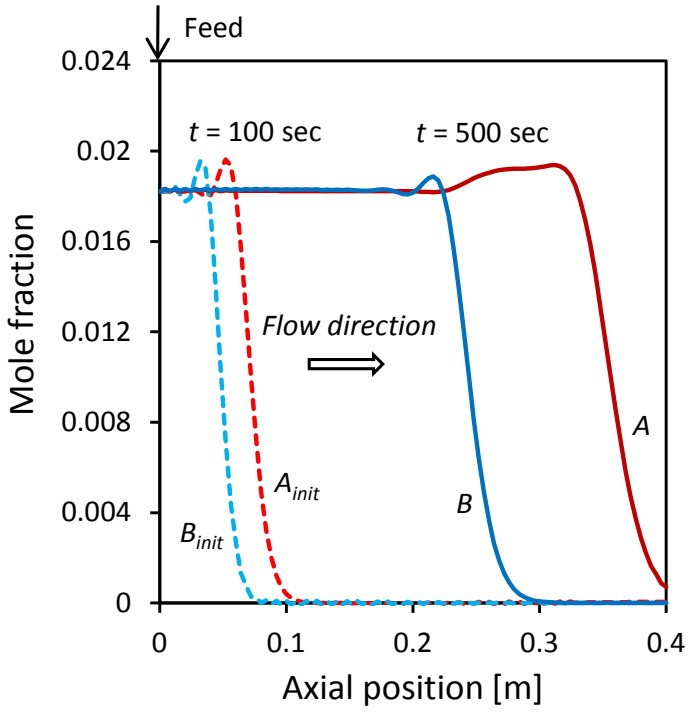

Figure 4.5: PSA internal profiles during adsorption step of a cycle at CSS condition. Operating conditions shown in Table 4.4

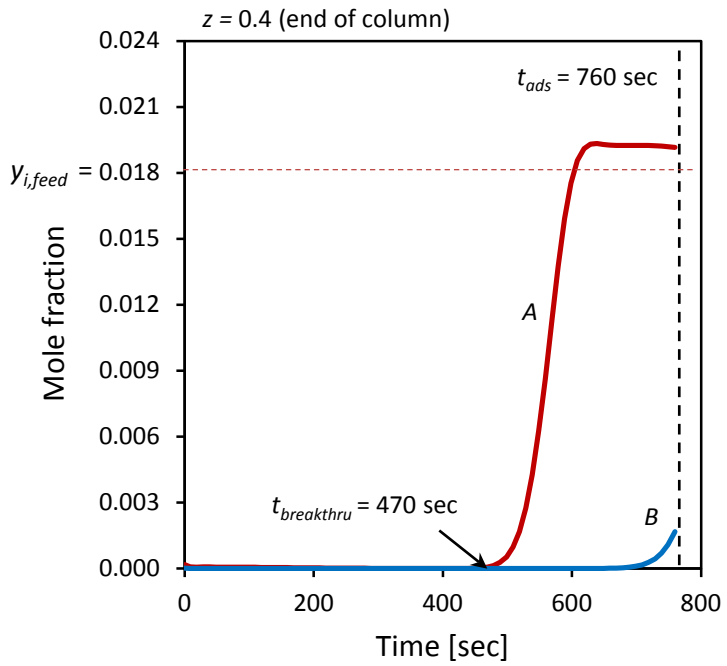

Figure 4.6: PSA raffinate product profiles during adsorption step of a cycle at CSS condition. Operating conditions shown in Table 4.4

In Figure 4.5 the time evolution of the adsorption wave fronts during the PSA process is shown for each component in the column. Component A traverses the column faster than component B due to their relative adsorption affinities. Also, component A has a slight overshoot of the feed concentration at the peak of the propagation front. This overshoot is due to incomplete regeneration of the column during the purge step. The overshoot effect actually contributes to slightly increase the target recovery during a step at the CSS condition.

In Figure 4.6 the raffinate product profiles are shown over time during the adsorption step. At about 750 sec, the unwanted component B begins to pollute the raffinate stream, and so the adsorption step is ended at the point where 99% raffinate purity is achieved. The average mole fraction of component A in the raffinate product is about 0.012, assuming the raffinate collection begins at a breakthrough time of about 470 sec. Therefore, the raffinate product concentration is equal to about two-thirds

of the feed concentration. Interestingly, this product concentration is nearly the same as that obtained in the SMB process. Nevertheless, the low value of 27.3% raffinate recovery is a disadvantage for PSA. This is probably because both enantiomers of enflurane are adsorbed relatively strongly to the stationary phase, and the separation factor is only about 1.5. Therefore, these enantiomers do not attain a high degree of separation from each other in a single column.

4.4.2 Pareto Plots of SMB and PSA Optimal Solutions

Each solution to the SMB and PSA optimization problems, given by Equations (4.12) and (4.15), are compared in Figure 4.7 by Pareto plots with optimal raffinate recovery of component A and optimal throughput values. These optimal solutions are also compared in Figure 4.8 by Pareto plots with optimal raffinate recovery of component A and optimal productivity of component A values. Note that for all optimal solutions 99% raffinate purity was achieved. The definitions of feed throughput and productivity are given in Appendix A.

From Figures 4.7 and 4.8 it is clear that PSA has much lower raffinate recovery than SMB; PSA suffers more from the low selectivity (about 1.5) between the enantiomers, as well as their significant affinities for the stationary phase. For the simplified 4-step PSA configuration analyzed in this work, a majority of component A is adsorbed during the adsorption step, and most of the adsorbed components are, in the classical configuration, vented out as waste in the following depressurization and purge steps, rendering low recovery. Whereas for SMB, the adsorbed component A is desorbed by nitrogen and then re-sorbed or eluted as raffinate product in the following zones.

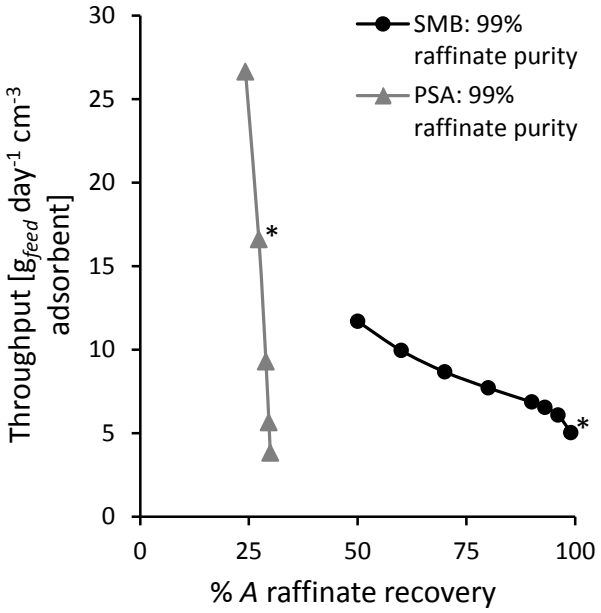

Figure 4.7: Pareto plot of optimal raffinate recovery and throughput for SMB and PSA. * indicates point where operating conditions are shown in Tables 4.3 and 4.4 for SMB and PSA respectively

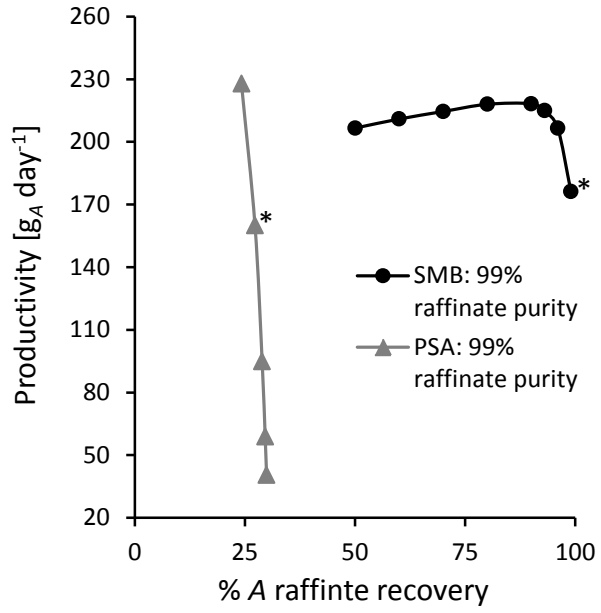

Figure 4.8: Pareto plot of optimal raffinate recovery and productivity of component *A* for SMB and PSA. Both SMB and PSA are assumed to use same mass of stationary phase, for equal capital investment. * indicates point where operating conditions are shown in Tables 4.3 and 4.4 for SMB and PSA respectively

The trade-off between the maximized throughput and target recovery requirements is investigated and shown in Figure 4.7. The productivity of the target component, also shown in Figure 4.8, is maximized by simultaneously increasing the throughput and raffinate recovery. Interestingly, the optimal raffinate recovery in PSA appears to have a linear dependence on the throughput. Even when the throughput is decreased to 3.8 g_{feed} day^{-1} cm^{-3} adsorbent, the recovery increased only to 29.9%, and this results in low productivity compared to SMB. The SMB process appears to have a maximum productivity of 218 g_A day^{-1} with a recovery of 90%, assuming a 4-column setup. On the other hand, the PSA process appears to have a greater productivity over 230 g_A day^{-1} with a recovery of only 24.3%, assuming the same mass of stationary phase as in the 4-column SMB process. Perhaps the PSA process also has a maximum productivity, but with reduced recovery it seems 4-zone SMB is more advantageous than the standard 4-step PSA for enantiomer separation, because the enantiomers are highly valuable products.

However, Figure 4.9 demonstrates a key advantage of the PSA process, which is reduced desorbent consumption. In the SMB process, desorbent is supplied continuously at the highest flow rate to facilitate fast desorption and regenerate the column in Zone 1. This causes the ratio of desorbent-to-feed flow rate, or D/F ratio, to be relatively large. On the other hand, the PSA process requires a lesser amount of desorbent for column regeneration due to its stepwise operation. Desorbent is only supplied during the pressurization and purge steps of the process, which constitute less than half of the cycle time. This can be a significant advantage if the product concentration must be high, or desorbent cost cannot be neglected in the process economics. The exact calculation of the D/F ratios are discussed in Appendix A.

The maximized production rate of the SMB was 218 g_A day^{-1} with a recovery of 90%, while the maximized product recovery of PSA was 29.9% at a much reduced throughput of 3.8 g_{feed} day^{-1} cm^{-3} adsorbent. The SMB throughput values

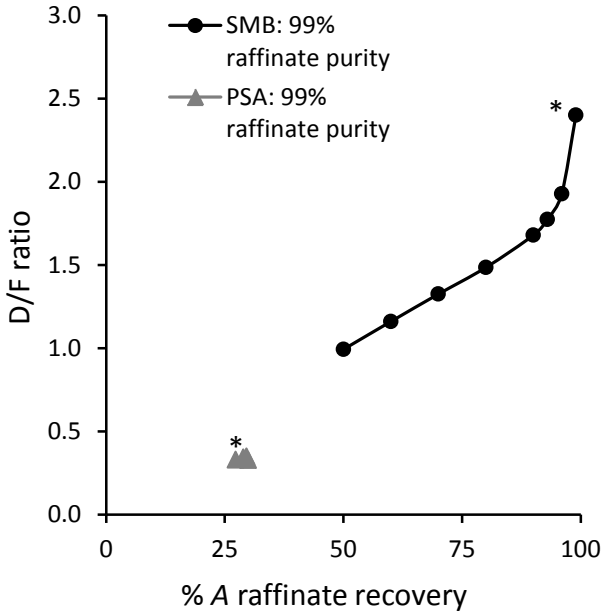

Figure 4.9: Pareto plot of optimal raffinate recovery and D/F ratios for SMB and PSA. * indicates point where operating conditions are shown in Tables 4.3 and 4.4 for SMB and PSA respectively

are far above those reported in the non-optimized experimental studies of Biressi *et al.* [16, 17]. This result can be attractive for industrial use as it indicates feasible operating conditions where a large amount of purified enfluranes may be produced for pharmacological studies. For further investigation on the feasibility of these processes, the column efficiency must be verified by an experimental study. Furthermore, the poor recovery of PSA may be improved by introducing a modified operating strategy or employing multiple columns while maintaining the high throughput demonstrated in this study.

4.5 Conclusion

In this work, the resolution of racemic gas mixtures by SMB and PSA is investigated by dynamic simulation and multi-objective optimization. The internal concentration profiles and operating conditions at the optimal solutions are investigated and analyzed by dynamic simulation. Furthermore, the trade-off of throughput and target recovery has been investigated systematically. It has been found that the SMB process achieves high recovery which can be greater than 99%, while the recovery using 4-step PSA considered in this work remains relatively low. Nevertheless, the higher throughput of the PSA process can be a significant advantage for inexpensive feed mixtures. Even at reduced recovery, the productivity of the target component can be greater in PSA than the maximum productivity possible in SMB. Also, the PSA process features a low D/F ratio compared to SMB and this is also economically advantageous if the product concentration must be high or desorbent cost cannot be neglected.

CHAPTER 5

PREDICTION-CORRECTION METHOD FOR OPTIMIZATION OF SMB CHROMATOGRAPHY

5.1 Motivation

In this chapter the prediction-correction (PC) method for SMB process development and optimization is introduced and demonstrated using experiments with a linear isotherm system. The goal of this work is to show that the PC algorithm for SMB process development, starting from a new separation problem and ending with optimal operating conditions, is efficient and robust [11].[1]

Using SMB for binary separations, pure extract and raffinate products can be obtained with relatively high productivity and reduced solvent consumption compared to batch chromatography even if the separation factor is small. The operating principles of SMB are previously discussed in Section 1.2.1. The determination of optimal operating conditions is not yet a straightforward task, especially if the sample volume available for lab and mini-plant tests is small or there is only a limited time for process development. Therefore, SMB is frequently applied using operating conditions that are known to be sub-optimal in terms of productivity and solvent consumption.

Typical steps in SMB process development for a new separation problem are to perform batch experiments, find some operating conditions that are expected to satisfy purity constraints based on design criteria that approximate SMB dynamics [58, 64, 74], then manually tune the operating conditions experimentally until the design specifications are met. Usually this effort is aided by mini-plant experiments and computer simulation of a process model [22, 26, 55]. In addition, there may be

[1] This chapter is published in Bentley and Kawajiri [11]

efforts to design more robust operating conditions where the separation performance is not adversely affected by slight disturbances in the flow rates, feed or desorbent compositions.

An important aspect of SMB process development is the selection of a process model, which is discussed in Section 3.1 and the determination of model parameters. There are a number of techniques that chromatographers have used for obtaining adsorption isotherm and kinetic parameters in the literature [9, 71]. Reviews of moment analysis of pulse injections, frontal analysis, elution by characteristic points, and inverse methods can be found [27, 36, 71, 72]. Batch experiments are typically used to estimate single-column model parameters and obtain a predictive process model for SMB. In Grosfils *et al.* [32] there is a comparison between different single-column models and a study of the identifiability of model parameters using pulse injections and parameter estimation. They used design of experiments to reduce the effort required to obtain reliable process model parameters for SMB. In Grosfils *et al.* [31] their SMB process model, which relies on careful descriptions of the extra-column dead volumes that exist in the real SMB unit, was validated by comparing it with SMB plant data. In Küpper *et al.* [52] a concept for SMB model parameter estimation using online measurements is proposed and demonstrated using computational simulations of an SMB process model. They conclude that the model parameters can be estimated over time by transient measurements of the extract, raffinate and recycle lines and can be adapted to physical changes in the column properties such as porosity. Yet their work requires online detection of entire internal concentration profiles over a step and no SMB optimization is performed using the estimated parameters.

There are other researchers who have worked on another aspect of SMB operation, that is the maintenance of the desired operation once process development is completed. The automatic control of the SMB processes is described in Klatt *et al.* [48], where the operating conditions and the assembled elution profile are measured during

the periodic SMB operation and adjustments are made automatically to correct deviations from the desired product purities. The sampling methods that are used by [48] are similar to those used in the PC method. Further work on optimizing control for SMB has been done at ETH Zurich by Grossmann *et al.* [35], where average product concentrations are measured during a cycle as feedback information for a controller. This measurement strategy also uses HPLC to analyze the product concentrations, which is more reliable than online UV detection, as a measurement technique. Their methodology assumes that a reliable set of process model parameters and optimal operating conditions for the SMB are known *a priori*. They do not consider updating the SMB model parameters using the product concentration data.

The PC algorithm is designed for optimal SMB process development. It makes use of a surrogate model (see Biegler *et al.* [14]), infrequent sampling of SMB outlet streams, parameter estimation, and dynamic optimization to reduce the time required to obtain reliable model parameters and optimize the SMB process in a systematic manner.

This chapter is organized as follows: The detailed steps of the PC algorithm are discussed in Section 5.2, the laboratory equipment is detailed in Section 5.3, and two case studies with a linear isotherm system are presented in Section 5.4 to show that the algorithm converges efficiently and that the algorithm is robust to poor initial parameter values.

5.2 Methodology

5.2.1 Prediction-Correction Algorithm

The prediction-correction (PC) algorithm for SMB process development is shown in Figure 5.1. This is an iterative scheme where the SMB model parameters are corrected by fitting SMB experimental data and the optimal operating conditions are predicted by re-optimizing the SMB model. The algorithm is terminated systematically with

clearly defined termination criteria.

This procedure assumes that a new mixture is to be resolved by SMB, and a reliable set of SMB model parameters is not yet known. The adsorbent type, SMB column configuration, desorbent and feed compositions, and other operating parameters such as temperature should be selected *a priori*. The procedure is as follows:

1. Initialize $k = 0$. A set of batch experiments are performed to estimate column porosity, adsorption isotherm and kinetic parameters.

2. Model-based SMB optimization is performed to obtain an initial set of optimal operating conditions.

3. Let $k = k+1$. An SMB experiment is performed using the k^{th} optimal operating conditions and a set of concentration data and product purities are obtained.

4. The adsorption isotherm and kinetic parameters are refined by fitting the SMB model to the experimental concentration data (correction step).

5. Model-based SMB optimization is repeated with the refined set of model parameters to obtain an updated set of optimal operating conditions (prediction step).

6. If termination criteria are satisfied the PC algorithm ends and no further switches of operating conditions are needed. If not, return to Step 3 and repeat.

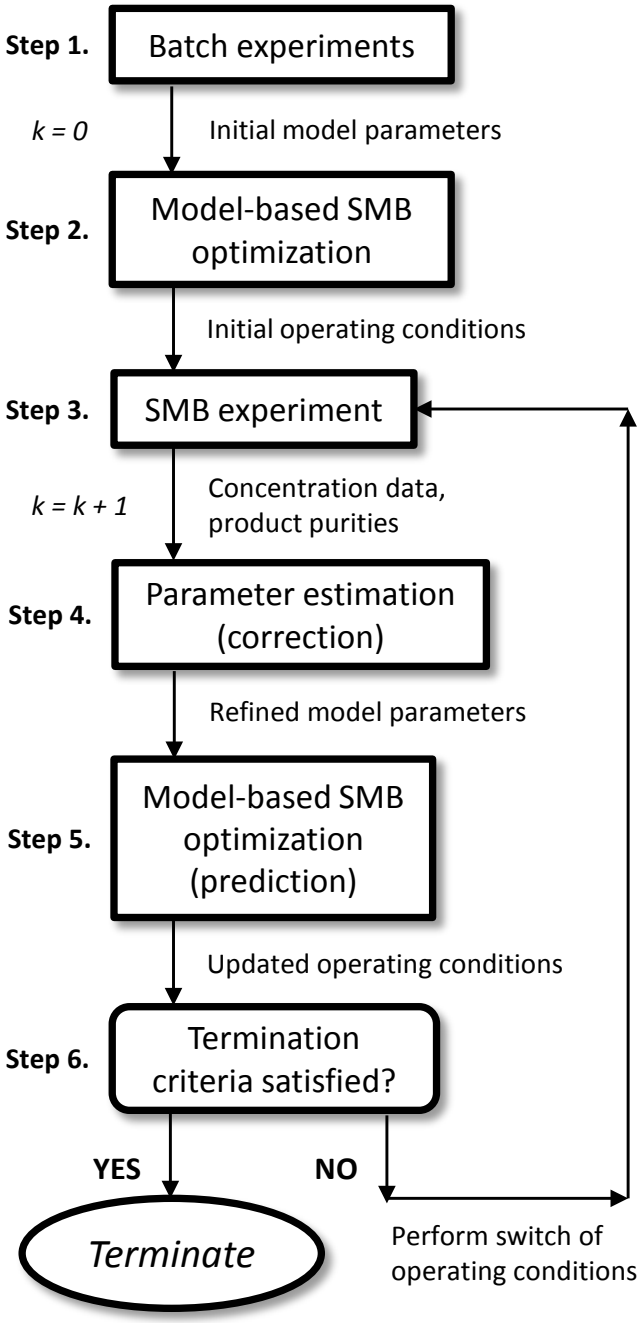

Figure 5.1: Prediction-correction (PC) algorithm for SMB process development

5.2.2 Step 1: Batch Experiments

The SMB model considers individual chromatographic columns, column connections, and inlet/outlet streams. The chromatographic column model consists of component mass balances in the liquid and stationary phases, adsorption isotherm relations, and mass transfer/diffusion relations where the only unknown parameters are the adsorption isotherm and kinetic parameters. There are more sophisticated models that could be used to include model parameter dependencies on flow rate, such as the van Deemter relation [36] showing the effect of flow rate on mass transfer coefficients. Furthermore, detailed column models that consider the dead volume of the real SMB unit can be found in the literature [60].

In this work a linear isotherm and the linear driving force (LDF) model in the stationary phase are used, so there is one equilibrium constant (Henry's constant) and one overall mass transfer coefficient to be determined for each adsorbing component in the system. Hence, the following batch experiments and calculations are needed:

1. Small-volume pulse injection of tracer compound to estimate overall porosity of the column

2. Small-volume pulse injection of feed mixture to estimate Henry's constants and mass transfer coefficients by moment analysis

The Henry's constant for each component is a function of the column porosity, and the estimate of the mass transfer coefficient is a function of the column porosity, plate number and flow rate. These batch experiments yield a set of initial model parameters that are not measured at various conditions, and they do not account for any dead volumes or mixing behaviors in the real SMB unit. In this approach, such models that require extra experimental effort are not necessary. These initial parameter estimates are used only to obtain an initial set of optimal operating conditions which are later corrected iteratively.

5.2.3 Steps 2 and 5: Model-Based SMB Optimization (Prediction Step)

The SMB model used in this work is given by Equations (3.1) - (3.3), (3.6), (3.7), (3.8) discussed in Section 3.1. This model resembles closely the kinetic model that is used by others for dynamic simulation of the SMB process [22, 31]. The SMB optimization problem formulation is given by Equation (3.10) discussed in Section 3.2.1. This formulation is based on the simultaneous approach discussed by Kawajiri and Biegler [46]. The model-based SMB optimization is performed initially in Step 2 of the PC algorithm as shown in Figure 5.1 and then again in Step 5 of each iteration. The numerical solution of the SMB optimization problem follows the simultaneous, single-discretization approach described in Section 3.2.2. The problem is written in gPROMS and solved using the SRQPD nonlinear programming solver. For initialization of the optimization problem in Step 2 of the PC algorithm, SMB operating conditions are selected so that the triangle theory constraints set forth in Mazzotti *et al.* [58] are satisfied, but these constraints are not needed in subsequent iterations.

It should be noted that the PC algorithm is designed for finding optimal operating conditions and reliable parameter values in the process development stage for a new separation problem. On the other hand, rejecting disturbances and dealing with unexpected changes in physical properties during continuous operation (pump flow rates, porosity, etc.) are out of scope of this work. To correct the operating conditions in a timely manner for such time-varying changes, an optimal control problem that takes into account the entire transient profile, not a CSS optimization problem, must be solved on-line. In addition, a reliable state estimation technique would enable fast and effective control actions [4, 35, 48]. For such problems, employing efficient and reliable computational methods for on-line calculations is crucial.

5.2.4 Step 3: SMB Experiment

In the SMB experiment the current optimal operating conditions are implemented and transient concentration data from the extract, raffinate and recycle lines are measured. Numerous sampling strategies are feasible. One such sampling strategy, which is employed in the following case studies, is as follows: At the moment the operating conditions are switched, the product streams (extract and raffinate, see Figure 5.2) are fed into empty containers and the cumulative product is collected. At the end of a number of steps a small sample is taken from the product containers and its composition is analyzed by HPLC. This generates a set of concentration data for each product line over time.

For each SMB experiment the product samples are collected at the end of a number of steps until the change in the measured concentration in the n^{th} sample is sufficiently small. For each sample in the k^{th} experiment, the following condition is checked:

$$\left| \frac{\sum_{i=A,B} c_i^{ext}(n-1) - \sum_{i=A,B} c_i^{ext}(n)}{\sum_{i=A,B} c_i^{ext}(n-1)} \right| \leq \epsilon_c^k \tag{5.1}$$

where $c_i^{ext}(n)$ is the concentration of component i in extract sample n, and ϵ_c^k is the tolerance for the change in concentration of the extract product in the k^{th} experiment. If the condition in Equation (5.1) is satisfied for sample n, then no more sampling needs to be done, and the next step of the PC method can begin. The condition set in Equation (5.1) is checked only for the extract samples since the most-retained component requires a longer time to reach the CSS condition.

During an experiment there may be significant contaminations in the product streams as well as significant concentrations in the recycle loop. To increase observability of the process, the recycle stream is sampled over a single step to obtain average concentrations, as shown in Figure 5.2. This sample is taken after the sampling of extract and raffinate products is finished. It should be noted that more frequent sampling from the recycle line may further increase the observability. However, this

was not done due to the additional complexity of modeling the opening and closing of the recycle loop.

5.2.5 Step 4: Parameter Estimation (Correction Step)

The parameter estimation is formulated as a maximum likelihood problem and the objective function is:

$$\phi_{PE}(\theta) = \sum_{p=1}^{NE} \sum_{l=1}^{NV_p} \sum_{n=1}^{NM_{pl}} \left[ln(\sigma_{pln}^2) + \frac{(\tilde{z}_{pln} - z_{pln})^2}{\sigma_{pln}^2} \right] \tag{5.2}$$

where θ is the set of model parameters to be estimated, NE is the number of experiments, NV_p is the number of variables measured in experiment p, NM_{pl} is the number of measurements of variable l in experiment p, σ_{pln}^2 is the variance of measurement n of variable l in experiment p, which is determined by the measured variable's variance model, $\tilde{z}_{pln}$ is measurement n of variable l in experiment p, and z_{pln} is model-prediction n of variable l in experiment p. The measured variables are the concentration data obtained from the SMB experiment(s), and the model-predicted variables are the concentration values calculated by numerical simulation of the SMB model. The SMB model equations were presented in Section 3.1.

The parameter estimation problem is formulated as:

$$\begin{aligned} &\min \quad \phi_{PE}(\theta) \\ &\text{s.t.} \quad \theta_{min} \leq \theta \leq \theta_{max} \\ &\text{Equations (3.1) - (3.3), (3.6), (3.7), (3.8)} \end{aligned} \tag{5.3}$$

where θ_{min} and θ_{max} are the lower and upper bounds on the set of model parameters to be estimated. The bounds on θ are used to avoid unreasonable changes in the parameter values, and it is confirmed that these constraints are inactive at the optimal solutions.

The SMB parameter estimation problem was written in gPROMS and solved using the SRQPD nonlinear programming solver [2]. The numerical optimization follows a

sequential method which is described in Kawajiri and Biegler [46]. The SMB model is used to simulate the SMB experiment, and then the objective function and constraints are checked by the optimization solver. Therefore, computation time of the parameter estimation problem scales with the number of SMB experiments that are simulated.

The parameter estimation routine in gPROMS also includes statistical analysis of the estimated parameters. The statistics of interest are the confidence intervals for the estimated parameters. These values represent bounds on the estimated parameters where 95% of the observed data is adequately described by parameter values within the interval. The details of this calculation can be found in the gPROMS documentation [2]. The 95% confidence interval for parameter m is:

$$\theta_m = \hat{\theta}_m \pm X_m(95) \tag{5.4}$$

where $\hat{\theta}_m$ is the value of parameter m estimated by solving the parameter estimation problem in Equation 5.3 and $X_m(95)$ is given by:

$$X_m(95) = t\left(\frac{95+1}{2}, N - N_p\right)\sqrt{V_{mm}} \tag{5.5}$$

where N is the number of experimental data points, N_p is the number of model parameters, $t(.,.)$ is the t-distribution with the probability level, equal to half of the confidence level plus one, and degrees of freedom, and V_{mm} is the m^{th} diagonal element of the variance-covariance matrix estimated by:

$$\begin{aligned} V &= \hat{H}^{-1}\Lambda V_{\tilde{z}}\Lambda^T\hat{H}^{-1} \\ \hat{H} &= \frac{\partial^2\phi_{PE}(\theta)}{\partial\theta^2} \\ \Lambda &= \frac{\partial^2\phi_{PE}(\theta)}{\partial\tilde{z}_{ijk}\partial\theta} \\ V_{\tilde{z}} &= \mathrm{diag}(\sigma^2_{ijk}) \end{aligned} \tag{5.6}$$

where $\phi_{PE}(\theta), \tilde{z}_{ijk}$, and σ^2_{ijk} are all defined in the parameter estimation objective function shown in Equation (5.2). The confidence interval is a good indication of the statistical precision of the parameter estimate.

An important element of the maximum likelihood objective function and the confidence interval calculation is the variance model definition for the experimental measurements. A variance model can be obtained for the concentrations measured by HPLC using calibration curve data. The calibration curve for each component may consist of three or more data points for each concentration level. From the calibration data, the deviation of each measured concentration from that predicted by the regression model used in the calibration curve can be calculated. The variance σ^2_{pln} may be dependent on the measured value z_{pln}. In this work a linear variance model is used:

$$\sigma^2_{pln} = (\alpha z_{pln} + \beta)^2 \tag{5.7}$$

where α and β are regression coefficients fit to the standard deviations calculated at each concentration level in the calibration curve. It is assumed that the linear variance model explains the positive correlation between concentration and variance observed in the HPLC. And a linear variance model with positive slope ($\alpha > 0$) lends additional weight to those experimental data points with low concentrations in the parameter estimation, since the smaller the variance of a measurement the greater the corresponding multiplier in the objective function shown in Equation (5.2).

5.2.6 Step 6: Termination Criteria

An important aspect of the PC algorithm is that it has systematic termination criteria. The following two criteria must both be satisfied before termination of the PC algorithm occurs. The termination criteria are:

1. Purity constraints are satisfied in the SMB experiment

2. Optimal objective function value is converged

The first condition means that at the current iteration, the SMB experimental product purities should meet or exceed the minimum purity limits set by the operator. The

second condition means that the $k+1^{th}$ SMB optimal objective value, $\phi_{SMB}(u_{k+1})$, should not differ significantly from the previous optimal objective value, $\phi_{SMB}(u_k)$. The following condition should be satisfied:

$$\Delta\phi_{SMB}(u_k) = \left| \frac{\phi_{SMB}(u_{k-1}) - \phi_{SMB}(u_k)}{\phi_{SMB}(u_{k-1})} \right| \leq \epsilon_{tol} \tag{5.8}$$

where ϵ_{tol} is the tolerance set for the change in the objective function between successive SMB optimization problems. If both of the termination criteria are satisfied then the $k+1^{th}$ SMB experiment is deemed to be unnecessary. Thus, the PC algorithm is terminated and the current operating conditions in the k^{th} experiment, u_k, are considered optimal.

5.3 Experimental

5.3.1 SMB Equipment

The experiments were performed using a laboratory scale SMB unit (CSEP C190, Knauer, Berlin, Germany). A schematic of the SMB unit is shown in Figure 5.2. The unit includes four double-piston pumps (P1 through P4), two ultra-violet detectors at the extract and raffinate outlet streams, and a rotary valve with sixteen positions. The ports of the rotary valve are connected to each other by continuous channels. All unoccupied positions were filled with short capillary tubing. Four HPLC columns (YMC-Pack ODS-A, YMC Co., Ltd., Japan), labeled (C1 through C4) were used in a 4-zone configuration with one column in each zone (1-1-1-1). The HPLC column dimensions are 250 mm length and 10 mm inner diameter. They are packed with a C18 stationary phase for reverse phase chromatography with an average particle size of 20 μm.

5.3.2 SMB Experimental Technique

During an SMB experiment the extract and raffinate lines were placed in empty containers and the cumulative products were collected. The sampling technique was

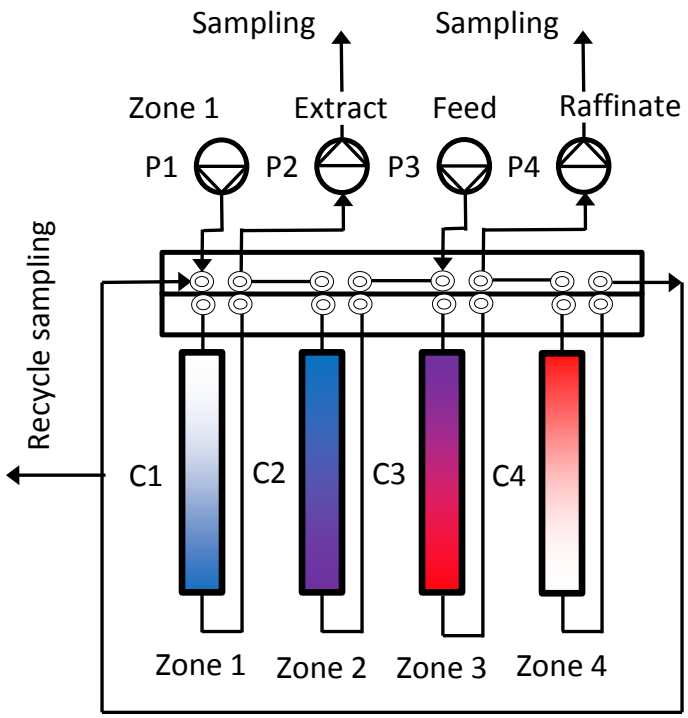

Figure 5.2: Schematic of SMB unit with four pumps (P1 through P4), and sampling points at the extract, raffinate and recycle lines. Four HPLC columns (C1 through C4) are in a 4-zone 1-1-1-1 configuration, connected to a rotary valve

described in Section 5.2.4. The composition of each sample was analyzed by a Shimadzu HPLC with an analytical C18 column (Daisopak, SP-120-10-ODS-BP, Daiso, Japan). The average SMB pump flow rates were measured periodically using a flow meter (Model 5025000, GJC Instruments Ltd.) at the extract outlet, raffinate outlet, and recycle line between Zone 4 and Zone 1 (referring to Figure 5.2) during each experiment to verify the operating conditions. The UV signals at the extract and raffinate points were monitored, but this data was not used in the parameter estimation because of poor baseline quality and the need for deconvolution of the signal [4, 35]. In addition, the average extract and raffinate product concentrations were sampled for an entire step after the first set of samples were taken and the product purities were checked against the target purity constraints.

5.3.3 Determination of Variance Model

Using the Shimadzu HPLC and the analytical C18 column, calibration curve data for uridine and guanosine were obtained. Uridine (CAS 58-96-8, EMD Biosciences) and guanosine (CAS 118-00-3, Spectrum Chemical Mfg. Corp.) were injected as one-to-one mixtures dissolved in 85% water 15% methanol. These data and the standard deviations at each concentration level for uridine and guanosine are shown in Figure 5.3.

A linear regression on the standard deviation data is performed to obtain the coefficients in the linear variance model shown in Equation (5.7). The coefficients $\alpha = 0.0045, \beta = 0.23$ are the average slope and intercept values for uridine and guanosine from the standard deviation data in Figure 5.3. It was observed that the variance has a slight positive correlation with concentration, and a linear variance model is the most simple way to quantify this relationship. An increase in σ^2_{pln} for both uridine and guaosine with increasing feed concentration was observed, but a notable difference in σ^2_{pln} for uridine and guanosine was not found at any concentration level. The observed variances are probably due to errors in the injection volume for repeated injections and perhaps also errors in baseline definition during the calculation of chromatogram peak areas.

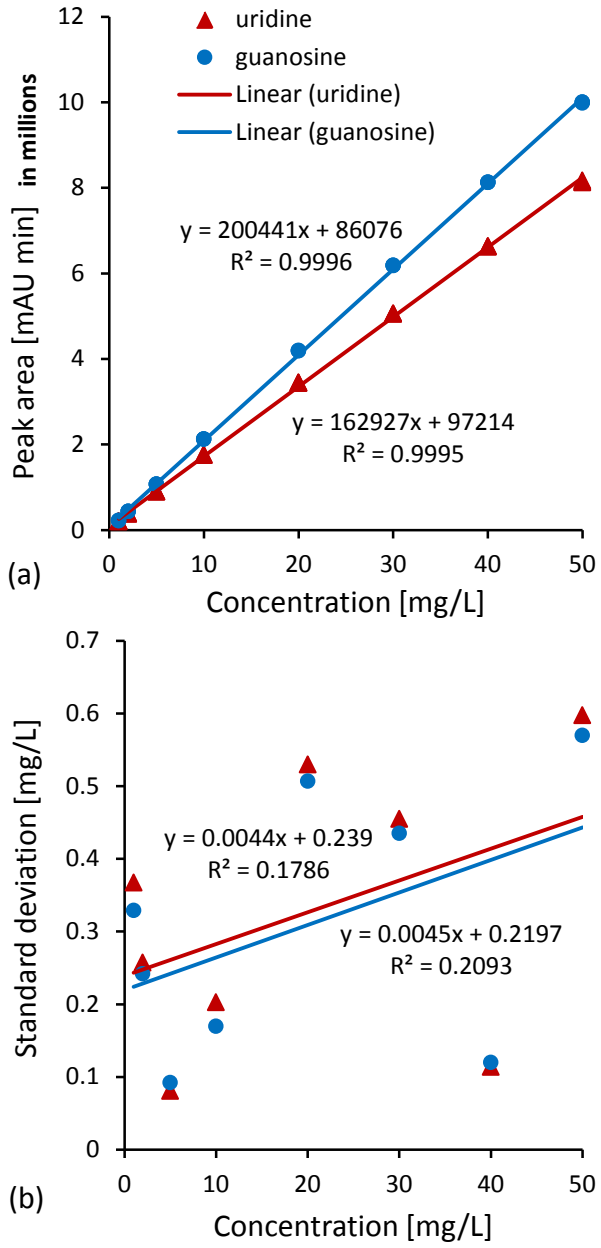

Figure 5.3: (a) Calibration curve using Shimadzu HPLC with three injections made at each concentration level. (b) Standard deviations of the measured concentration at each concentration level. Regression equations and coefficients are included

5.4 Results

5.4.1 Convergence of PC Algorithm

The PC algorithm is shown to converge efficiently in this section. This means that only a few changes of SMB operating conditions are needed to reach the purity constraints with optimal productivity.

The vector of initial parameter values, θ_0, was obtained by batch experiments on a single HPLC column, which was one out of the four columns used in the SMB unit. The desorbent used in this case study was 90% water 10% methanol. The feed was 39 mg L^{-1} uridine, called A, and 39 mg L^{-1} guanosine, called B, dissolved in the desorbent. The overall porosity of the column was found to be $\epsilon_b = 0.820$ by measuring the retention time of uracil, which is often used in reversed phase chromatography to measure the porosity. Nevertheless, there is a small increase in the retention of uracil when the amount of methanol in the desorbent is decreased, and the value of ϵ_b is therefore increased when the water content in the mobile phase is increased. The Henry's constants, H_i for components A and B were calculated by measuring the retention times of uridine and guanosine after a 30 μL pulse injection of the SMB feed mixture. The flow rate for these tests was 3.0 mL min^{-1} and the operating temperature was 40 °C. The mass transfer coefficients, k_i were calculated by measuring the peak width at half peak height for uridine and guanosine using the same pulse injection. This set of parameters was refined by parameter estimation after each SMB experiment. The initial parameter set and each parameter estimation solution are shown in Table 5.1.

Table 5.1: Refinement of θ_k by parameter estimation

Parameter	Initial, θ_0	Refined, θ_1	Refined, θ_2	Refined, θ_3
H_A	0.846	1.00	0.983	0.971
H_B	2.75	2.82	2.84	2.80
k_A [min^{-1}]	103	52	90	52
k_B [min^{-1}]	161	81	58	81

The SMB optimization problem, described in Section 3.2.1 was solved in the each iteration using θ_k with the purity constraints $\text{Purity}_A^{raf} \geq 96\%$ and $\text{Purity}_B^{ext} \geq 96\%$, and $F_{max} = 10$ mL min^{-1}. The objective function convergence tolerance, ϵ_{tol} in Equation (5.8) was set to 0.05. The vector of optimal operating conditions, u_k, is predicted to satisfy the purity constraints with maximum feed throughput. These operating conditions were implemented in SMB experiment k until the termination criteria were met. The optimal operating conditions are shown in Table 5.2 together with the product purities obtained in experiment k and the normalized change in throughput from Equation (5.8). The m-values are the liquid-to-solid flow rate ratios defined by Equation (3.14). In all optimal solutions the Zone 1 flow rate reached the upper bound of 10 mL min^{-1}. This happens so that higher concentrations of components can be sufficiently desorbed when the feed throughput is maximized.

Table 5.2: Updates of u_k and termination criteria

Control variable	u_0	u_1	u_2^*	u_3
Step time, t_{step} [min]	2.624	2.677	2.713	2.700
Zone 1 flow rate ratio, m_1	2.870	3.019	3.120	2.997
Zone 2 flow rate ratio, m_2	0.7716	0.9456	0.9156	0.9121
Zone 3 flow rate ratio, m_3	2.808	2.825	2.787	2.799
Zone 4 flow rate ratio, m_4	0.6715	0.7954	0.06578	0.7705
Termination criteria	$k = 1$	$k = 2$	$k = 3$	-
Purity_A^{raf} [%]	92.8	94.7	97.8	-
Purity_B^{ext} [%]	89.6	98.3	96.2	-
$\Delta\phi_{SMB}(u_k)$	0.095	0.017	0.039	-

In this case study the PC algorithm required only three iterations for the termination criteria to be met. This corresponds to only two changes of the SMB operating conditions from the initial guess. It is clear from Table 5.2 that the product purity constraints were violated in SMB experiments at $k = 1$ and $k = 2$. The termination criteria were satisfied at $k = 3$ because the product purities in SMB experiment 3 were both $\geq 96\%$ and $\Delta\phi_{SMB}(u_3) \leq 0.05$. Since the termination criteria were satisfied at $k = 3$, the optimal operating conditions u_3 were not used, and u_2^* was considered

optimal.

The SMB experimental data and model predictions for $k = 1$ through $k = 3$ are displayed together in Figure 5.4. From Figure 5.4 it is obvious that the fitting of the experimental data points is good for θ_3, which is the refined parameter vector from the parameter estimation solution at $k = 3$. The most pronounced improvement seen in the figure is the fitting of the component A profiles and the recycle line data.

The simulated concentration profiles have discontinuities at those time points where the next operating conditions are initialized, as seen in Figure 5.4. This discontinuity is also observed in the experiment by using an empty container to collect the extract and raffinate products at the moment the operating conditions are switched. For the recycle line a different sampling strategy was used. The recycle line was not collected in a cumulative way during the experiment. Instead it was sampled once by collecting the average concentration over a step after the extract and raffinate sampling was completed. This was done assuming that after a sufficient number of cycles the cumulative concentration measurement equals the average concentration measurement over a step. This single sample for the recycle line was included in the parameter estimation.

Compared to the change in the Henry's constants there was a significant change in the values of the mass transfer coefficients from θ_0 to θ_3. This is because the mass transfer coefficients are less sensitive parameters in the SMB model, and their confidence intervals are large, as discussed later. From u_0 to u_2^*, the operating conditions were varied around the optimal operating conditions, and yet the parameter estimates for θ_1 and θ_3 remained within reasonable ranges.

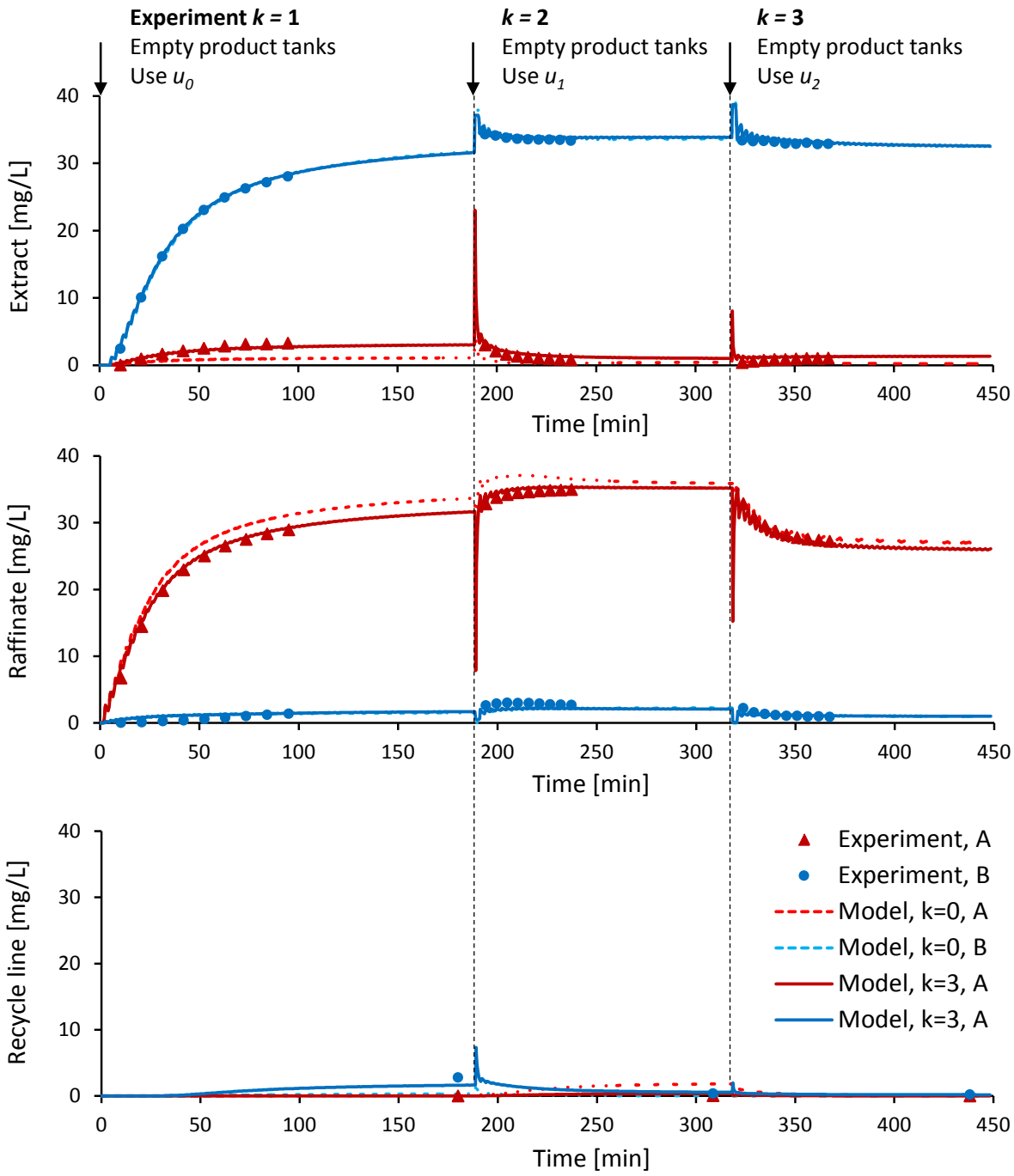

Figure 5.4: Cumulative concentration data for extract, raffinate and recycle lines from $k = 1$ to $k = 3$ and the parameter estimation fitting. The dotted lines are the simulated profiles using θ_0 and the solid lines are the simulated profiles using θ_3. The operating conditions were switched at the indicated time points and the product containers were emptied to restart the cumulative concentration profiles

The optimal operating conditions for each iteration of the PC algorithm are shown in Figure 5.5 in the m_2-m_3 and m_4-m_1 planes to illustrate how the optimal operating conditions evolved as the parameters were refined at each iteration of the PC algorithm. The boundaries of the triangle region are the values of H_A and H_B in θ_3, and are derived from the triangle theory discussed in Section 1.2.2. In general, the changes in operating conditions for each experiment illustrate the move toward improved product purities from the initial operating condition with poorly estimated parameters. The change from u_1 to u_2 in the m_2-m_3 plane was because the extract product was too pure in $k = 2$, and the raffinate product needed to be further purified. The m_4-m_1 values of a given optimal solution are usually not unique since desorbent consumption was not considered in the SMB optimization objective function. In u_3 the value of m_4 went back to around the same value as in u_1.

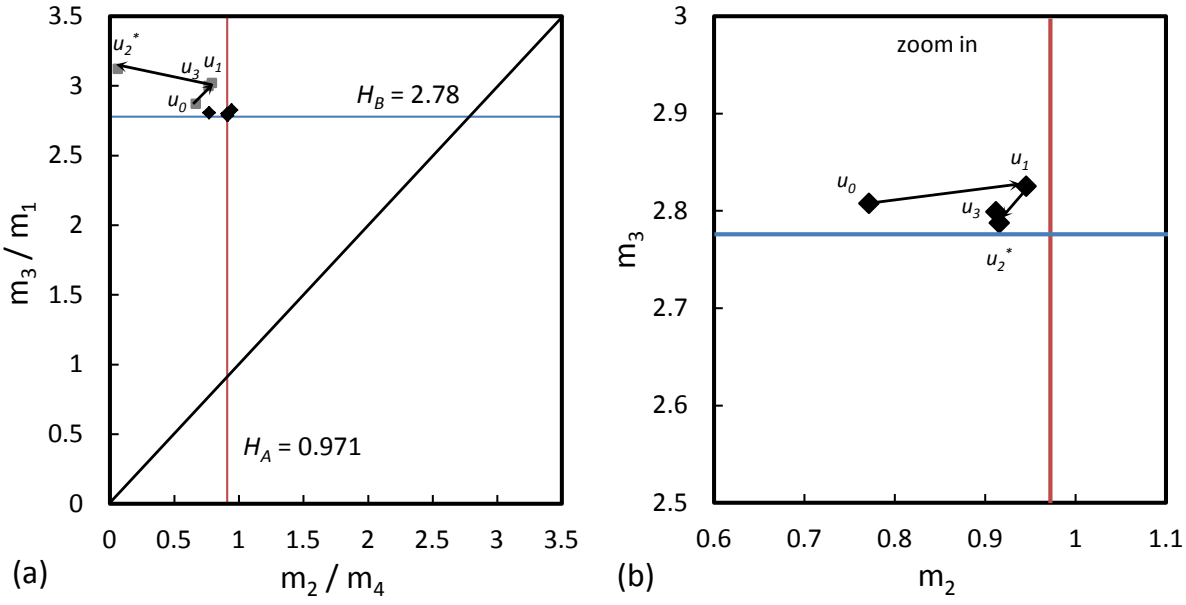

Figure 5.5: (a) Operating conditions u_0 through u_3 labeled on the m_2-m_3 (diamonds) and m_4-m_1 (squares) planes with H_A^3 and H_B^3 as triangle region boundaries. (b) Zoom in on m_2-m_3 values for u_0 through u_3. Note that u_3 was not implemented because the algorithm was terminated at the optimal u_2^*

In Figure 5.6 the improvement of model parameters from $k = 0$ to $k = 1$ is shown. The most pronounced improvement in the fitting of the experimental data is in the component A profiles. Model mismatch is observed in the component A profiles and recycle line data using θ_0, hence the need for the correction step. The optimization constraints on product purities were both 96%, yet the measured purities were 89.6% for extract and 92.9% for raffinate. This mismatch is due to the initial estimation of the model parameters from batch experiments and the existence of dead volumes in the SMB unit. The poor product purities were corrected in the next SMB experiment at $k = 1$ as shown in Table 5.2.

It should be noted from Figure 5.6 that the simulated profiles exhibit oscillations at the beginning of the experiment. This is not due to numerical instability of the solver, but is a result of product concentration profiles within a step. The product concentrations that enter the extract and raffinate tanks have decreasing and increasing patterns respectively during a step. These patterns are observed distinctly at the beginning of this experiment where the cumulative amounts of the components in the tanks are still small.

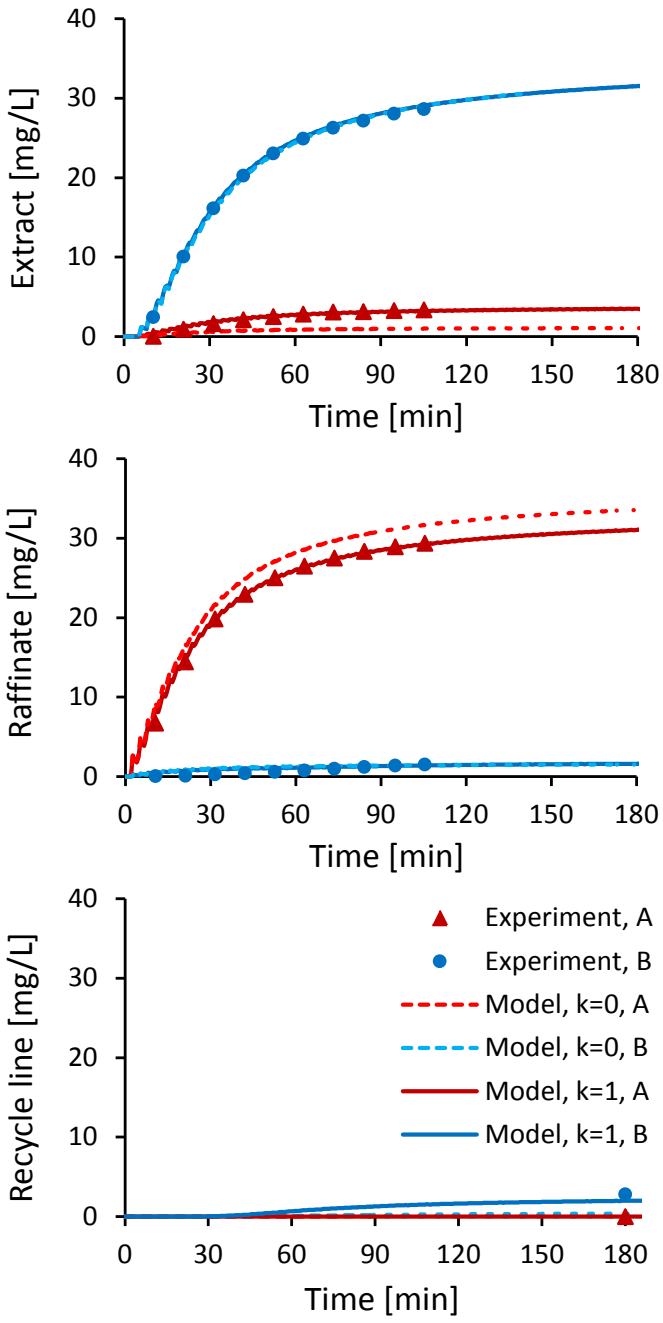

Figure 5.6: Cumulative concentration data for extract, raffinate, and recycle lines and the parameter estimation fitting. The dotted lines are model prediction using θ_0 and the solid lines are model prediction using θ_1

The parameter estimation problem given by Equation (5.3) was solved as described in Section 5.2.5 and the refined model parameters are shown in Table 5.1. The overall column porosity was kept constant at the initial measured value of 0.820. The following lower and upper bounds were employed in the parameter estimation problem:

$$2/3H_{i,0} \leq H_i \leq 3/2H_{i,0}$$

where $H_{i,0}$ is the value of the Henry's constant for component i determined by batch experiments, and

$$\epsilon_k \leq k_i \leq 1/\epsilon_k$$

where ϵ_k is a small positive constant. This constant was selected to be 0.01 based on the results of some sensitivity analysis of the mass transfer coefficients in the SMB model for this system. It was observed that if the value of k_i was too large then the SMB model produced concentration profiles that were nearly identical and the sensitivity of k_i was lost due to numerical inaccuracy. It is confirmed that these bounds are inactive at the optimal solution in each iteration. It was also noted by Dunnebier and Klatt [22] that the kinetic model, which uses only k_i as a lumped parameter to describe band broadening effects, can exhibit some numerical inaccuracy for high efficiency columns. They concluded that the general rate model is more appropriate for numerical simulation of chromatographic columns with a large value of k_i. Yet the general rate model is undesirable because of correlations between the four additional transport parameters that are included. It may be too difficult to reliably estimate all the parameters simultaneously. For the purposes of this work, the kinetic model with only one transport parameter per component has sufficient accuracy.

Some important observations of the changes in parameter values from θ_0 to θ_1 should be noted. As expected, the Henry's constants in θ_1 were increased from θ_0 by the parameter estimation due to the effect of dead volumes in the SMB unit. This

increase is caused by an increase in the apparent retention times of the components in each column because they are further held-up in the dead volumes. In addition, the startup dynamics of the SMB process expose the effect of mass transfer in the SMB model. For example, if mass transfer is fast, then the SMB system reaches the CSS condition sooner. The initial mass transfer coefficients, which were overestimated in the batch experiment, were corrected by parameter estimation. From Figure 5.6, it is seen that k_B was decreased to fit the guanosine contamination in the recycle line. Likewise, k_A was decreased to fit the uridine contamination in the extract product.

5.4.2 Confidence Intervals of Parameter Estimates

To confirm the reliability of the optimal parameter set, the confidence intervals at 95% statistical confidence were analyzed. In Figure 5.7 the computed confidence intervals for the Henry's constants and mass transfer coefficients are shown for each iteration of parameter estimation. These statistics were calculated by the parameter estimation routine in gPROMS, and these values depend on the specification of the variance model for experimental measurements discussed in Section 5.2.5 on parameter estimation.

In general, the confidence intervals decreased from one parameter estimation result to the next. The values of the confidence intervals for H_A and H_B were tight relative to the parameter values of 0.971 and 2.80 respectively and slight improvement was observed. Compared to the Henry's constants, the values of the confidence intervals for k_A and k_B were not tight relative to the parameter values of 52 and 81 min^{-1} respectively. Yet the confidence intervals for k_A and k_B improved significantly from $k = 1$ to $k = 3$. The larger confidence intervals for the mass transfer coefficients occur because of significant variance in the measurements of concentration data, various flowrates in the four SMB zones, and unknown mixing behaviors in the column connections and the main rotary valve. The decrease in the confidence intervals for

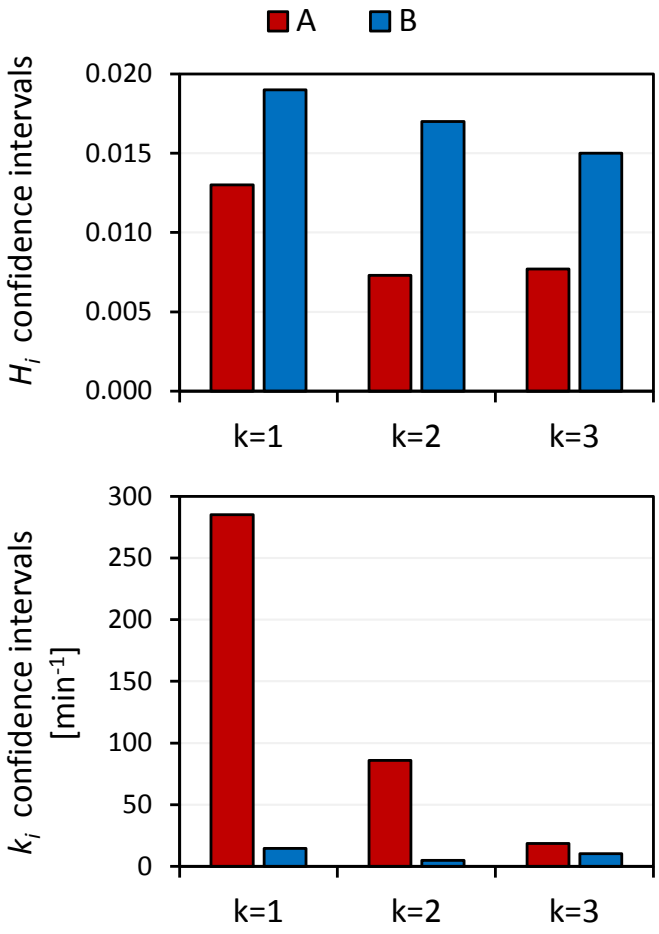

Figure 5.7: Henry's constants and mass transfer coefficients 95% confidence intervals for each parameter estimation result from θ_1 through θ_3

k_i is an indication that the final parameter values are more reliable than the initial guess, because these parameters more specifically predict all three SMB experimental results.

5.4.3 Robustness of PC Algorithm

The robustness of the PC algorithm is demonstrated for a poor initial guess of model parameters. The system for this case study was 50 mg L^{-1} uridine and 50 mg L^{-1} guanosine dissolved in 95% water 5% methanol. An HPLC column was used to perform batch experiments which had significantly different separation performance

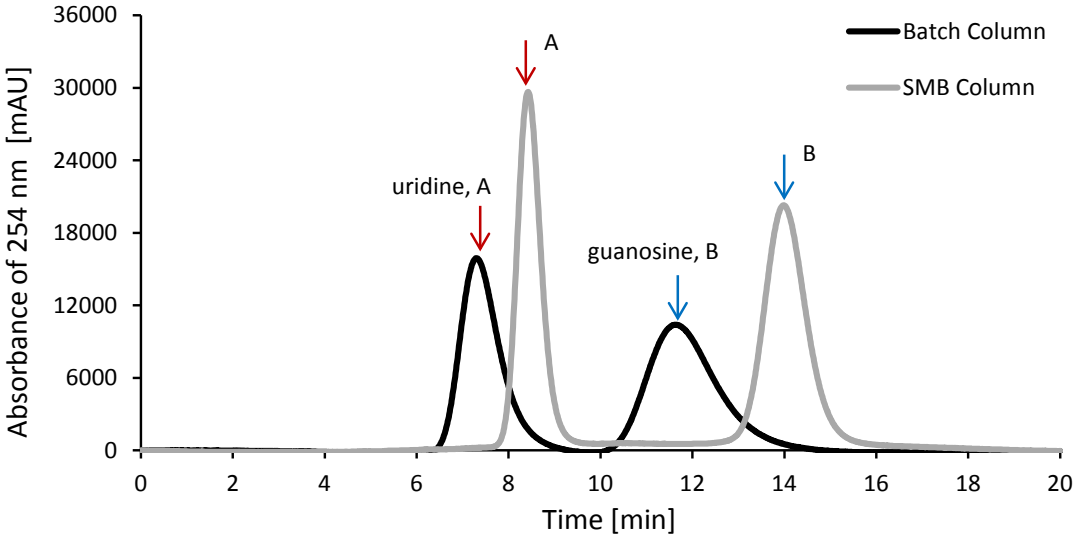

Figure 5.8: Comparison of chromatograms for column used in batch experiments and an SMB column. $F = 3$ mL min^{-1}, $c_{A,feed} = c_{B,feed} = 50$ mg L^{-1}, injection volume 30 μL, temperature 40 °C

from the SMB columns used in the experiment. This case study can be considered as a simulation of scale-up where the column packing is inconsistent in a large-scale system, or the lot-to-lot reproducibility of adsorbent is poor. In Figure 5.8 there is a comparison between the performance of both the "Batch Column" and an "SMB Column". The chromatograms are the result of 30 μL injections of the feed mixture of uridine and guanosine on the columns with different performance. The flow rate for these tests was 3.0 mL min^{-1} and the operating temperature was 40 °C.

The overall porosity of the columns was calculated to be $\epsilon = 0.806$ by measuring the retention time of uracil. The vector of initial model parameters, θ_0, was calculated by moment analysis using the "Batch Column" chromatogram. The same model parameters were also calculated by moment analysis using the "SMB Column" chromatogram for comparison. The vector of model parameters obtained from the "SMB Column" chromatogram is θ_{ref}. The initial parameter set was refined by parameter estimation after an SMB experiment to obtain θ_1. The initial parameter set, refined parameters, and reference parameters are shown in Table 5.3. Note the significant

Table 5.3: Refinement of θ_0 by parameter estimation and comparison with θ_{ref}

Parameter	Initial, θ_0	Refined, θ_1	Reference, θ_{ref}
H_A	1.41	2.91	2.11
H_B	4.96	7.17	6.63
k_A [min^{-1}]	20.5	58.1	76.2
k_B [min^{-1}]	23.8	3.80	77.3

change in the Henry's constants from θ_0 to θ_1; over 100% in H_A and 44% in H_B. Also, the values of the Henry's constants in θ_1 are approaching those in θ_{ref}, but they are increased because of the additional hold-up in the SMB dead volumes.

The SMB experimental data and parameter estimation fitting are displayed in Figure 5.9. There was significant model mismatch observed in the prediction using θ_0 in both component A and B profiles in all the sampling lines. The expected purities from the model-based optimization were both 99%, but the measured values were 62.0% in extract and 75.6% in raffinate.

The parameter estimation and optimization, as described before, were performed once in this case study to show that the model parameters could be refined to fit the experimental data with reasonable parameter values, and that the operating conditions could be updated to move in a direction of improved product purities. The optimal operating conditions were calculated for θ_0 and θ_1 and the results are shown together with SMB experimental purities in Table 5.4. The change in operating conditions is shown in Figure 5.10 to illustrate the large step in a single iteration of the PC algorithm. In this single step the product purities were each increased to 99.9%, and the throughput was reduced by about 50%. This means that the PC algorithm takes aggressive steps to enable efficient convergence if the initial model parameter estimates are poor.

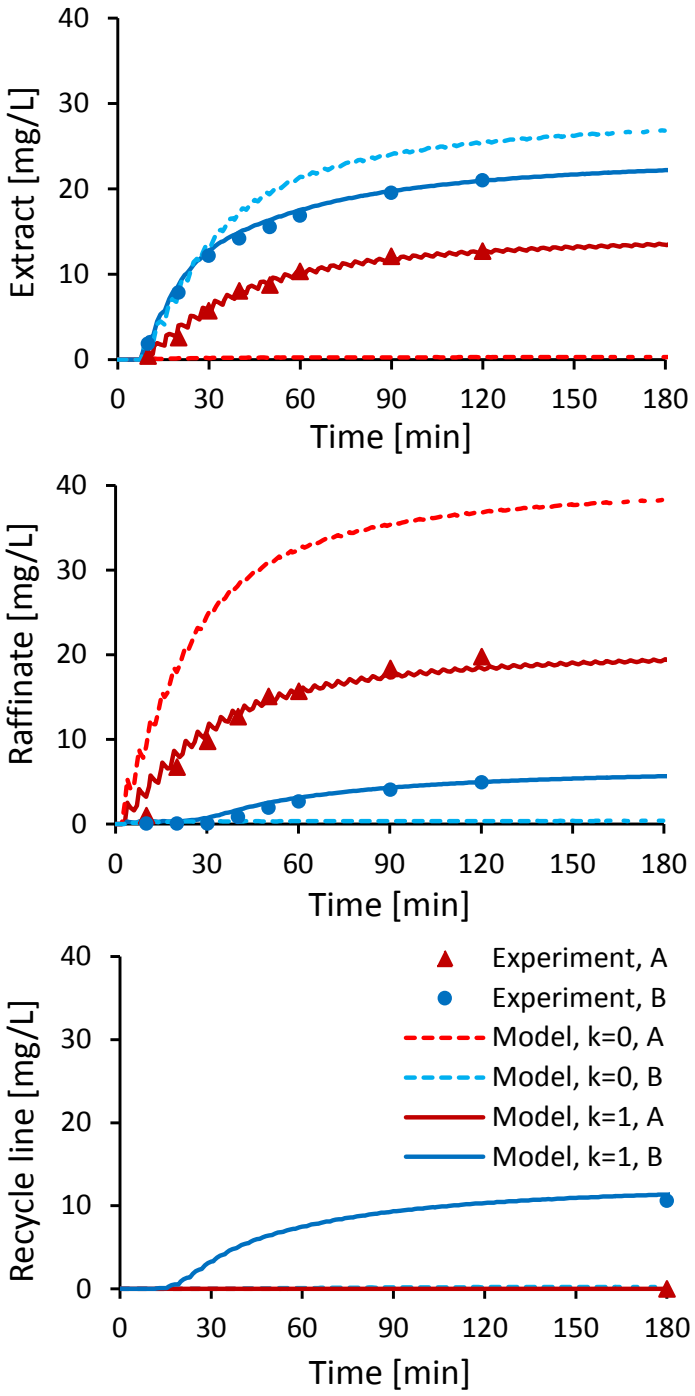

Figure 5.9: Cumulative concentration data for extract, raffinate, and recycle lines and parameter estimation fitting. Dotted lines are model prediction using θ_0 and solid lines are model prediction using θ_1

Table 5.4: Update of u_0 after parameter estimation and experimental purities

Control variable	u_0	u_1
t_{step} [min]	3.843	5.952
m_1	5.930	11.46
m_2	1.636	3.073
m_3	4.228	5.022
m_4	0.9993	2.634
Product purities	$k = 1$	$k = 2$
Purity_A^{raf} [%]	75.6	99.9
Purity_B^{ext} [%]	62.0	99.9

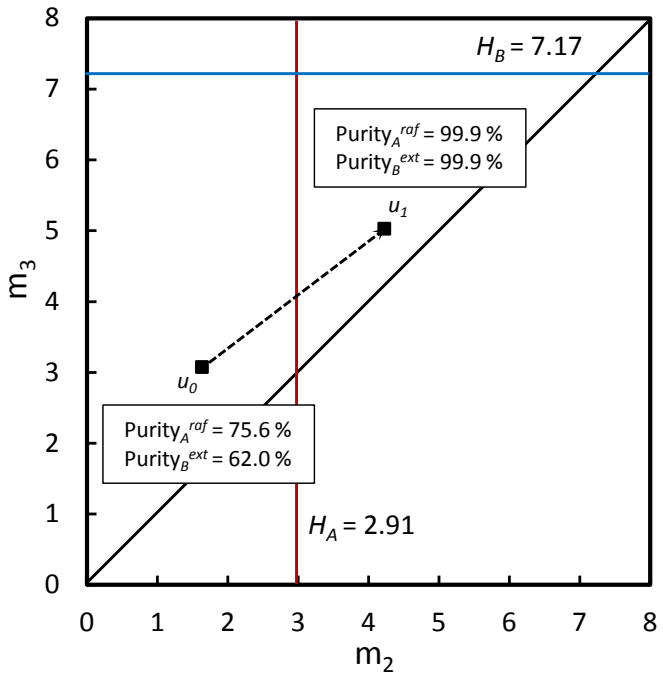

Figure 5.10: Optimal operating conditions u_0 and u_1 on the m^2-m^3 plane with H_A^1 and H_B^1 as boundaries of the triangle region. The experimental purities at each operating condition are shown

5.5 Conclusion

The prediction-correction algorithm for SMB process development has been proposed and tested. It was found to be an efficient algorithm in numerous laboratory experiments with a linear isotherm system, and in the first case study convergence was achieved in only two switches of the operating conditions. In the second case study the product purities were improved by about 30% in a single step when the initial model parameter estimates were poor. The PC algorithm proceeds in an automatic and sequential manner until it terminates itself so that an SMB expert is not required to manually tune the SMB operating conditions. It should also be noted that this algorithm is designed to function with any choice of the isotherm model. This work demonstrates the PC algorithm with a linear isotherm. The parameter estimation technique is demonstrated for the determination of nonlinear isotherm parameters in the next chapter.

CHAPTER 6

EXTENSION OF PC METHOD FOR SIMULTANEOUS MODELING AND OPTIMIZATION OF NONLINEAR SMB SEPARATIONS

6.1 Motivation

In this chapter the prediction-correction (PC) method for SMB process development and optimization is extended by the inclusion of a model-selection step for nonlinear systems. The efficiency and robustness of the proposed algorithm is demonstrated using experiments with a nonlinear isotherm system. The goal of this work is to build on the results of the previous chapter by showing that startup SMB experimental data can be used to simultaneously model and optimize nonlinear systems.[1]

In Chapter 5 the usefulness of SMB for binary separations, and the typical steps of process development, have already been discussed. Yet operating SMB in a regime where nonlinear adsorption isotherms are operative is an even more challenging task, as discussed by [36, 58]. It is challenging to determine parameter values for the mathematical model, and to solve the SMB optimization problem. This difficulty is compounded for the SMB operator if the sample volume available for lab and mini-plant tests is small or there is only a limited time for process development. Therefore, SMB is frequently applied using operating conditions that are known to be sub-optimal in terms of productivity and solvent consumption, and in some cases the feed concentration is reduced to avoid operation in the nonlinear adsorption regime.

The typical process development scheme for a new separation problem relies on

[1] This chapter is submitted to Journal of Chromatography A, 2012.

modeling with results from batch experiments, cyclic steady state SMB experiments, and manual tuning. A new separation problem poses many challenges for the process designer including the estimation of reliable SMB model parameters for each component of the mixture. Once model parameters are determined, usually by batch experiments, operating conditions are selected based on design criteria that approximate SMB dynamics [58, 64, 74]. By observing the SMB performance at CSS, the operating conditions are tuned manually until process specifications are met. Sometimes mini-plant experiments and computer simulation of a process model are used to aid in the design [22, 26, 55].

Perhaps the most important aspect of SMB process development is the selection of a process model, including adsorption isotherm, and the determination of model parameters. This task is crucial for nonlinear SMB systems where the performance of the process is sensitive to the increased concentrations in the unit. Reliable estimates of isotherm model parameters are needed in order to predict performance. A review of batch experiments for modeling was given in Section 5.1. There is some work reported where researchers used design of experiments to reduce the effort required to obtain reliable model parameters for nonlinear SMB systems, although they do not consider isotherm model selection [32].

In most case studies of nonlinear SMB process development in the literature, the adsorption isotherms of each component are characterized by batch experiments and then an isotherm model is assumed and used to fit the data. For example, in Heuer *et al.* [39] a careful perturbation analysis is used to estimate modified competitive Langmuir isotherm parameters for the design of enantiomer separation by SMB. Even though the estimated parameters were reliable for single-column tests, there was still significant model mismatch in the prediction of product concentrations and purity values. Indeed, there is no guarantee that the SMB modeling based on results of batch experiments will accurately predict SMB performance. In Grosfils *et al.* [31]

a less-reliable inverse method is used to determine competitive Langmuir isotherm parameters from two pulse injections. Using an SMB model with careful measurements of dead volumes in a real SMB plant, the process simulation was compared with plant data via UV detector signals. The inverse method has been shown to be a reliable parameter estimation technique in predicting batch experimental results for enantiomer separations [27], and is useful for isotherm model selection; however, the model may not be reliable for SMB optimization where the concentrations can be significantly higher.

Some other work has been done to attempt parameter estimation using SMB experimental data. In Araújo *et al.* [10] a hybrid inverse method is used to determine competitive Langmuir isotherm parameters for an SMB model using numerous batch experiments and a periodic state represented on a single-column set-up. The model parameters are refined by parameter estimation using the single-column cyclic steady state data, but these are only an approximation of real SMB dynamics and no optimization of the SMB process is performed.

There are other researchers who have worked on on-line optimizing control of the SMB process to correct operating conditions in the presence of disturbances. This work has been discussed previously in Section 5.1. In Erdem *et al.* [25] and Abel *et al.* [4], the claim is that the feedback controller, which is based on a simplified SMB model with linear isotherm, can be used to optimize even nonlinear SMB systems. Their methodology assumes that a reliable set of process model parameters and optimal operating conditions for the SMB are known *a priori*. They do not consider updating the SMB model parameters using product concentration data. The on-line control strategy presented by these groups, especially in "cycle-to-cycle" control [33, 35] uses a similar sampling strategy to the one used in the PC method. However, the application of the information is for control, not process development. In Grossmann *et al.* [33] they use a generalized Langmuir isotherm in the SMB model

for some application in nonlinear SMB systems. Yet fast controller actions and stability may not be guaranteed if there is significant model-mismatch when a set-point is defined for the controller. The controller has also been demonstrated to stabilize the SMB unit after disturbances in some nonlinear systems experimentally, yet the process development needed to be carried out before the controller could be implemented to maintain the desired oepration [34, 54].

The PC algorithm is designed for optimal SMB process development. It makes use of a surrogate model (see Biegler *et al.* [14]), infrequent sampling of SMB outlet streams, parameter estimation, model selection, and dynamic optimization to reduce the time required to obtain reliable model parameters and optimize the SMB process in a systematic manner. The model selection step is added from the previous PC algorithm presented in Chapter 5, and it is now applied to a nonlinear isotherm system.

This chapter is organized as follows: The detailed steps of the extended PC algorithm are discussed in Section 6.2, experimental equipment is discussed in Section 6.3, and case studies with a nonlinear isotherm system are presented in Section 6.4 to show how the model selection works, that the algorithm converges efficiently and that the algorithm is robust to poor initial guess of isotherm model.

6.2 Methodology

6.2.1 Extended Prediction-Correction Algorithm

The extended PC algorithm for nonlinear SMB process development is shown in Figure 6.1. This is an iterative scheme, following the same basic steps presented in Section 5.2, where the isotherm model may be selected fitting SMB experimental data, and the optimal operating conditions are predicted by re-optimizing the SMB model. During process development for a new separation problem the adsorption isotherm is unknown. Instead of spending valuable time and resources performing

batch experiments to explore the adsorption isotherm for each component, a set of SMB startup data is used to perform model selection and parameter estimation. This method is similar to inverse modeling of competitive frontal analysis, only SMB data is used to correct the SMB operation on-line by parameter estimation followed by model-based optimization.

This procedure assumes that a new mixture is to be resolved by SMB, and a reliable isotherm model and SMB model parameters are not yet known. The adsorbent type, SMB column configuration, desorbent and feed compositions, and other operating parameters such as temperature should be selected *a priori*.

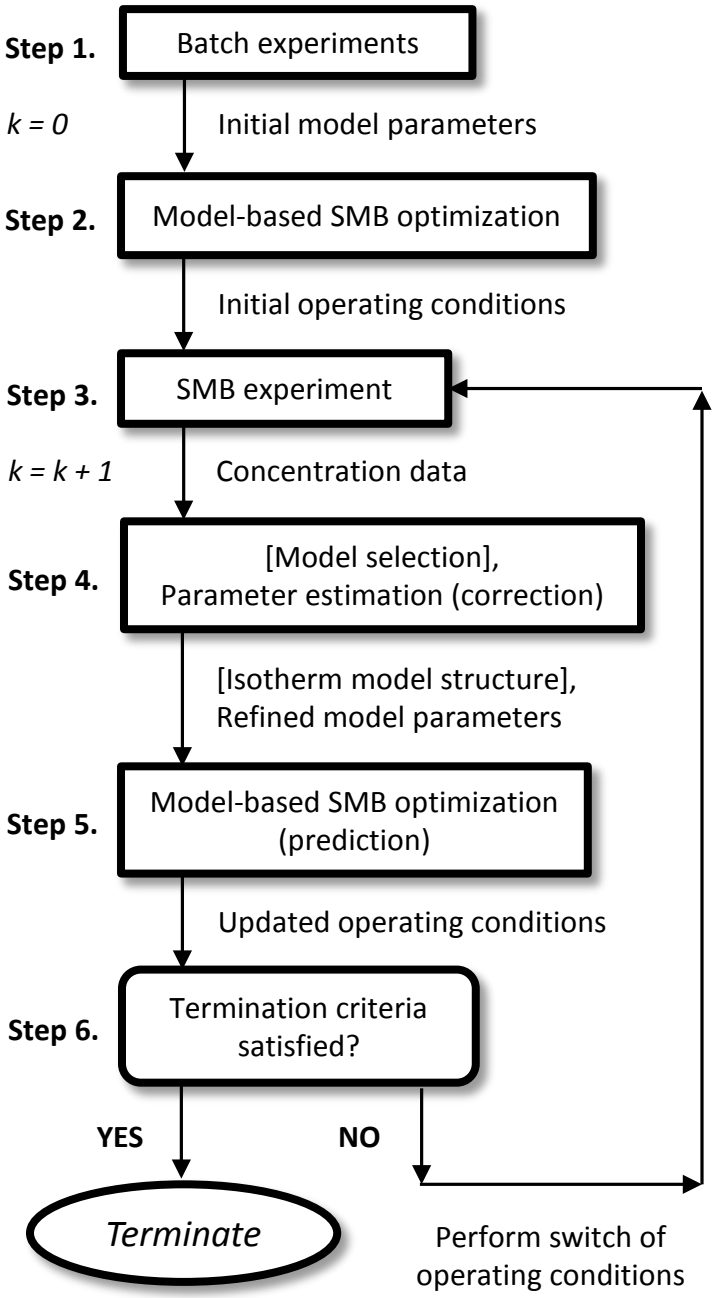

Figure 6.1: Extended prediction-correction (PC) algorithm for SMB process development with model selection step

The only difference in the extended PC algorithm from that presented in Figure 5.1 is the model selection step following the SMB experiment. By adding model selection in Step 4, it is possible to optimize the SMB with a given isotherm model and then discover if a different isotherm model can significantly improve prediction of real SMB performance. This is a useful step if the initial guess of isotherm model is inadequate to describe the real system. For example, it may be assumed that the system is linear at first and then a nonlinear isotherm model can be selected, following systematic criteria, which fits the SMB experimental data more reliably.

Within the individual steps of the PC algorithm, most of the details of the procedure are the same as those presented in Section 5.2. Only the differences for nonlinear isotherm selection will be highlighted in the next sections, namely the batch experiments of Step 1, and the model selection of Step 4. For details on SMB optimization, SMB experiments, parameter estimation, and termination criteria, see Section 5.2. In addition, a different nonlinear programming solver was used for SMB optimization in this work, which will be discussed later.

6.2.2 Step 1: Batch Experiments

Pulse tests are performed to measure the overall porosity of the packed bed in a column and determine initial adsorption isotherm and kinetic parameters for each component in the feed mixture. The following pulse tests should be done:

1. Small-volume pulse injection of tracer compound to measure the overall porosity of the column.

2. Small-volume pulse injection of feed mixture (low concentration) to estimate the Henry's constants and mass transfer coefficients by retention times and the number of theoretical plates (NTP) for each component.

3. Increased-volume pulse injection of feed mixture (increased concentration) for parameter estimation by the inverse method.

The main difference between the this procedure and that described in Section 5.2.2 is the pulse test chromatograms can be used to estimate initial isotherm parameters for any isotherm model using the inverse method [27, 32, 36]. The chromatographic column model equations presented in Section 3.1 can be used to numerically simulate the pulse tests. The simulation can be performed with any isotherm model, given in general by Equation (3.3). If a linear isotherm is used, then the initial guess of Henry's constants can be obtained from a single pulse test at low concentration. This will save time and resources during Step 1 of the PC algorithm, but may lead to poor initial operating conditions for the SMB if the real system indeed behaves nonlinearly. For other isotherm models, such as the single-component Langmuir isotherm, additional information is required about the saturation capacity of the column.

In this work, a single-column model is written in gPROMS using Equations (3.1) - (3.3). The chromatograms obtained from pulse tests are used to solve a least-squares error minimization problem in gPROMS for parameter estimation. The methods involved in this calculation are the same as those described earlier in Section 5.2.5.

6.2.3 Step 4: Model Selection and Parameter Estimation (Correction Step)

After the initial SMB experiment the isotherm model selection step takes place. The startup SMB experiment is like a loading test, because initially the concentrations are small in the unit, and they gradually build up to the CSS concentration profiles. Observing this increase in the concentration profiles gives opportunity to measure nonlinear isotherm parameters if necessary.

The isotherm model selection may be done systematically for any number of isotherm models. There is a trade-off in model selection between the number of independent model parameters and the maximum likelihood estimation. The Akaike information criteria may be used to select from multiple models minimizing a factor

that takes into account both of these objectives [8]. A simplified model selection procedure is used by comparing the number of parameters and the parameter estimation solutions in Equation (5.3) given in Section 5.2.5 for three isotherm models. The models are ranked based on the number of parameters, and their optimal objective function values are compared. The selection is based on the following prioritization and comparison:

1. The models are ranked in increasing order depending on the total number of parameters and the number of parameters in the isotherm equation for each component. For example, the linear isotherm, Equation (1.2), has first priority, the single-component Langmuir isotherm, Equation (3.4), has second, and the competitive Langmuir isotherm, Equation (3.5) has third.

2. The optimal objective function values are compared for each pair of isotherm models, and the model with lesser priority is only selected if there is a sufficient decrease in the objective function value. The following comparison is made for each pair of isotherm models:

$$\Delta\phi_{PE}(r,s) = \left|\frac{\phi^r_{PE} - \phi^s_{PE}}{\phi^r_{PE}}\right| \leq \epsilon_{MS}, \quad r = 1, 2, \ldots, n_{mod} - 1 \qquad (6.1)$$
$$s = 2, 3, \ldots, n_{mod}, \quad s > r$$

   where ϕ^r_{PE} is the optimal objective function value for model r, ϵ_{MS} is the tolerance set on model selection, and n_{mod} is the number of isotherm models. If the condition specified by Equation (6.1) is satisfied, then model s is selected instead of model r.

The value of ϵ_{MS} is chosen to be a positive value less than 1.0, such as 0.5. This systematic approach will ensure that the selected model will simultaneously satisfy a small number of parameters and have sufficient fitting of the experimental data.

The computation time of the parameter estimation problem was found to scale with the number of SMB experiments that are simulated, and the computation is

longer if there are more parameters in the isotherm model to be determined. For model selection, multiple parameter estimation problems can be solved in parallel using the same set of SMB experimental data. This is one motivation for selecting a model with less parameters, such as the single-component Langmuir isotherm. If competitive adsorption can be neglected in the isotherm model, then the PDEs of the SMB model become decoupled and the solution of the discretized ODE system is more efficient.

6.2.4 Numerical Solution of SMB Optimization

In this work on the PC algorithm for nonlinear SMB systems the simultaneous, full-discretization method, described in Section 3.2.2, is used. This method requires that the PDE system given by Equations (3.1) - (3.3) in Section 3.1 be fully discretized in time and space yielding a large-scale optimization problem with algebraic constraints. Therefore the size of the problem scales with the number of columns in the SMB model and the number of discretization points in time and the axis of the columns, and can have a quite large number of variables, around 10^5. The SMB model was written and discretized in AMPL, and the IPOPT solver is used, which is based on an interior point algorithm [15, 28]. The time domain was discretized using 3^{rd}-order orthogonal collocation which works to reduce the overall number of algebraic constraints in the problem formulation. This solver was also systematically compared with SRQPD in gPROMS for SMB optimization by [46], and it was found that AMPL with the IPOPT solver is more efficient. This result is also confirmed by the present work.

There exists a trade-off between computational complexity and model accuracy. The isotherm selection step is important for exploiting this fact. For example, if a linear isotherm is assumed in Step 1 of the PC algorithm, then the initial SMB optimization is rather fast and it is easier to find a good initial guess for optimization using the triangle theory for linear systems. Yet, if the linear model is assumed

throughout the PC algorithm, then there may be an increased number of iterations required to converge on the optimal operating conditions. On the other hand, if a nonlinear isotherm is assumed at first, then it requires more effort with nonlinear triangle theory to find a good initial guess of operating conditions, and the computational time for optimization and parameter estimation is greater. Yet, if the model fits well the experimental data, then there may be a reduced number of iterations in the PC algorithm. This highlights a key difference between the single-component Langmuir and competitive Langmuir isotherm models: they have the same number of model parameters overall, yet the competitive Langmuir isotherm is more computationally complex in the SMB optimization problem due to coupling of the PDEs. In the following case studies the single-component Langmuir isotherm is considered for model selection, even though it may not be a physically realistic model for describing the real adsorption phenomena for the mixture in a SMB unit. The single-component Langmuir model may be useful to reduce computational effort and may be sufficient to optimize the operation. This is the concept motivating the use of a surrogate model [14].

6.3 Experimental

6.3.1 SMB Equipment and Experimental Technique

The experimental equipment used in this work is the same as that described in Section 5.3.1 in the previous chapter. Although, in some case studies eight C18 columns were used in the SMB unit instead of four. In addition, the experimental technique used in this work is the same as that described in Section 5.3.2. The samples were analyzed by the same HPLC system described in the previous chapter.

6.3.2 Determination of Variance Model

Using the Shimadzu HPLC and the analytical C18 column, calibration curve data for cyclopentanone and cyclohexanone were obtained. Cyclopentanone (Alfa Aesar,

CAS# 120-92-3, USA), C5, and cyclohexanone (Alfa Aesar, CAS# 108-94-1, USA), C6, were injected as one-to-one mixtures dissolved in 50% water 50% methanol. Three injections of 10 μL each were made at various feed concentrations in the HPLC analyzer. The flow rate was 1.0 mL min^{-1} and the temperature was 40 °C. Standard deviations of the peak area measurements were calculated at each concentration level to establish a linear variance model for use in the parameter estimation routine in gPROMS. The calibration curve data is shown in Figure 6.2.

A linear regression on the standard deviation data is performed to obtain the coefficients in the linear variance model shown in Equation (5.7) in Section 5.2.5. The coefficients for C5 were $\alpha = 1.1 \times 10^{-3}$ and $\beta = 9 \times 10^{-4}$. The coefficients for C6 were $\alpha = 1.1 \times 10^{-3}$ and $\beta = 4 \times 10^{-4}$. The standard deviations for both C5 and C6 increase with increasing feed concentration. This relationship is modeled most simply by a linear regression. The increasing variance with feed concentration may be due to error in the injection volume for the three samples. There may also be error in the baseline definition during the calculation of peak areas, and this error may be intensified at higher concentrations due to the nonlinearity of the adsorption isotherms for C5 and C6.

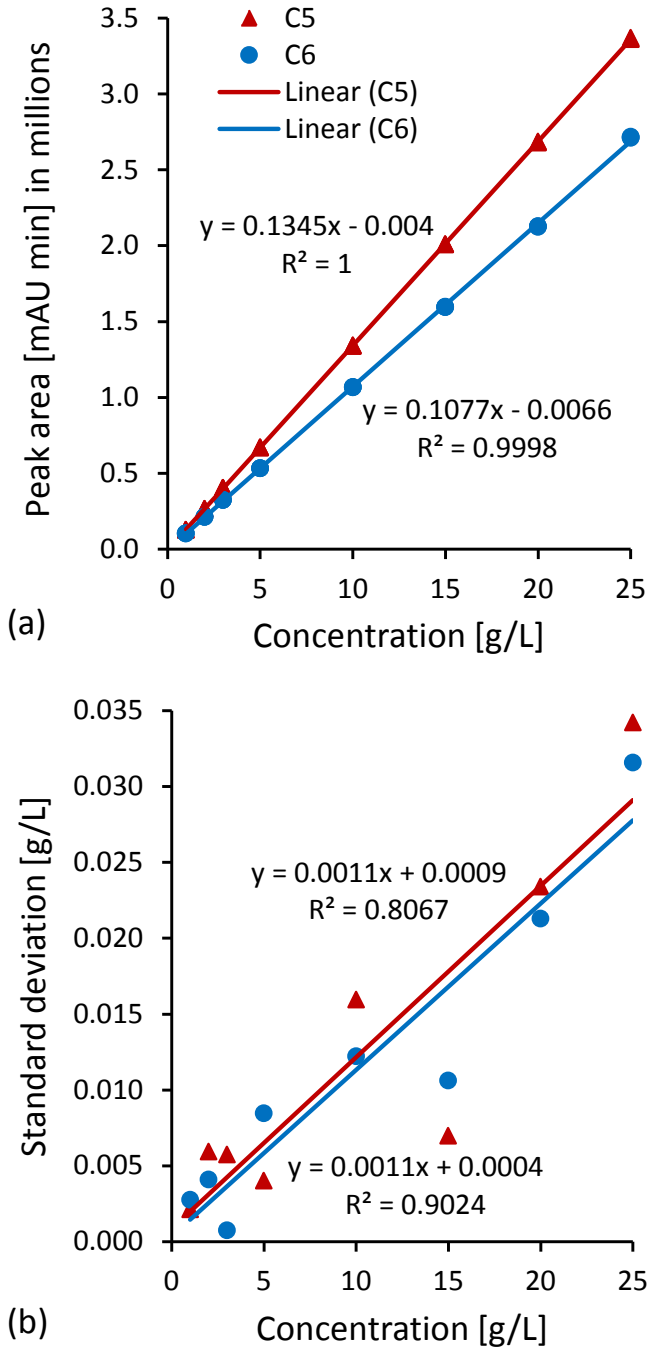

Figure 6.2: (a) Calibration curve using Shimadzu HPLC with three injections made at each concentration level. (b) Standard deviations of the measured concentration at each concentration level, the regression equations and coefficients are included

6.4 Results

6.4.1 Demonstration of Isotherm Model Selection

A crucial step in the PC algorithm for nonlinear systems is isotherm model selection. In order to demonstrate isotherm model selection for a nonlinear system the following case studies were done with cyclopentanone (C5), also called component A, and cyclohexanone (C6), also called component B, where A is less-retained and B is more-retained on the reversed phase column. Three case studies are considered, Case A, B and C, as shown in Table 6.1.

Table 6.1: System configuration details for three case studies with C5 and C6

Variable	Case A	Case B	Case C
n_{col}	4	8	4
Zone configuration	1-1-1-1	2-2-2-2	1-1-1-1
$c_{feed,C5}, c_{feed,C6}$ [g L^{-1}]	34, 34	34, 34	20, 20
Desorbent, [% water, % methanol]	[60, 40]	[60, 40]	[60, 40]
Temperature, [°C]	40	40	40
Initial isotherm model	s-Langmuir	linear	s-Langmuir
F_{max} [mL min^{-1}]	6.5	6.5	5.0
$Purity^{raf}_{A,min}$ [%]	97	97	97
$Purity^{ext}_{B,min}$ [%]	97	97	97
Purity safety margin, [%]	1.0	1.0	1.0

6.4.1.1 Initial Pulse Tests

In all case studies, the PC algorithm was initiated at $k = 0$ by pulse tests on a single SMB column for parameter estimation. The column porosity was measured by a 2 μL injection of uracil at a flow rate of 3.0 mL min^{-1}, and the value was $\epsilon_b = 0.678$. This porosity value was fixed in all the case studies. The Henry's constants, mass transfer coefficients and nonlinear isotherm parameters for C5 and C6 were estimated simultaneously using the inverse method with two small-volume injections of the feed mixture on the SMB column. Figure 6.3 shows the experimental chromatograms for C5 and C6 with injection volumes of 40 and 80 μL at a flow rate of 3.0 mL min^{-1}. The

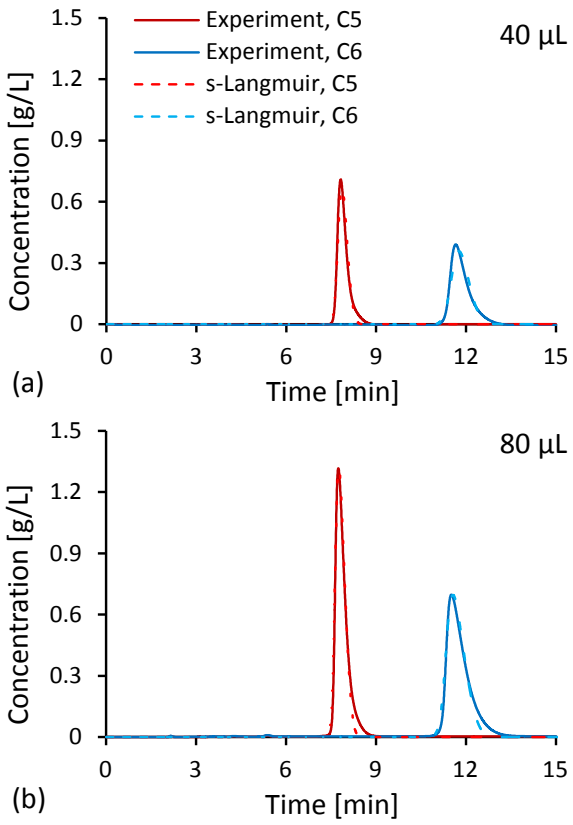

Figure 6.3: Chromatograms of C5 and C6 with (a) 40 μL and (b) 80 μL injection, with $c_{feed,C5} = c_{feed,C6} = 34.0$ g L^{-1}, $F = 3.0$ mL min^{-1}, $T = 40$ °C, and inverse method fitting using s-Langmuir model

310 nm UV signal from the detector was converted into concentration units for C5 and C6 so that the parameter estimation problem, given by Equations (5.2) and (5.3) in Section 5.2.5, could be solved in gPROMS. The simulated chromatograms are also shown in Figure 6.3 using the estimated model parameters for the s-Langmuir isotherm. The inverse method problem was solved for three isotherm models: linear (Equation (1.2)), single-component Langmuir, called s-Langmuir (Equation (3.4)), and competitive Langmuir, called c-Langmuir (Equation (3.5)). The initial parameter values estimated for each model are shown in Table 6.2 in the next section.

The experimental chromatograms exhibit some tailing due to asymmetry of the injection pulse as well as nonlinearity of the isotherm. The concentrations of C5 and

C6 in the column are probably not large enough to characterize the nonlinearity of the isotherm. However, these are only initial estimates of the Langmuir isotherm parameters which are refined later by the PC algorithm.

6.4.1.2 Isotherm Model Selection from SMB Experiment

Isotherm model selection was performed during the first iteration of the PC algorithm at $k = 1$. The optimal operating conditions were implemented in the SMB and the cumulative average product concentrations were sampled during four cycles of operation. The recycle line was also sampled once to improve observability of the SMB internal concentration profiles. This data was used to solve the parameter estimation problems for three isotherm models.

In Figure 6.4 there is a comparison of three isotherm models fit to the experimental concentration data obtained in Case A. Using the linear model there are four model parameters, including the mass transfer coefficients, estimated simultaneously. Accordingly, with the s-Langmuir and c-Langmuir models there are six estimated parameters. In Table 6.2 the initial parameters, refined parameters, 95% confidence intervals, and normalized objection function values for the parameter estimation problems are shown for Case A. The values of ϕ^r_{PE} shown in Table 6.2 are normalized by ϕ^1_{PE}, where 1 represents the linear model.

From Figure 6.4 it is clear that the linear isotherm model does not fit the experimental data, while the s-Langmuir model has improved fitting, and the c-Langmuir model exhibits the best fit. In Figure 6.4a and 6.4b it can be seen that the C6 profiles are fit better than the C5 profiles. The C5 profiles are more difficult to fit because C5 is the less-retained component in the SMB; nonlinear and competition effects may be observed in the raffinate data where the wave front is steepest. By comparison, the C6 profiles are easier to fit because C6 is the more-retained component and the extract data comes from the tailing end of the internal concentration profiles. In

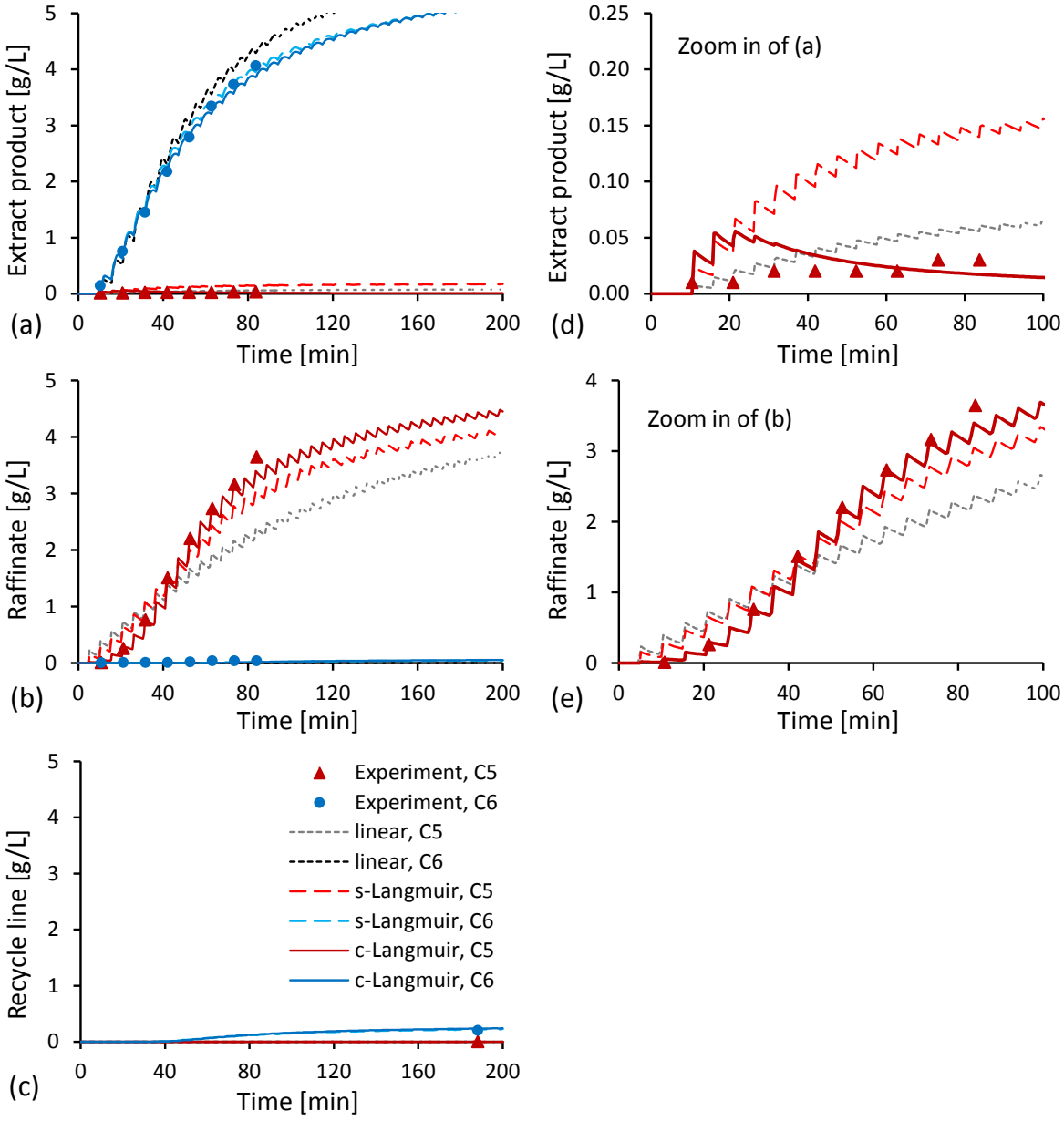

Figure 6.4: Experimental (a) extract, (b) raffinate and (c) recycle line data using optimal operating conditions of Case A, with simulated profiles using linear, s-Langmuir and c-Langmuir isotherms with refined parameter set θ_1. Zoom-in of C5 profiles in (d) extract and (e) raffinate streams to accent differences in model predictions

Table 6.2: Comparison of initial and refined parameter sets for three isotherm models after parameter estimation using SMB startup data in Case A

Linear isotherm	Initial, θ_0	Refined, θ_1	95% confidence interval
H_{C5}	1.793	1.593	5.3×10^{-4}
H_{C6}	3.743	2.771	6.4×10^{-4}
k_{C5}, [min^{-1}]	310	186.5	4.5
k_{C6}, [min^{-1}]	180	108.1	88
ϕ^1_{PE}	1.0		
s-Langmuir isotherm	**Initial, θ_0**	**Refined, θ_1**	**95% confidence interval**
H_{C5}	1.793	1.766	8.6×10^{-4}
H_{C6}	3.743	3.413	7.3×10^{-4}
b_{C5}, [L g^{-1}]	0.0225	0.0121	8.2×10^{-5}
b_{C6}, [L g^{-1}]	0.0405	0.0337	3.0×10^{-4}
k_{C5}, [min^{-1}]	310	372*	-
k_{C6}, [min^{-1}]	180	26.8	0.99
ϕ^2_{PE}	0.38		
c-Langmuir isotherm	**Initial, θ_0**	**Refined, θ_1**	**95% confidence interval**
H_{C5}	1.793	2.011	1.6×10^{-3}
H_{C6}	3.743	3.581	4.6×10^{-3}
b_{C5}, [L g^{-1}]	0.0207	0.0115	9.4×10^{-5}
b_{C6}, [L g^{-1}]	0.0378	0.0367	2.4×10^{-4}
k_{C5}, [min^{-1}]	310	372*	-
k_{C6}, [min^{-1}]	180	130.7	11
ϕ^3_{PE}	0.080		

* indicates active upper bound for a parameter value

Figure 6.4d and 6.4e note that the profiles for C5 are only fit well by the c-Langmuir isotherm, indicating that significant competition exists in the SMB using conditions of Case A.

In agreement with these experimental observations, it can be concluded from the objective function values in Table 6.2 that the c-Langmuir model is the best choice to fit the data. The objective function value for the s-Langmuir model is 61% less than that of the linear model, and the objective function value for the c-Langmuir model is 79% less than that of the s-Langmuir model. In Table 6.2 it can also be seen why the linear isotherm should not be selected in this case study. The values of the Henry's constants are dramatically reduced in the refined parameter set, called θ_1. Note that

H_{C6} was reduced by about 26%, which indicates that the retention of C6 is much less than observed in single-column pulse tests. This apparent reduction of retention happens because the optimizer is accounting for nonlinearity of the isotherm.

Another observation from Table 6.2 is that systematic selection between s-Langmuir and c-Langmuir isotherms is enabled by the PC algorithm. The estimated parameter values for these models are similar, especially in the nonlinear b_i values. However, there is more than 50% decrease in the objective function value for the c-Langmuir isotherm compared to the s-Langmuir isotherm. Therefore, based on the selection criteria explained in Section 6.2.3, the c-Langmuir model is to be selected for the next iteration of the PC algorithm.

From Table 6.2 it should be noted that the value of the mass transfer coefficient for the less retained component, called k_{C5} reached the upper bound in $k = 1$ using the s-Langmuir and c-Langmuir models. The mass transfer coefficient is related to the number of theoretical plates (NTP) of a column, and the sensitivity of this parameter may be insufficient from the first set of experimental data. This issue is more distinctive when there is a combination of nonlinearity and fast mass transfer, which are highly correlated effects. The former contributes to the steepness of wave fronts and the latter describes overall band broadening. This is what happened in the case studies when a nonlinear system and HPLC columns with high efficiency, or large NTP values, are used. However, the PC algorithm can be continued even with this over-estimation of the mass transfer coefficient for C5, which can be corrected later by additional experimental data.

In Figure 6.5 the normalized values of each parameter estimation objective function are shown for the three case studies and for the three isotherm models. In each case study, the value of ϕ^3_{PE}, where 3 corresponds with the c-Langmuir isotherm, was significantly less than the other objective function values. Therefore, in all three case studies the c-Langmuir isotherm was distinguished from the others after the first

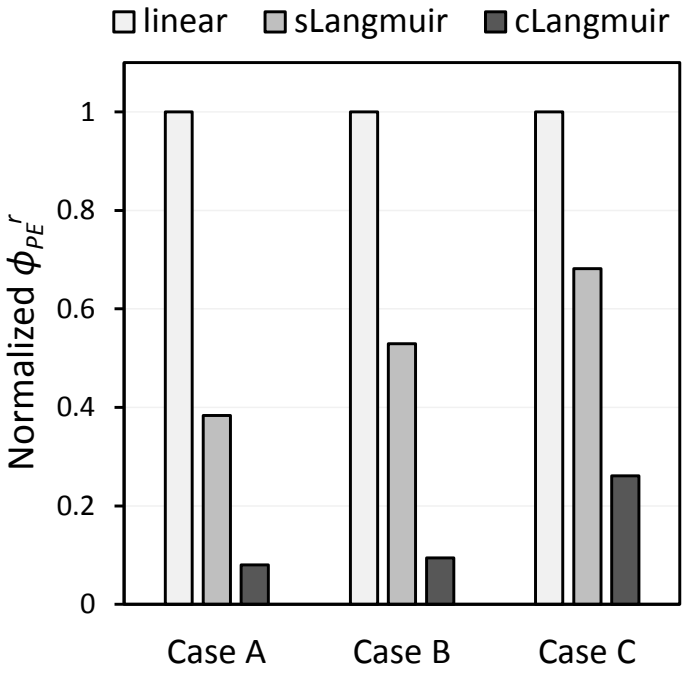

Figure 6.5: Parameter estimation objective function values normalized by ϕ_{PE}^{1} in three case studies with C5 and C6

SMB experiment.

6.4.2 SMB Performance Improvement After Isotherm Model Selection

In this section the robustness of the PC algorithm is demonstrated by Case B showing that even if a poor isotherm model is selected at first and the initial SMB performance is poor, isotherm model selection can correct the model structure and estimate parameter values for the re-optimization of the SMB. The SMB performance can be dramatically improved in the next iteration of the PC algorithm after model selection.

In Case B, the first SMB experiment had very poor purity values with 84% C6 in the extract and 62% C5 in the raffinate, because a linear isotherm was assumed initially despite the true adsorption behavior being nonlinear. The experimental data in $k = 1$ was used to perform model selection and the results were consistent with those

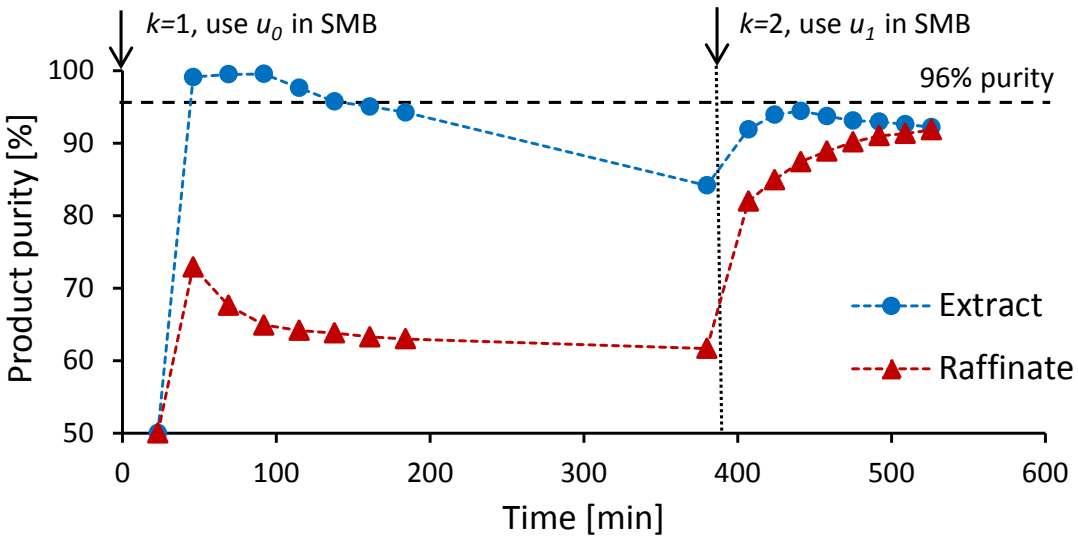

Figure 6.6: Experimental product purities plotted for $k = 1$ where u_0 is obtained using linear isotherm, and $k = 2$ where u_1 is obtained using c-Langmuir isotherm in Case B. The target product purity is 96%. The dotted lines are not the model prediction, just connecting the data points

discussed in Section 6.4.1.2. The parameter estimation objective function values for each isotherm model are shown in Figure 6.5 for Case B. Refined model parameters for the c-Langmuir isotherm were used to obtain the next optimal operating conditions, called u_1 which were implemented in $k = 2$. The improvement in product purities is shown in Figure 6.6 after the operating conditions are switched from u_0 to u_1 in the SMB. After the switch, the measured purities in the extract and raffinate products improved by 8% and 30% respectively. The operating conditions u_0 were kept for 3 hrs after collecting samples in $k = 1$ before implementing the next conditions u_1. This was done to allow sufficient time for model selection and re-optimization of the process. The most difficult parameter estimation problem in gPROMS involves the simulation of multiple SMB experiments, and most problems take less than 60 min of CPU time. The SMB optimization problem usually takes less than 15 min of CPU time in AMPL.

To show how the optimal operating conditions were updated from $k = 1$ to $k = 2$,

Figure 6.7 shows triangle diagrams with regions of complete separation [58], superimposed for the linear and c-Langmuir models with u_0 and u_1 and the experimental product purities. The separation regions are drawn using refined parameter values, called θ_1. The move from u_0 to u_1 shows the reduction in feed throughput after re-optimization, which was about 60%. Based on the c-Langmuir triangle diagram, the position of u_1 is much closer than u_0 to the theoretical optimal operating conditions, which explains the improvement in observed purity values.

A clear advantage of the PC algorithm over conventional SMB process development methods is that a reliable set of nonlinear isotherm parameters can be obtained from a single SMB experiment that takes only hours, and these parameters can be used to obtain optimal operating conditions for the process. Although, one or two more iterations of the PC algorithm may be necessary to satisfy the termination criteria, this means that the SMB production can be modeled and optimized in a matter of hours.

6.4.3 Convergence of PC Algorithm

In this section the PC algorithm is shown to converge in Case C for a nonlinear system. For the termination criteria in the PC algorithm, the tolerance on change in feed throughput, ϵ_{tol}, was 0.015 because the nonlinear SMB performance is very sensitive to the feed flow rate.

The initial model parameters for the s-Langmuir model were used in $k = 0$, and after performing model selection on the first set of SMB data, the c-Langmuir model was selected. This result is consistent with the model selection shown in Section 6.4.1.2, and the parameter estimation objective function values in Case C for each model are shown in Figure 6.5.

Table 6.3 shows the iteration history of the c-Langmuir model parameter values determined by the PC algorithm. It should be noted that the final values of the

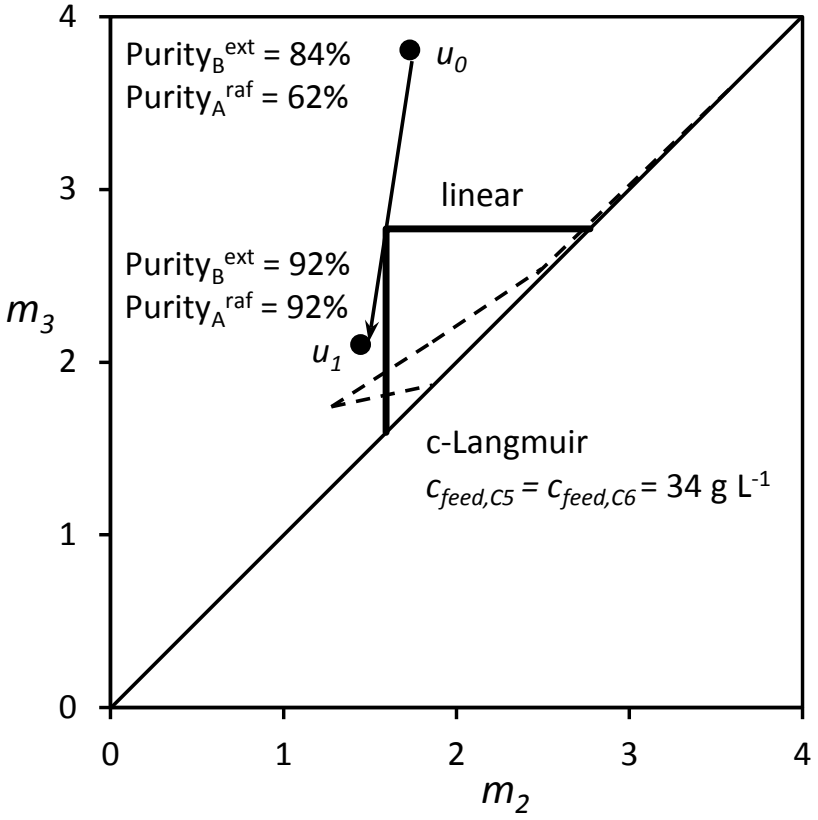

Figure 6.7: Optimal m_2 and m_3 values from operating conditions u_0 and u_1 with linear and c-Langmuir triangle regions determined by refined parameter sets, θ_1 in Case B. Experimental product purities are included

Henrys constants are greater by a few percent than the initial estimates. This can be explained by the fact that there are dead volumes in the real SMB unit with column connections, rotary valve and pumps that are not described explicitly in the SMB model. The values of the c-Langmuir isotherm parameters, called b_i, fluctuate in each iteration. The greatest change observed is in b_{C5} from θ_1 to θ_2. In general the values of the mass transfer coefficients estimated by the PC method are reduced by more than 50% of the initial guess when k_i's are obtained by the inverse method. This agrees with previous results in the case study with uridine and guanosine [11] where the apparent mass transfer rates in the real SMB unit were about 50% less than the initial guess obtained from pulse tests. This reduction is probably due to mixing and various flow rates in the real SMB unit with column connections, rotary valve and pumps. The k_i values are largely insensitive in the SMB model, thus it is not surprising that their estimated values vary greatly from iteration to iteration. Note that in θ_2, it can be seen that k_{C5} has an active upper bound which is 15% greater than the initial value. This is an indication of the steep concentration profiles for C5, the less-retained component, observed in the raffinate product. The large value of k_{C5} was unexpected because the apparent mass transfer rates in the SMB unit are usually less than the initial guess using pulse tests. Nonetheless, in the final iteration, $k = 3$ the value of k_{C5} was corrected to be a small fraction of the initial guess.

Table 6.3: Refinement of SMB model parameters in Case C using c-Langmuir isotherm in $k = 1$ to $k = 3$

Parameter	Initial, θ_0	Refined, θ_1	Refined, θ_2	Refined, θ_3
H_{C5}	1.793	1.870	2.202	2.134
H_{C6}	3.743	3.578	3.814	3.819
b_{C5}, [L g^{-1}]	0.0207	0.00302	0.0223	0.017
b_{C6}, [L g^{-1}]	0.0378	0.0424	0.0360	0.042
k_{C5}, [min^{-1}]	310	148	372*	18.7
k_{C6}, [min^{-1}]	180	44.8	110	71.5

* indicates active upper bound for parameter value

In Figure 6.8 the convergence of the SMB experiments to optimal productivity with high purity constraints is shown. The SMB experiments are performed relatively quickly with a small number of samples taken in each iteration. In $k = 2$ and $k = 3$ only six measurements were taken to observe the transition in operating conditions. It can be seen how the concentration profiles evolve after switching the operating conditions, and the improvement of the model fitting is shown by plotting simulated profiles using θ_0 and θ_3. The most significant improvement in the model fitting is in the C5 profiles of the extract and raffinate products. Another observation is that product concentrations are increased in the final iteration with an increase of about 400% in the raffinate stream. The simulated C5 raffinate profile has some steep oscillations in each step of operation, as seen in Figure 6.8. As observed in [11], these oscillations are not due to numerical instability of the solver, but instead are a result of internal concentration profiles during a step. The product concentrations that enter the extract and raffinate tanks have decreasing and increasing patterns respectively during a step. These patterns are observed distinctly at the beginning of each experiment where the accumulated volume of components in the tanks is still small.

The simulated concentration profiles have discontinuities at the time points where the next operating conditions are initialized, as seen in Figure 6.8. This discontinuity is also observed in the experiments by collecting the extract and raffinate products in empty containers at the moment the operating conditions are switched. The recycle line was not collected in a cumulative way during the experiment, but was sampled once by collecting the average concentration over a step, as discussed in Section 5.2.4. This was done assuming that after a sufficient number of cycles the cumulative concentration measurement equals the average concentration measurement over a step. This single sample for the recycle line was included in the parameter estimation.

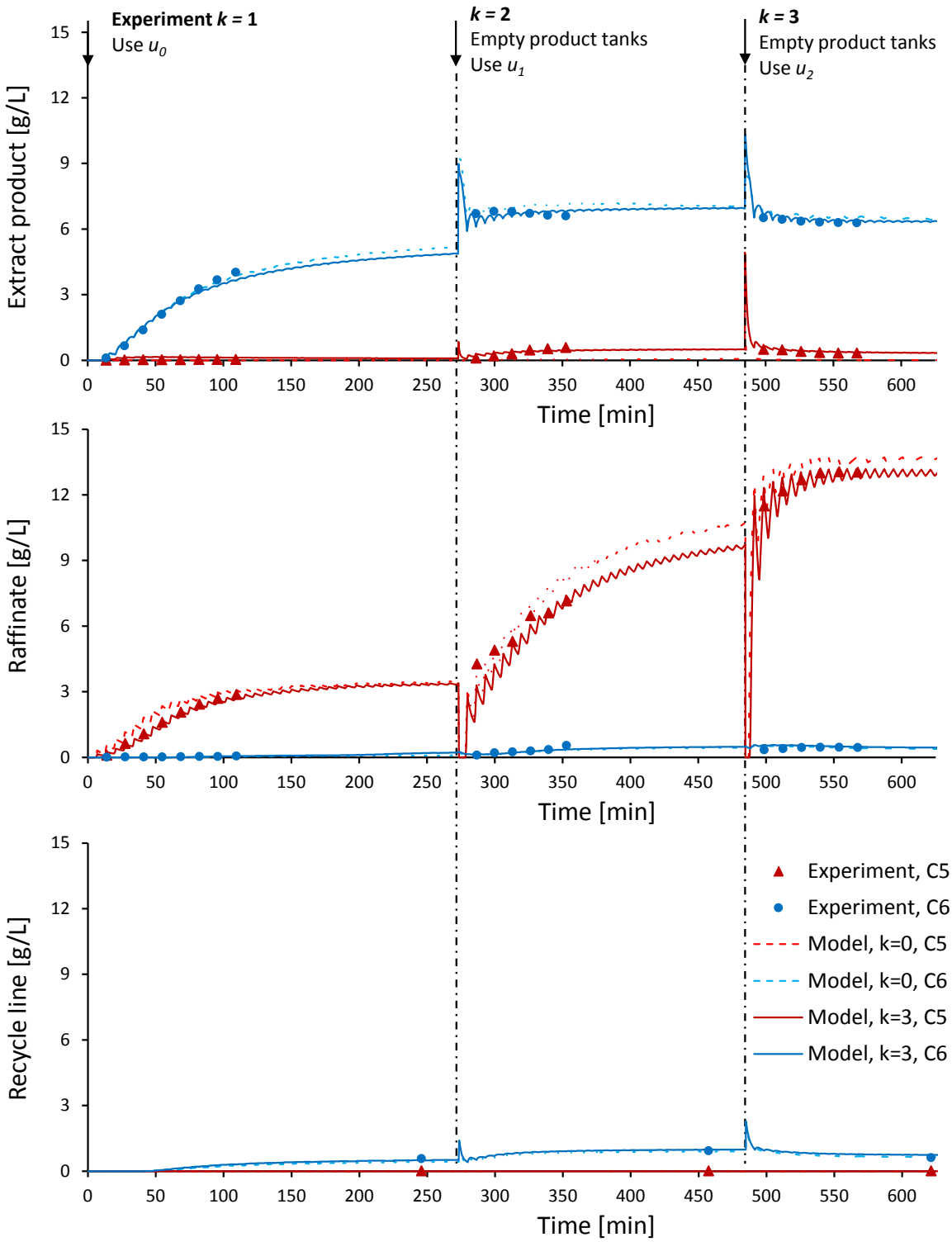

Figure 6.8: Experimental extract, raffinate, and recycle line cumulative concentration data for three iterations of the PC algorithm in Case C. The simulated profiles are plotted using θ_0 and the final parameter set θ_3

Table 6.4: Optimal operating conditions and termination criteria in each iteration for Case C

Control variable	u_0	u_1	u_2	u_3
t_{step}, [min]	6.83	6.61	6.83	6.83
m^1	3.26	3.01	3.18	3.25
m^2	1.64	1.23	1.36	1.44
m^3	2.17	1.85	1.93	2.01
m^4	-0.72	0.84	1.10	0.92
Termination criteria	$k=1$	$k=2$	$k=3$	
Purity_A^{raf}, [%]	98.2	93.9	97.8	
Purity_B^{ext}, [%]	99.2	91.0	98.0	
$\Delta\phi_{SMB}^k$	0.215	0.117	0.014	

Table 6.4 shows the optimal operating conditions in each iteration of the PC algorithm for Case C, along with the product purities and the change in feed throughput for each SMB experiment. In addition, Figure 6.9 shows how the change in feed throughput affects the experimental purity values in each iteration. It should be noted that the optimal solutions u_0 through u_3 do not differ greatly, yet the experimental purities and the product concentrations are significantly affected by even slight changes in the step time and feed throughput. The termination criteria are satisfied in the third iteration because both products have purity values greater than 96% and the change in the optimal feed throughput between u_2 and u_3 is less than 1.5%. Therefore, u_2 is considered optimal the optimal set of operating conditions for CSS production.

In Figure 6.10 it can be seen how the operating conditions change after each SMB optimization in order to improve both the product purities and feed throughput. The complete separation region is drawn using θ_3 and it is seen that the initial operating conditions u_0 were close to the tip of the triangle even though the s-Langmuir model was used to solve for u_0. Indeed, the product purity values were high in the first experiment. The step from u_0 to u_1 appears to be overly aggressive because the feed flow rate increased by 22% and the product purities decreased below the minimum

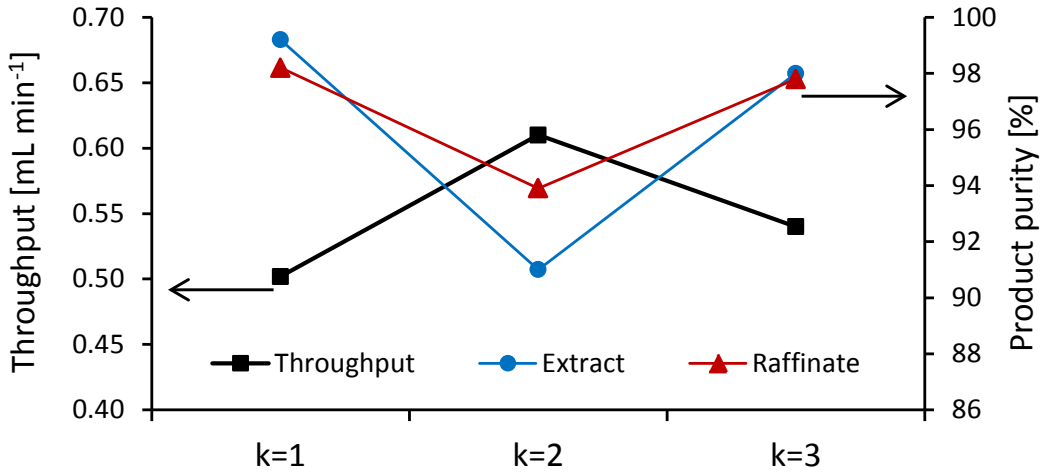

Figure 6.9: Experimental throughput values are shown on the left axis, and experimental extract and raffinate purity values are shown on the right axis for three iterations of the PC algorithm in Case C

constraint of 96%. Nonetheless, the step from u_1 to u_2 was a good adjustment because the purities were a few percent greater than 96%, and the throughput was improved by 8% from $k = 1$ to $k = 3$.

6.4.4 Validity of Model Parameters

In this section, it is shown that the values of c-Langmuir isotherm parameters estimated using the PC algorithm in the case studies are reliable when compared with those measured by single-component frontal analysis (FA) and perturbation analysis (PA). It is not necessary to perform FA or PA to use the PC method, however it is worthwhile in this research to check the reasonableness of model parameter values against well-established parameter estimation techniques. The nonlinear isotherm parameters are more difficult to estimate, especially when competitive adsorption is involved, yet it is shown that the values obtained by the PC method are reliable in the SMB model.

In Figure 6.11 single-component FA data for C5 and C6 are compared with the

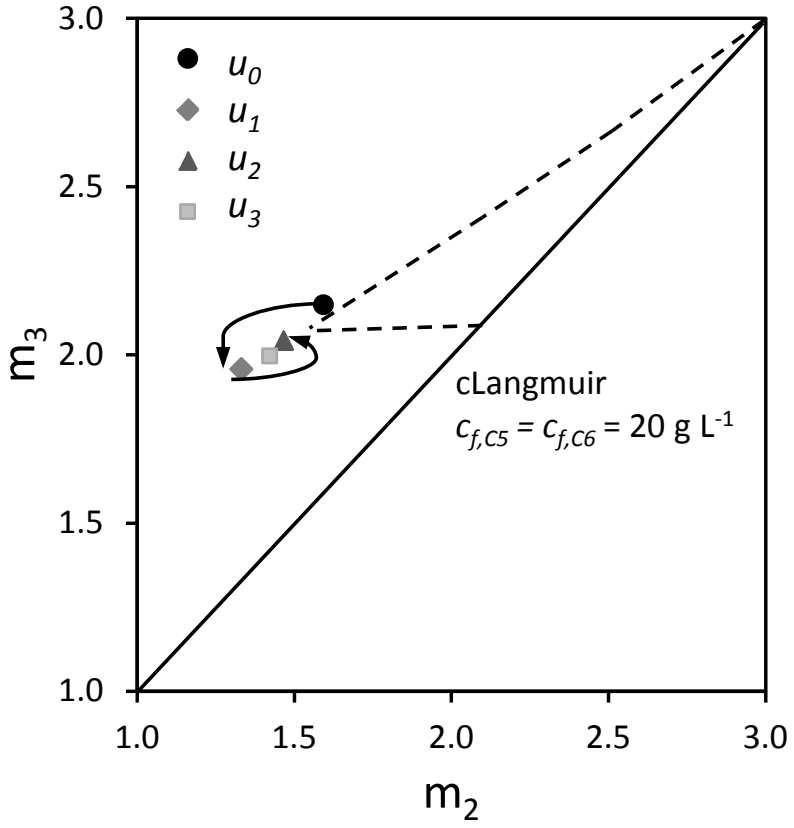

Figure 6.10: Optimal m_2 and m_3 values in Case C for u_0 through u_3 with the c-Langmuir triangle region determined by refined parameter set θ_3

model using the c-Langmuir isotherm parameters obtained by the PC method in $k = 3$ of Case C. The FA tests were performed by injecting step inputs of single components up to 70 g L^{-1} into an SMB column with 60% water and 40% methanol as mobile phase, flow rate of 3 mL min^{-1}, and temperature of 40 °C. It can be seen that C6 has stronger nonlinearity than C5 on the reversed phase column, and both components exhibit deviations from linear adsorption at 34 g L^{-1}, which was the feed concentration of each component used in Cases A and B. In this comparison the c-Langmuir model reduces to the s-Langmuir model because the FA tests were performed with single components, so there is no competition term in the isotherm model.

Note that Figure 6.11 shows that the PC model fits the C5 isotherm better than the C6 isotherm, especially over the concentration ranges of interest for Cases A and B. The PC model predicts both single-component isotherms relatively well at the low-to-moderate concentration range, although the deviation increases for C6 at higher concentrations. We find that a better estimate for b_{C5} than b_{C6} is obtained by the PC method because nonlinear effects are directly observed in the raffinate stream, which is downstream of the feed location, where C5 is pure. From Figure 6.4 it was noted that the c-Langmuir isotherm fit the C5 profiles in the raffinate and extract while all isotherm models fit the C6 profiles reasonably well. This indicates that the nonlinearity of C6 is not completely observed at the tailing end of the concentration profiles of the SMB which are collected in the extract product.

In Table 6.5 the c-Langmuir isotherm parameter values obtained by inverse method, frontal analysis, and PC method are compared. Theoretical saturation capacities, called q_i^{sat} are obtained from the following equation:

$$q_i^{sat} = \frac{H_i}{b_i} \quad i = A, B \tag{6.2}$$

The parameters H_i and b_i are correlated by the theoretical saturation capacity of the stationary phase. The b_is estimated by the PC method are within a reasonable

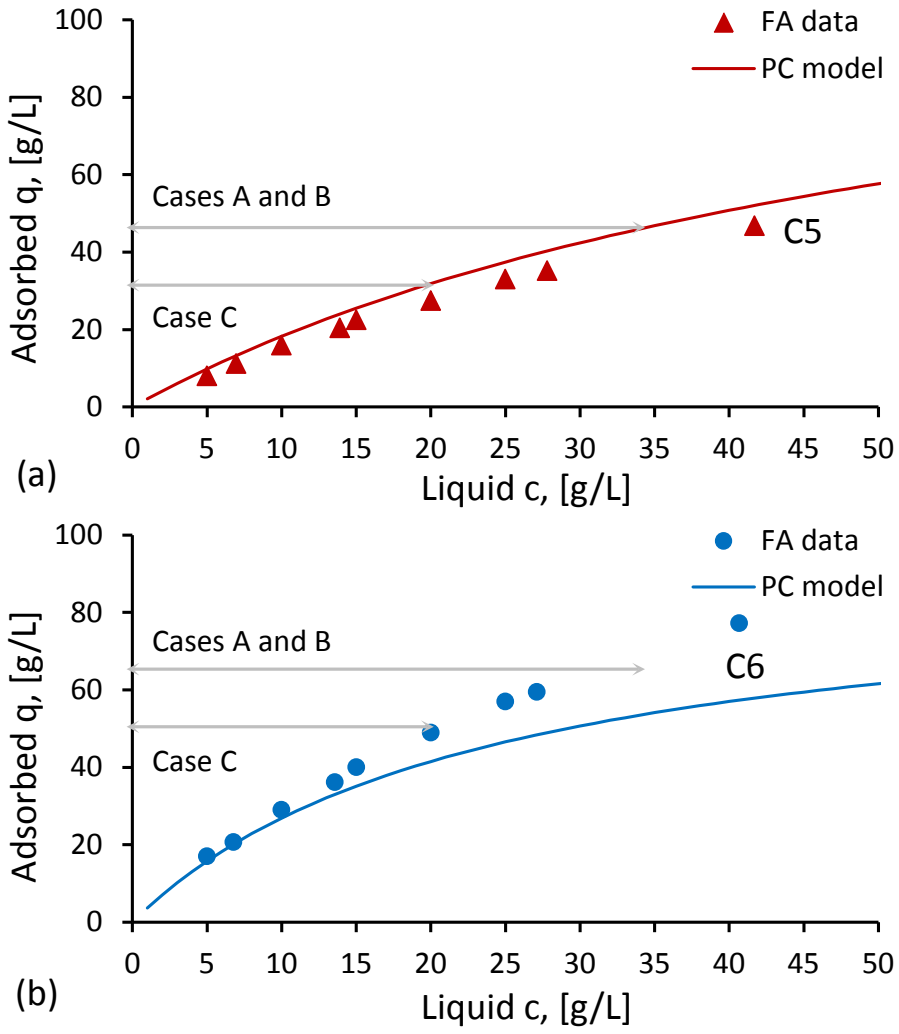

Figure 6.11: Comparison of single-component FA data for (a) C5 and (b) C6 with c-Langmuir model parameters obtained by PC method in Case C. Relevant concentration ranges are shown for Cases A, B, and C

Table 6.5: Comparison of c-Langmuir isotherm parameter values estimated by three methods. The PC method parameters are from θ_3 in Case C

Parameter	Inverse method	Single-component FA	PC method
b_{C5}, [L g^{-1}]	0.0207	0.0107	0.017
b_{C6}, [L g^{-1}]	0.0380	0.0197	0.042
q^{sat}_{C5}, [g L^{-1}]	86.6	152	130
q^{sat}_{C6}, [g L^{-1}]	98.5	176	91

range when compared to those obtained by single-component FA, and it seems that in Case C the initial guess of c-Langmuir b_is obtained by the inverse method were also fairly reliable. If the underlying assumptions of the fundamental Langmuir equation are reasonable in this practical application of multi-component adsorption, it is expected that the values of b_i obtained by single-component FA will match those of the competitive FA [20]. The SMB startup experiment is essentially a competitive loading test on the SMB columns, and non-ideal competitive adsorption behavior can be observed that is lost in the single-component FA experiment.

For further validation of estimated c-Langmuir parameters using the PC method competitive PA was performed. An SMB column was used with 60% water 40% methanol as mobile phase, flow rate of 2.5 mL min^{-1}, and temperature of 40 °C. The column was equilibrated with five different solutions of C5 and C6 that were prepared to imitate various internal locations of the SMB unit. A 30 μL injection of $c_{feed,C5} = c_{feed,C6} = 20$ g L^{-1} was made at each equilibrium level, and the retention times of the C5 and C6 peaks were recorded. The results of the PA are summarized in Figure 6.12 where each equilibrium state is shown as a category on the horizontal axis. The values of dq_i/dc_i were calculated, based on the method described by [39], for the experimental results and the model predictions using c-Langmuir parameters obtained by both the PC method and single-component FA. The values of b_{C5} and b_{C6} obtained by FA were used in the competitive Langmuir isotherm to calculate dq_i/dc_i at each equilibrium state [57]. The percent deviations shown in Figure 6.12

were calculated by the following formula:

$$\left| \frac{(dq_i/dc_i)^j_{exp} - (dq_i/dc_i)^j_{mod}}{(dq_i/dc_i)^j_{exp}} \right| \text{x } 100\% \tag{6.3}$$

where j is the index for the equilibrium condition, *exp* is the experimental value, and *mod* is the model-predicted value of the local derivative of the adsorption isotherm. Equal values of the Henrys constants were used in the PC and FA model parameter sets in order to evaluate the estimates of b_i for competitive adsorption. This result shows that the c-Langmuir model parameters obtained by the PC method can predict the retention times of perturbation peaks more reliably than the c-Langmuir parameters measured by single-component FA, especially around the feed concentration of 34 g L^{-1} each C5 and C6. Using the solution where c_{C5} = 34.0 g L^{-1} and c_{C6} = 34.0 g L^{-1}, the predicted dq_i/dc_i values using the FA parameters were off by 144% and 114% for C5 and C6 respectively. This means that the assumptions of the fundamental Langmuir theory, such as one molecule - one site interaction, or no interaction among adsorbing components, may not hold in this case study.

Another way to test the reliability of the optimal parameter set obtained by the PC method is to analyze the confidence intervals for each estimated parameter at 95% statistical confidence. In Figure 6.13 the computed confidence intervals for the Henry's constants, c-Langmuir parameters and mass transfer coefficients are shown in each iteration of the PC algorithm for Case C. These statistics were calculated by the parameter estimation routine in gPROMS, which depend on the specification of the variance model for experimental measurements discussed in Section 6.2.3. In general, the confidence intervals decreased from one parameter estimation result to the next. The values of the confidence intervals for H_{C5} and H_{C6} were tight relative to the parameter values of 2.134 and 3.819 respectively and slight improvement was observed. The values of the confidence intervals for b_{C5} and b_{C6} were also tight relative to the parameter values of 0.017 and 0.042 L g^{-1} respectively and slight improvement was observed. Comparatively, the values of the confidence intervals for k_{C5} and k_{C6}

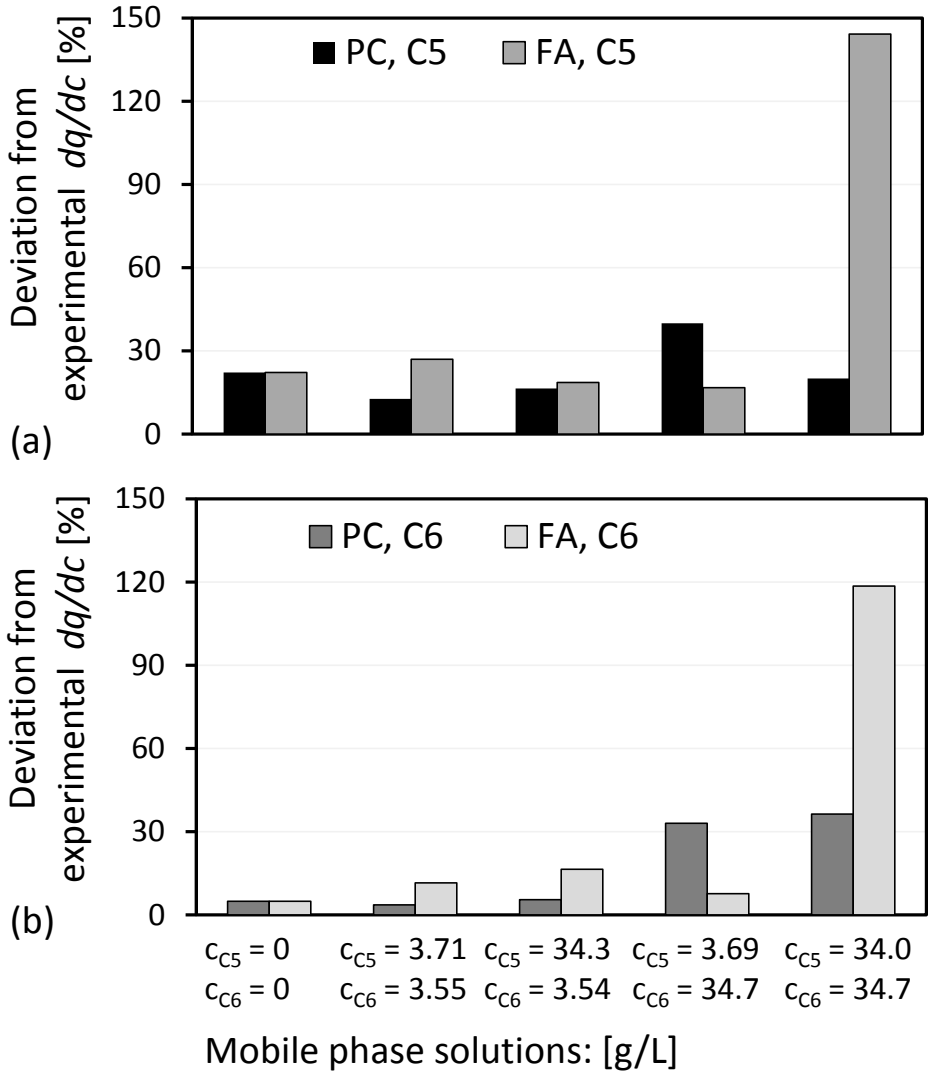

Figure 6.12: Comparison of experimental dq_i/dc_i values to those predicted by c-Langmuir model parameters obtained by PC method in Case C and single-component FA for (a) C5 and (b) C6

were loose relative to the parameter values of 18.7 and 71.5 min^{-1} respectively. Yet the confidence interval for k_{C5} improved significantly from $k = 1$ to $k = 3$. This is a similar trend to that observed in the linear case study discussed in Chapter 5 and the larger confidence intervals for the mass transfer coefficients are another indication of their insensitivity in the SMB model.

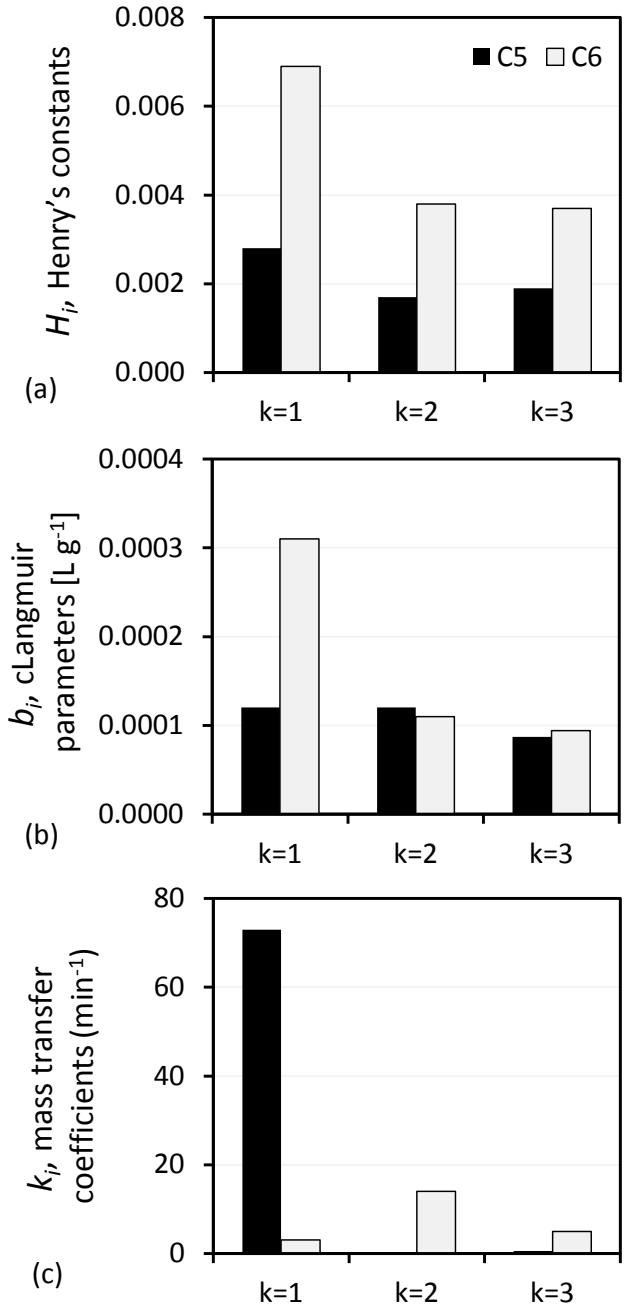

Figure 6.13: 95% confidence intervals for each SMB model parameter in each iteration of the PC algorithm in Case C

6.5 Conclusion

The prediction-correction algorithm for nonlinear SMB process development is extended with isotherm model selection and tested. It is found to be an efficient and robust algorithm in numerous laboratory experiments with a nonlinear isotherm system. In all case studies with cyclopentanone and cyclohexanone the competitive Langmuir isotherm is distinguished from the linear and single-component Langmuir models, and the isotherm parameters are determined from SMB startup data. The parameter values estimated using the PC method are comparable to those obtained using batch techniques such as moment analysis, inverse methods and frontal analysis. In one case study the robustness of the PC algorithm is demonstrated where the operating conditions are corrected from a poor initial point in a single step after isotherm model selection. The product purities were improved by 8% in the extract and 30% in the raffinate. In another case study the PC algorithm is shown to converge to optimal operating conditions in only three iterations while maintaining high purity constraints and increasing the feed throughput of the process by 8%. The PC algorithm proceeds in an automatic and sequential manner until it terminates so that an SMB expert is not required to manually tune the SMB operating conditions. It should be noted that this algorithm is designed to function with any choice of isotherm model, and up to six model parameters have been simultaneously determined using the PC method in this study.

CHAPTER 7

EXPERIMENTAL INVESTIGATION OF OPTIMAL STARTUP STRATEGIES FOR SMB

7.1 Motivation

In this chapter there is a demonstration of optimal startup operation for SMB chromatography. The startup acceleration problem is posed as a piece-wise optimal control problem and the solution is implemented in a laboratory scale SMB unit to show that significant reduction in startup time and desorbent consumption is achieved.

The operating principles of SMB chromatography have been presented in Section 1.2.1. In this chapter the focus is on transient operation of SMB, where during startup the concentration profiles of each component are not yet established in the unit. The goal is to reduce the time it takes for the SMB unit to reach the CSS conditions by manipulating the control variables over time. Usually the SMB products are discarded when the product concentrations are low. During transient operation the product concentrations may be too low or the purity may be off-specification. The time it takes to reach the CSS condition from a clean bed can be quite long when compared with the total operation time. In some cases, where only a few grams or kilograms of feed are to be processed by SMB, there may not be enough time for the SMB unit to reach the CSS condition before shutdown is required.

As discussed by [56], there may be a common scenario in the pharmaceutical production where the same SMB unit is used to purify small batches of different mixtures sequentially. In Figure 7.1 there is an illustration of this scenario with a three-phase production campaign, where the transient SMB operation is taking a significant portion of the total operation. If the transient operation is optimized, as

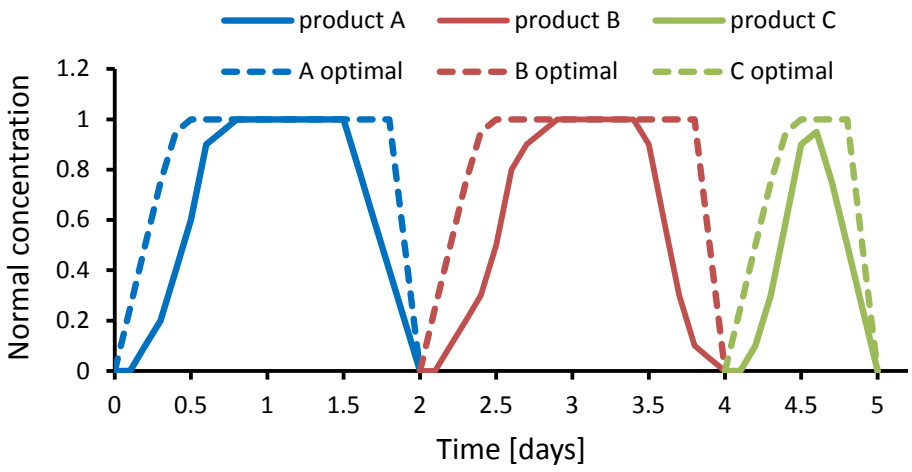

Figure 7.1: Illustration of normalized product concentration over time for SMB operated with nominal verses optimal startup control for a three-phase production campaign

shown by the solid lines in the figure, then the feed can be produced continuously to meet specifications, even during startup and shutdown, and more feed can be processed as indicated by the increased area under the dashed curves.

Some other researchers have applied heuristic startup and shutdown strategies such as pre-loading the columns with feed and having pre-elution, including recovery of adsorbed products during shutdown. Both numerical simulation and experimental demonstration of these techniques is shown by Xie *et al.* [85]. They found that the startup time of an SMB cascade system could be reduced by pre-loading the SMB columns with the feed mixture. That is, the feed pump was activated only to build up the concentration profiles in the unit before the operating conditions for CSS production were implemented. However, they do not use any model-based optimization of the control variables during transient operation.

Li *et al.* [56] presented a systematic startup optimization method using nonlinear programming. Building on the methodology used by [56], optimal startup controls are calculated and implemented in a lab-scale SMB unit using a linear isotherm system. The optimization problem is not yet fully explored, in other words, the solutions

shown in this work may not be the global optimal control strategy. Yet this work demonstrates experimentally the feasibility of a model-based optimization approach to startup acceleration.

This chapter is organized as follows: the methods used in solving the SMB startup acceleration problem are discussed in Section 7.2, experimental equipment and the determination of model parameters for a linear isotherm system is discussed in Section 7.3, and case studies are presented in Section 7.4 to show that startup acceleration using model-based optimization is feasible.

7.2 Methodology

The methods used to solve the startup acceleration problem are discussed in this section. Before solving the startup acceleration problem the SMB unit is optimized for CSS operation. The following section will show how the CSS optimal operation is determined, and then the startup acceleration problem will be discussed in detail.

7.2.1 CSS Optimal Operation

The optimal operating conditions for the SMB unit to achieve maximum productivity with high purity constraints is determined by the PC method which is discussed in Chapter 5. The steps of the PC algorithm are shown in Section 5.2.

To summarize the PC method, initial SMB model parameters are obtained by batch experiments on a single HPLC column. The SMB model is described in detail in Section 3.1, and this is used to solve the SMB optimization problem given by Equation (3.10) in Section 3.2 using the initial model parameters. The optimal solution from the SMB optimization is implemented in an SMB experiment, and cumulative product concentrations are collected over time during SMB startup. The SMB model parameters are corrected by solving the parameter estimation problem given by Equation (5.3) in Section 5.2.5, fitting the SMB experimental data, and

the SMB is re-optimized using the corrected parameters. This sequence of SMB experiments, followed by parameter estimation and re-optimization, is repeated until the termination criteria are satisfied. At that point the optimal operating conditions for CSS operation of the SMB are determined. The results of the PC method for parameter estimation and SMB optimization are shown in Section 7.3.

7.2.2 Nominal Startup Strategy

In order to demonstrate the advantage of startup acceleration for SMB, nominal startup is carried out and compared with the accelerated startup strategies. The nominal startup strategy in SMB operation is to use constant operating conditions equal to those obtained for CSS optimal operation. This is the typical operating strategy for SMB because of its simplicity; there is only one set of operating conditions to implement, and the system will approach the desired CSS performance. However, nominal startup often results in long startup times with significant consumption of desorbent, and there is no guarantee that the products collected during startup will meet the desired specifications of purity or product concentration. In typical SMB operations, the products are discarded during some cycles of transient operation, and only the products with high concentration and high purity are collected.

7.2.3 Startup Acceleration Strategy

The idea of startup acceleration is to change the operating conditions of the SMB unit over time so that the system reaches the optimal CSS performance as soon as possible. Startup acceleration is essentially an optimal control problem that may be stated in a straightforward manner as:

$$\min \quad \phi_{SA}(u(t)) \;=\; t_{startup} \tag{7.1}$$

$$\text{s.t.} \quad \|C(t,u(t)) - C^*(t)\|^2_{t=t_{startup}} \;\leq\; \epsilon_{SA} \tag{7.2}$$

Equations (3.1) - (3.3), (3.6), (3.7), (3.8)

where $\phi_{SA}(u(t))$ is the objective function for startup acceleration, $u(t)$ is the vector of control variables as a function of time, $t_{startup}$ is the startup time, $C(t, u(t))$ is a vector of the total internal concentration profile for each component in each column as a function of time, $C^*(t)$ is a vector of the CSS total internal concentration profile for each component in each column as a function of time, and ϵ_{SA} is the tolerance for the difference between the startup concentration profile and the CSS concentration profile. Initially, $C(0) = 0$ and as time increases, the SMB model, given by Equations (3.1) - (3.3), (3.6), (3.7), (3.8), is solved to determine $C(t, u(t))$. The vector function $C^*(t)$ is already solved by determining the optimal CSS operation for a given SMB system. To find the optimal control profile, $u^*(t)$, is not trivial due to PDE constraints of the SMB model. As discussed by Li *et al.* [56], this optimization problem is ill-conditioned, and may not be solved reliably.

Instead of trying to solve the straightforward statement of startup acceleration given by Equation (7.1), in this work the problem statement is approximated in two ways. First, the optimal control profile is approximated by a sequence of step-wise constant operating conditions. This is done by decomposing the startup time horizon into stages. The decomposition of time horizon is shown schematically in Figure 7.2a, and the approximation of the control profile is shown in Figure 7.2c. Each stage is a set of SMB steps where constant operating conditions are used. Therefore, in the decomposed problem, $u(t) = u_n, t \in [t_{n-1}, t_n]$ where u_n is the vector of operating conditions for stage n, t_n is the time that stage n ends. The second approximation of the startup acceleration problem statement involves solving the optimization over decomposed stages of the time horizon. In part (b) of the figure, the time horizon is normalized using the equation:

$$\tau_n = \frac{t - t_{n-1}}{t_n - t_{n-1}}, \quad n = 1, 2, \ldots, P \tag{7.3}$$

where τ_n is the normalized time for stage n, and P is the total number of stages for the startup period. The decision is made *a priori* about how many stages will be

used, and how many steps of SMB operation take place within each stage. The idea behind these approximations is that only the constant operating conditions for stage n, u_n, need to be solved in stage n of the optimization problem.

Therefore, the startup acceleration is decomposed into a sequence of stage-wise optimization sub-problems where each sub-problem is formulated as:

$$\begin{aligned}
\min \quad \phi_{SA,n}(u_n) &= t_{step,n}\|C(1,u_n) - C^*(1)\|^2 + \epsilon_{reg}\|u_n - u^*_{CSS}\|^2 && (7.4)\\
\text{s.t.} \quad \text{Purity}_A^{raf} &\geq \text{Purity}_{A,n,min}^{raf} && (7.5)\\
\text{Purity}_B^{ext} &\geq \text{Purity}_{B,n,min}^{ext} \\
F_x &\leq F_{max}, \quad x = 1,2,3,4 && (7.6)\\
F_1 - F_2 &\geq 0, \quad F_1 - F_4 \geq 0 \\
F_3 - F_2 &\geq 0, \quad F_3 - F_4 \geq 0
\end{aligned}$$

Equations (3.1) - (3.3), (3.6), (7.7), (3.8)

where ϵ_{reg} is a coefficient for the penalty function that should guide the optimizer to choose the CSS operation conditions, u^*_{CSS}, as the sub-problems are solved stage-wise. The purity values were defined by Equation (3.11) in Section 3.2. The purity constraints in these optimization sub-problems are not necessary, yet they are used in one startup acceleration strategy to preserve the product quality during startup. The flow rates in each zone are also constrained to maintain feasible and safe operation of the SMB unit.

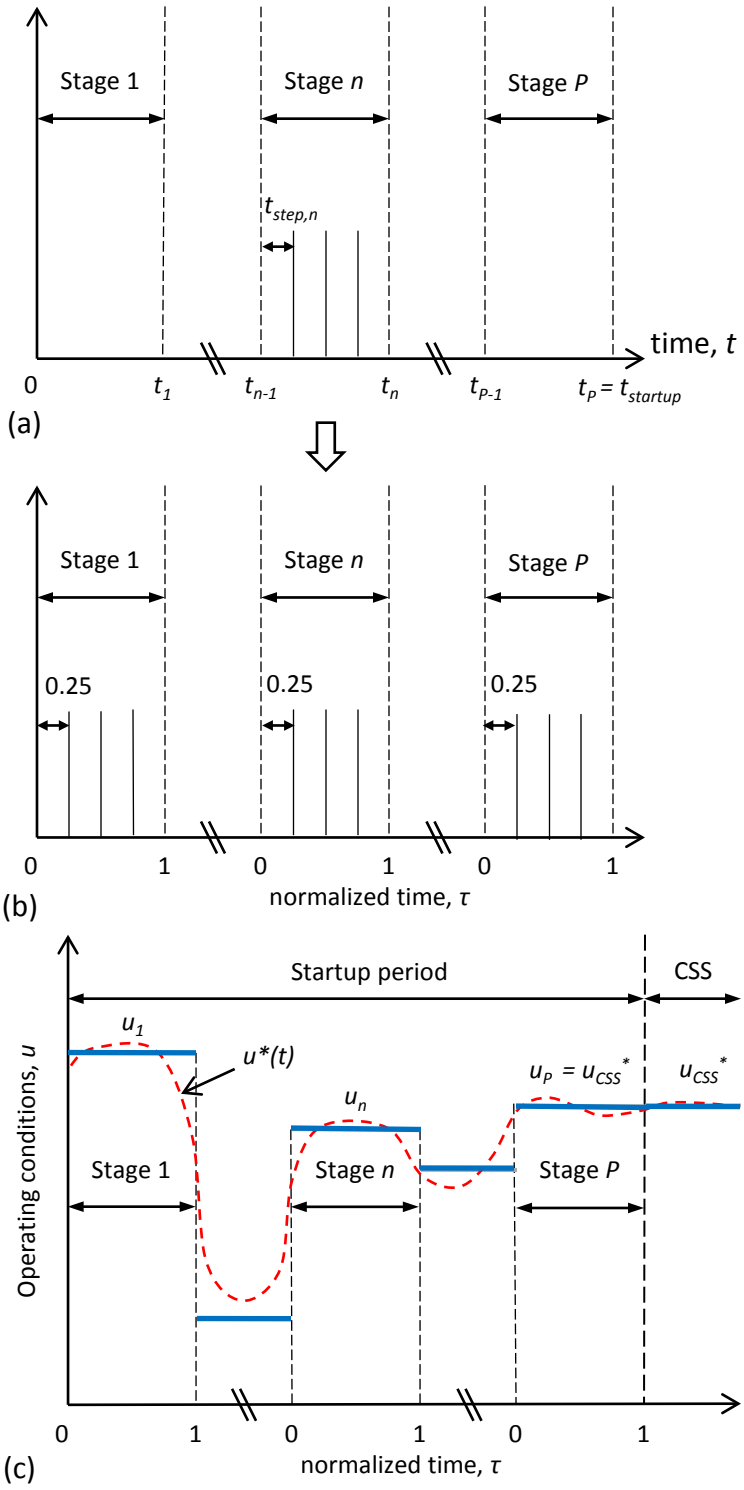

Figure 7.2: (a) Schematic of startup time horizon decomposed into stages. (b) Normalized time horizon with fixed 4 steps per stage. (c) Piece-wise constant operating conditions approximating the optimal control profile, $u^*(t)$

Overall, the approximated SMB startup problem is solved iteratively following the algorithm proposed by Li *et al.* [56]. The steps of the solution algorithm are shown below:

1. Initialize at $n = 1$

2. Set number of SMB steps in stage n, initial guess of u_n, and update initial concentration profile, $C_n(\tau = 0)$ of stage n

3. Solve stage-wise sub-problem given by Equation (7.4) with or without purity constraints specified

4. Check tolerance of convergence to CSS condition given by Equation (7.2). If condition is satisfied, then CSS is reached and the algorithm is terminated in stage n. If condition is not satisfied, then let $n = n + 1$, return to Step 2 of the algorithm, and repeat.

For updates of the initial concentration profile in stage n, the final concentration profile from stage $n - 1$ is used. Therefore, $C_{n-1}(\tau = 1) = C_n(\tau = 0)$.

For the work presented here, each stage is a cycle of SMB operation consisting of 4 steps, and this strategy is also used by [56]. However, the decisions about how many stages for startup and how many steps per stage have not been fully explored in simulation or in experiment, and remain open questions for further research.

In this work, for the purity constrained startup acceleration sub-problems given by Equation (7.5), variable purity constraints are used in each stage in order to allow for some contamination in the extract and raffinate products during the first two stages of SMB operation, as this allows the concentration profiles in the unit to build more rapidly. Yet the high-purity constraints are confirmed to be satisfied by the end of the startup phase of SMB operation.

Each SMB startup sub-problem is solved using the nested, single-discretization

approach, described in Section 3.2.2. There are no CSS conditions explicit in the sub-problems, so the number of decision variables is much less than in the simultaneous optimization methods. The DAE system resulting from single-discretization of the SMB model is integrated for the time horizon of a single-stage, and the the objective function and constraints are checked. Each sub-problem was written in gPROMS and solved using SRQPD, which is described in Section 4.3.2 in an iterative scheme until the number of stages specified for the startup period are solved. The CSS concentration profile at the end of a cycle, called $C^*(\tau = 1)$, was solved based on simulation of the SMB model in gPROMS using the optimal CSS operating conditions, called u^*_{CSS}, which are obtained by the PC method described in the next section. In this work, the number of startup stages was found to be 4, thus $P = 4$ and $u_4 = u^*_{CSS}$, following the algorithm proposed by Li *et al.* [56].

7.3 Experimental

7.3.1 SMB Equipment and System Parameters

The SMB unit, C18 columns, and HPLC equipment used in this work are the same as those described in Section 5.3.1. In addition, the experimental techniques used for the PC method in this work are the same as those described in Section 5.3.2. The components of the feed mixture are uridine, A, and guanosine, B, dissolved in the desorbent, which is 90% water and 10% methanol. The SMB model parameters are obtained by the PC method as described in Chapter 5. Two iterations of the PC method are performed using the SMB unit with eight C18 columns to obtain the vector of parameter values, θ_2, used in this study. The CSS optimal operation is shown to satisfy the target purity constraints of 95% in the extract and raffinate products after re-optimizing the SMB with these refined parameters. The initial and refined parameter values are shown in Table 7.1. The initial parameters, called θ_0, were obtained from pervious SMB experiments with uridine and guanosine following

the PC mehtod, shown in Table 5.1 detailed in Section 5.4.1.

Table 7.1: Refinement of θ by parameter estimation following the PC method

Parameter	Initial, θ_0	Refined, θ_1	Refined, θ_2
H_A	0.971	0.901	0.911
H_B	2.80	2.58	2.59
k_A [min^{-1}]	52	52	52
k_B [min^{-1}]	81	81	26

The SMB design and model parameters used in the startup acceleration experiments are given in Table 7.2. The nominal operating conditions, u^*_{CSS}, are shown in Table 7.3. From the given inlet/outlet flow rates, all the flow rates in the SMB system can be calculated. An SMB experiment using optimal operating conditions is performed to test the reliability of the model parameters, and the cumulative product concentration profiles are shown in Figure 7.3. This SMB experiment is performed using the PC method technique, and the SMB model is shown to predict the experimental behavior quite well, although there is some model mismatch in the raffinate profile for component A. The model mismatch is probably due to the fact that the refined model parameters, θ_2, were obtained using experimental data with eight columns in the SMB unit, and the experiment shown in Figure 7.3 was performed using four columns. Yet, the product purities both exceed 95% during CSS operation, and the feed throughput is relatively high for this lab-scale unit.

Table 7.2: System parameters for separation of uridine and guanosine

Parameter	Value
Overall porosity, ϵ_b	0.82
Henry's constant for uridine, H_A	0.911
Henry's constant for guanosine, H_B	2.59
Mass transfer coefficient for uridine, k_A [min^{-1}]	51.7
Mass transfer coefficient for guanosine, k_B [min^{-1}]	26.1
Column diameter, d_c [m]	0.01
Column length, L [m]	0.25
Number of columns, n_{col}	4
Operating temperature, T [°C]	40
Feed concentration of uridine, $c_{A,feed}$ [mg L^{-1}]	42.05
Feed concentration of guanosine, $c_{B,feed}$ [mg L^{-1}]	40.75

Table 7.3: Nominal operating conditions, u^*_{CSS}

Control variable	Value
Step time, t_{step} [min]	3.79
Zone 1 flow rate, F_1 [mL min^{-1}]	7.0*
Feed flow rate, F_{feed} [mL min^{-1}]	1.46
Extract flow rate, F_{ext} [mL min^{-1}]	1.91
Raffinate flow rate, F_{raf} [mL min^{-1}]	1.58

* indicates active upper bound from constrained optimization problem

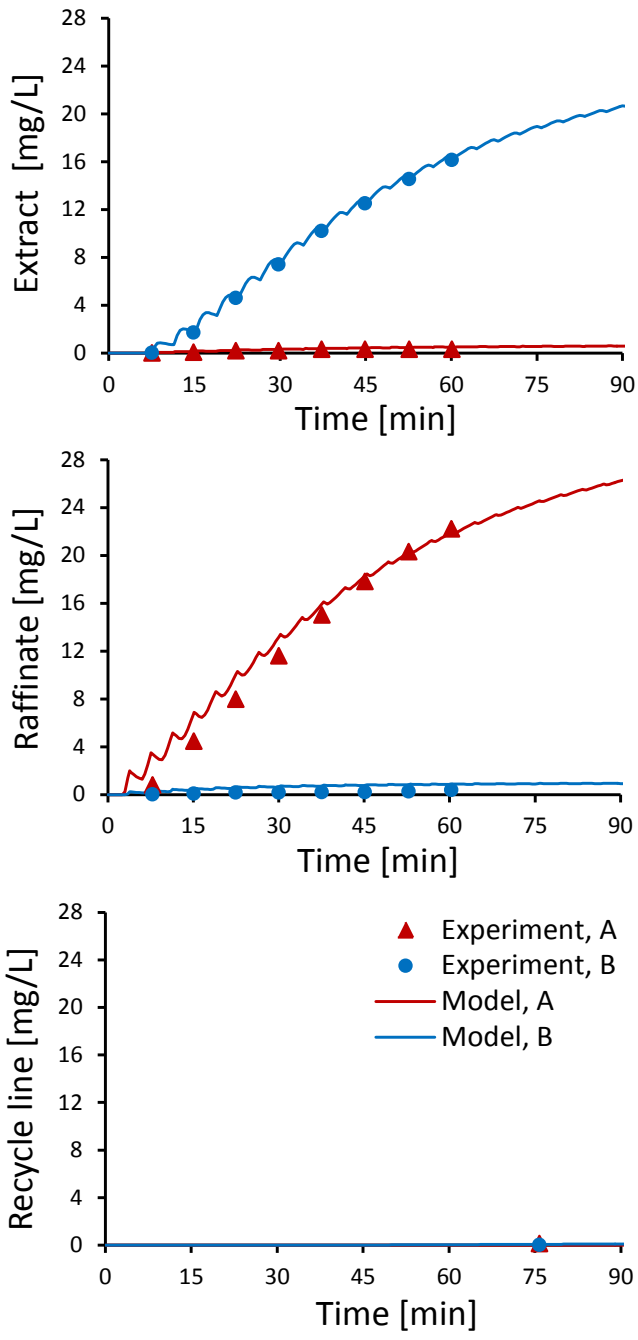

Figure 7.3: Cumulative extract, raffinate, and recycle line concentrations using optimal operating conditions in the SMB unit. The model prediction using refined parameters, θ_2, from Table 7.2 is shown

7.3.2 SMB Startup Experiments

For the SMB startup experiments, the unit is washed with desorbent sufficiently to equilibrate the columns with the mobile phase. For nominal startup, at $t = 0$ the operating conditions are switched to u^*_{CSS}, and the extract and raffinate products are collected once per cycle for a duration of t_{step}, so the average concentration over a step is observed. Based on simulation of the experiment with the SMB model, it is predicted that the system will take a certain number of cycles to reach the CSS concentration values. The time to reach the CSS condition for each component in each product stream is defined using the following equations where relative concentration changes are checked for each measurement:

$$t^{startup}_{ext,i} = \min\{t_n : \left|\frac{c^{ext}_{i,CSS} - c^{ext}_i(n)}{c^{ext}_{i,CSS}}\right| \leq \epsilon_{c,ext,i}, \forall t \geq t_n\} \tag{7.7}$$

$$t^{startup}_{raf,i} = \min\{t_n : \left|\frac{c^{raf}_{i,CSS} - c^{raf}_i(n)}{c^{raf}_{i,CSS}}\right| \leq \epsilon_{c,raf,i}, \forall t \geq t_n\}$$

$$i = A, B$$

where $t^{startup}_{ext,i}$ and $t^{startup}_{raf,i}$ are the times for component i to reach the CSS condition in the extract and raffinate products, t_n is the time that sample n is measured, $c^{ext}_i(n)$ is extract concentration of component i in cycle n, $c^{raf}_i(n)$ is raffinate concentration of component i in sample n, $c^{ext}_{i,CSS}$ and $c^{raf}_{i,CSS}$ are the average concentrations for a step in the extract and raffinate products for component i at the CSS condition, $\epsilon_{c,ext,i}$ is the tolerance on the concentration of component i in the extract, and $\epsilon_{c,raf,i}$ is the tolerance on the concentration of component i in the raffinate. The CSS convergence criteria in Equations (7.7) need to be satisfied for all subsequent samples where $t \geq t_n$ as well. The overall startup time of the SMB process, t_{CSS}, is defined as max $\{t^{startup}_{ext,A}, t^{startup}_{ext,B}, t^{startup}_{raf,A}, t^{startup}_{raf,B}\}$. Therefore, the startup time is limited by the concentration profile that takes the longest to satisfy the CSS condition.

The tolerances in Equations (7.7) are selected based on the relative concentration

values of each component either in the extract or raffinate products. This is done to de-emphasize the convergence of the contaminations in the extract and raffinate products, which have low concentration and may take significantly longer to reach the CSS concentration, yet have a minor effect on product purity. During the SMB startup experiment, the number of cycles that are predicted to satisfy the CSS conditions are sampled, and the CSS conditions are confirmed if there is only a small change in the product concentrations observed over consecutive cycles.

For the accelerated startup experiments performed in this work, it was fixed *a priori* that there would be four stages during startup and four steps, or one cycle, in each stage. The experiments were carried out as follows: At $t = 0$ the operating conditions are switched to u_1, the optimal operating conditions determined for Stage 1, solving the startup acceleration problem. For the first cycle of operation there is no sampling. After cycle 1 is complete, the operating conditions are switched to u_2, and the first sample is taken from the extract and raffinate products during the first step of the second cycle. The operating conditions are switched to u_n in stage n, and the products are sampled once per cycle at the beginning of each cycle. After Stage 4, the CSS optimal operating conditions are used, and sampling continues until the same number of samples are taken as in the nominal startup experiment.

Taking a sample once per cycle is a somewhat coarse measurement of the SMB startup time. In other words, it would be better to have more continuous data, measuring the average concentration over each step of the process. As a consequence of the discrete sampling method, in this work the observed startup times for each experiment have a margin of error equal to plus-or-minus one SMB cycle. Nevertheless, it may be difficult to take more frequent samples of the extract and raffinate products to increase sampling continuity using this technique because the various columns in the SMB may have differing performance, and this could lead to significant differences in

the observed extract and raffinate products over individual steps of operation. Therefore, it is more consistent to measure the products during the same step of each cycle, where the extract and raffiante products are coming from consistent locations in the SMB.

7.4 Results

In this section the experimental results for nominal startup, accelerated startup without purity constraints, and accelerated startup with purity constraints are presented and compared in terms of startup time, average product concentration, desorbent consumption, and cumulative product purities. All results are presented for the SMB unit and system with parameters given in Table 7.2 shown in Section 7.3.1. First the experimental data and model predictions for the different startup strategies are compared. It is of interest to see how well the SMB model can be relied upon for prediction of startup acceleration and calculation of control profiles.

In Figure 7.4 the experimental data and model-predicted product concentration profiles (average concentrations over each step of operation) for the nominal startup strategy are shown. The operating conditions for the nominal startup strategy are in Table 7.3. It can be seen in the figure how the model prediction follows quite well the experimental startup process using the nominal strategy. The CSS condition is confirmed by using Equation (7.7) in Section 7.3.2 with given tolerances. If $\epsilon_{c,ext,A} = \epsilon_{c,raf,B} = 0.04$ and $\epsilon_{c,ext,B} = \epsilon_{c,raf,A} = 0.01$, then the startup time using the nominal strategy is found to be about 170 min. The model predicted that the CSS condition would be satisfied after about 130 min using the same tolerance values. This indicates some model mismatch in the prediction of the contaminant profiles in the extract and raffinate streams. The nominal SMB operating conditions, u^*_{CSS} were also used in the experiment shown in Figure 7.3, but the cumulative product concentrations were measured instead of the average product concentrations over a step.

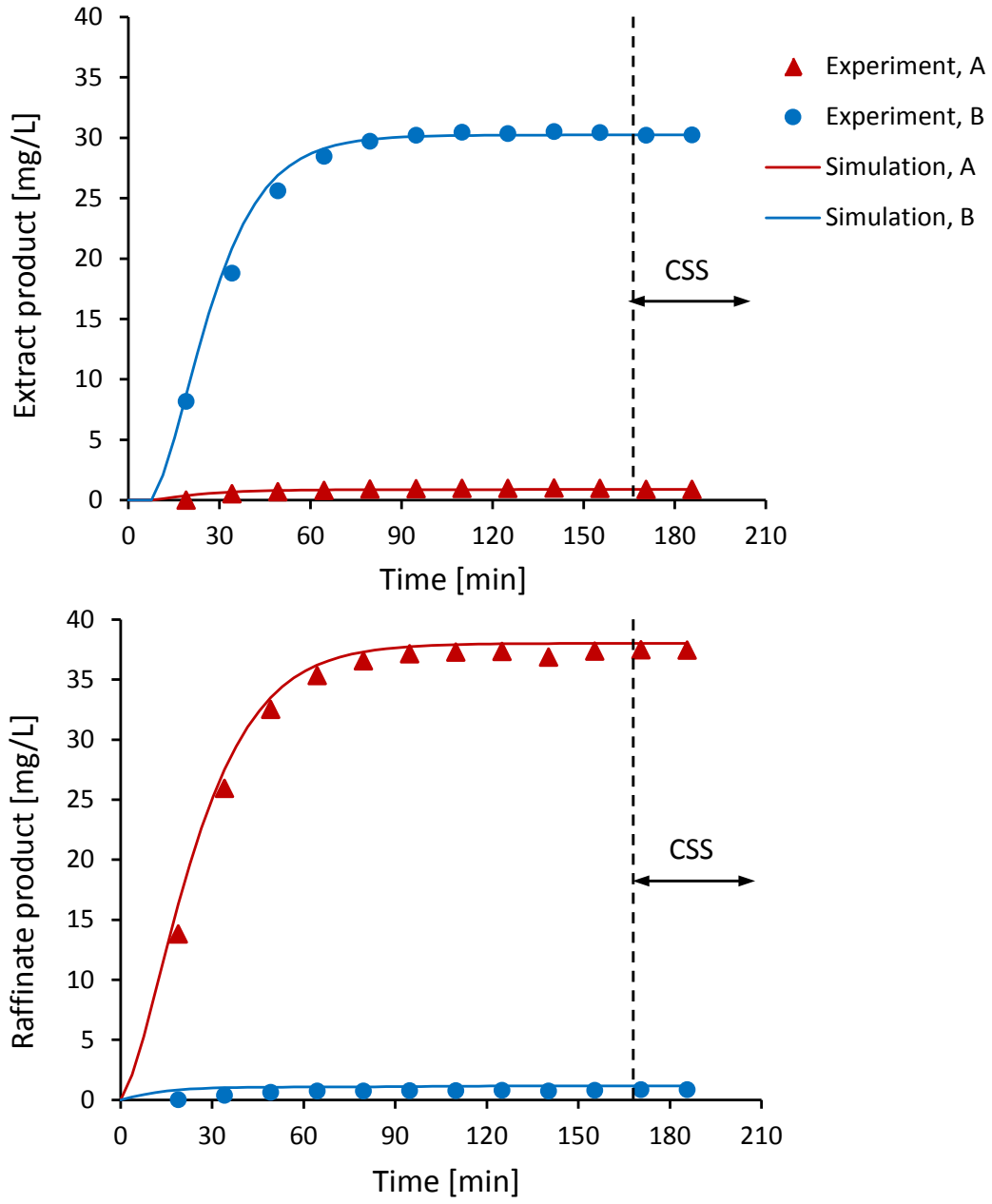

Figure 7.4: Experimental data and model-predicted product concentration profiles using nominal startup strategy. Operating conditions u^*_{CSS} were used, and model parameters in Table 7.2 were used for prediction

In Figure 7.5 the experimental data and model-predicted product concentration profiles for the accelerated startup strategy without purity constraints are superimposed over the nominal startup results. The control variable profiles for the accelerated startup strategy are shown in Figure 7.6. Significant model mismatch is apparent in Figure 7.5 in the first few cycles of operation, and this is probably because there are sharp changes in the operating conditions during Stage 1 and Stage 2. The model prediction does fit the CSS performance and the product concentrations are built-up rapidly in the SMB unit. If the same tolerances in Equation (7.7) are used, $\epsilon_{c,ext,A} = \epsilon_{c,raf,B} = 0.04$ and $\epsilon_{c,ext,B} = \epsilon_{c,raf,A} = 0.01$, then the CSS conditions are satisfied at around 99 min and this time is close to that predicted by the model for accelerated startup. The operating conditions used in this strategy cause a significant contamination in the extract during the first two stages of operation. It may be that the first two cycles of extract product would need to be discarded or reprocessed later in order to improve the extract purity using this startup strategy.

In Figure 7.6 the operating conditions for the four stages of startup operation are shown for the different accelerated startup strategies. These were calculated as discussed in Section 7.2 for stage-wise startup acceleration. It is apparent that the operating conditions for the unconstrained startup acceleration, shown in Figure 7.6a, have sharp changes from one stage to the next. The feed flow rate is increased from the CSS value by 126% in Stage 1, and then it is reduced dramatically in Stage 2. Such sharp changes in operation can lead to model mismatch as shown in Figure 7.5. The operating conditions for startup acceleration with 95% purity constraints, shown in Figure 7.6b, have smoother changes overall and this can result in more predictable SMB operation.

In Figure 7.7 the experimental data and model-predicted product concentration profiles are shown for the accelerated startup strategy with 95% purity constraints superimposed on the nominal startup results. The control variable profiles for the

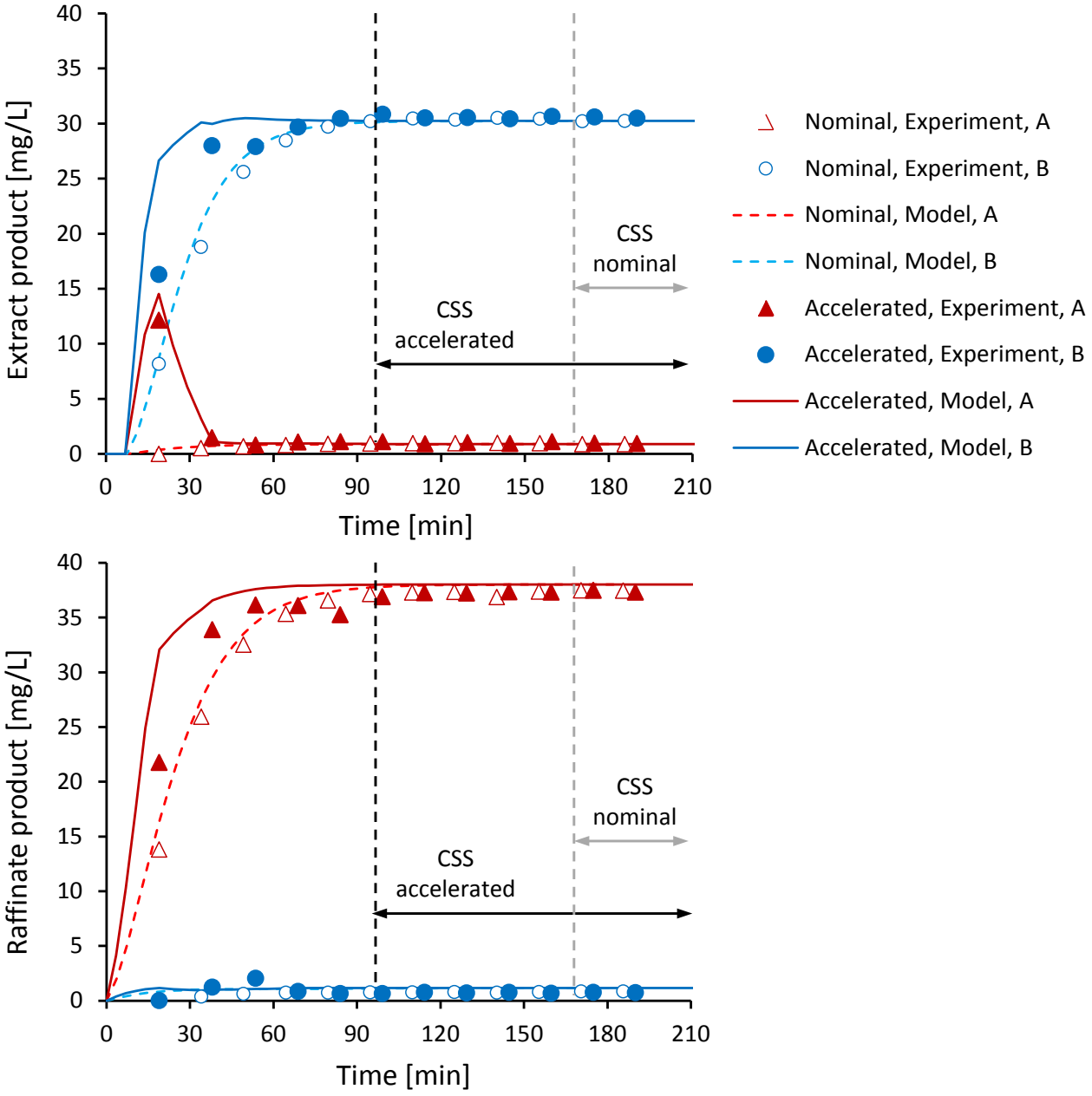

Figure 7.5: Experimental data and model-predicted product concentration profiles using accelerated startup strategy superimposed over nominal startup results

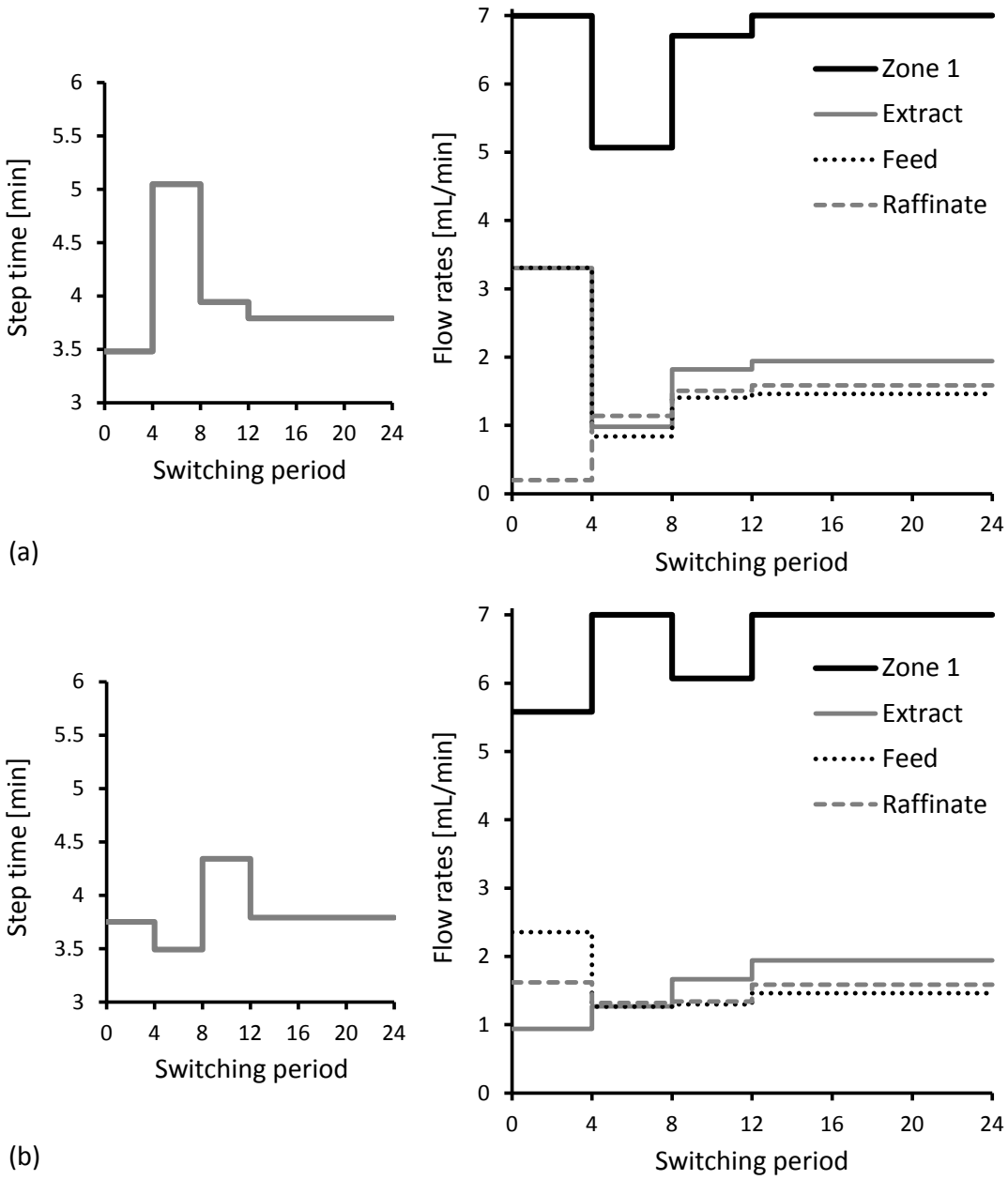

Figure 7.6: Comparison of SMB operating conditions used for (a) accelerated startup and (b) accelerated startup with 95% purity constraints satisfied by end of Stage 3 (switching period 12)

accelerated startup strategy with purity constraints is shown in Figure 7.6b. It can be seen in Figure 7.7 how the model prediction fits quite well the experimental behavior, even in the first few cycles, and this is probably because there are relatively smooth changes in the operating conditions during the three stages where operating conditions are switched to achieve startup acceleration. The model prediction fits well the CSS performance and the product concentrations are built-up rapidly in the SMB unit. If the same tolerances in Equation (7.7) are used, $\epsilon_{c,ext,A} = \epsilon_{c,raf,B} = 0.04$ and $\epsilon_{c,ext,B} = \epsilon_{c,raf,A} = 0.01$, then the CSS conditions are satisfied at around 95 min, and this time is close to that predicted by the model. The operating conditions used in this strategy cause some contamination in the extract and raffinate during the first two stages of operation, yet the product purities are satisfied in the cumulative product tanks after 3 hrs of operation. There is no need to discard any of the products collected in the initial stages of operation.

In solving the purity constrained startup acceleration, the stage-wise optimization problem, shown in Equation (7.4), was constrained by variable minimum product purity constraints in order to allow some contamination in the first stage and accelerate the startup. In Stage 1, $\text{Purity}^{ext}_{B,1,min} = 85\%$, and in Stage 2, $\text{Purity}^{ext}_{B,1,min} = 90\%$, and in Stage 3, $\text{Purity}^{ext}_{B,1,min} = 95\%$, which is the threshold purity in the extract at CSS. The same constraints were set for the raffinate purity of component A, but these constraints were inactive in each of the three stages of optimization.

The startup times reported in Figures 7.4, 7.5, and 7.7 depend on the tolerance values selected for CSS convergence in Equation (7.7). In order to show a complete comparison of the experimental startup times for the three startup strategies, Figure 7.8 shows the time it takes for each experimental concentration profile to satisfy the CSS conditions of Equations (7.7) depending on the tolerance values. The time for each component in the extract stream to reach the CSS condition is denoted $t^{startup}_{ext,i}$, which depends on $\epsilon_{c,ext,i}$. The time for each component in the raffinate stream to

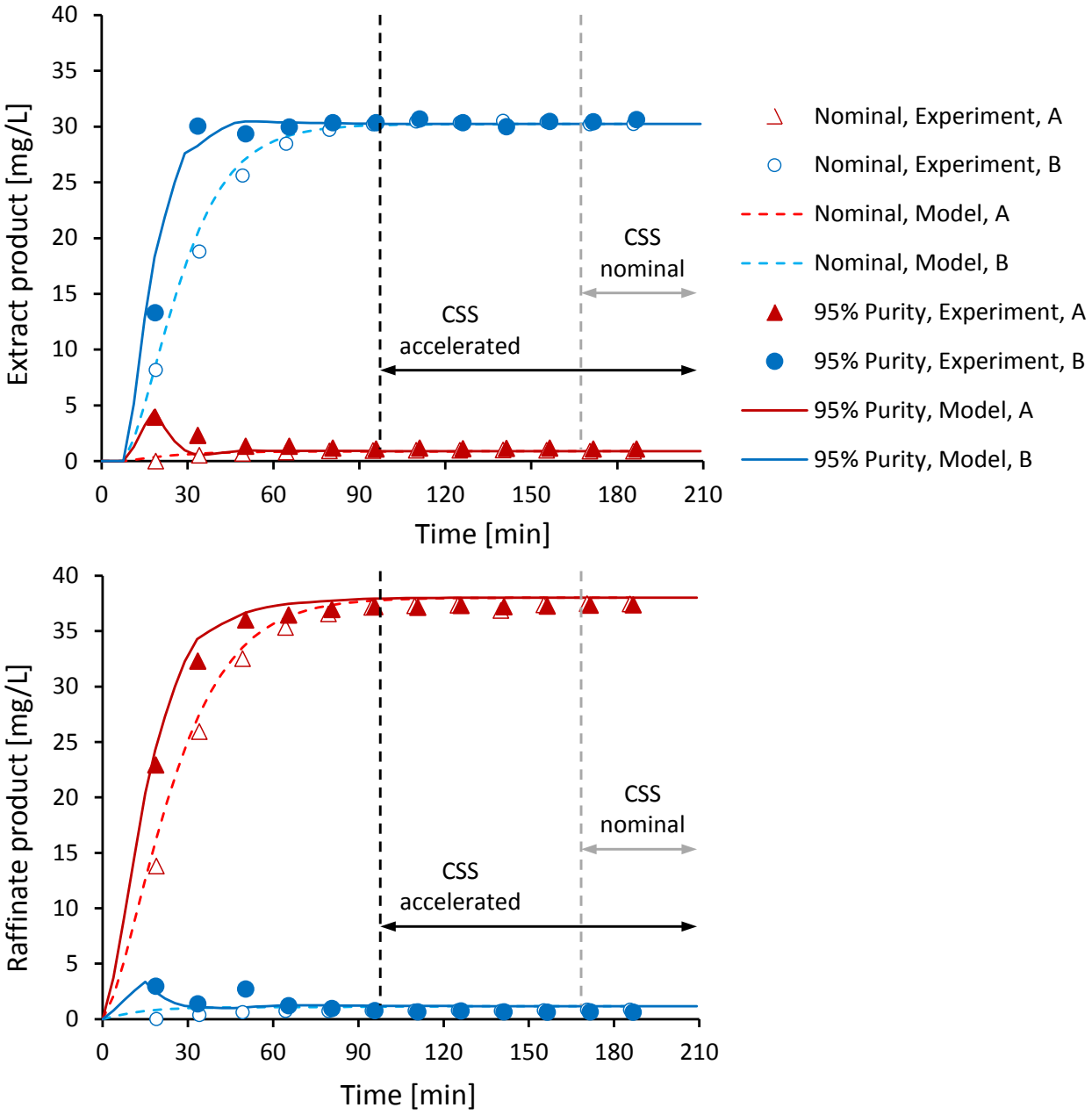

Figure 7.7: Experimental data and model-predicted product concentration profiles using accelerated startup strategy with 95% purity constraints superimposed with nominal startup results

reach the CSS condition is denoted $t_{raf,i}^{startup}$, which depends on $\epsilon_{c,raf,i}$.

From Figure 7.8 it is clear that the startup time generally decreases as the CSS tolerance is loosened. For the nominal strategy the contamination profiles, extract A and raffinate B, the startup time is relatively insensitive to $\epsilon_{c,ext,A}$ and $\epsilon_{c,raf,B}$, unless the tolerance is significantly increased. To compare the startup times for each strategy, there are clearly some values of the tolerance where little-to-no difference is observed between the accelerated and nominal startup, and there are other tolerance values where the difference is more than 50% reduction.

In Figure 7.9, there is a comparison of the three startup strategies in terms of startup time observed experimentally and predicted by the SMB model using $\epsilon_{c,ext,A} = \epsilon_{c,raf,B} = 0.04$ and $\epsilon_{c,ext,B} = \epsilon_{c,raf,A} = 0.01$. The startup time can be expressed in terms of the number of cycles or the absolute time of operation. From this result, it is apparent that the accelerated startup strategy yields about 42% reduction in startup time, and the accelerated startup strategy with 95% purity constraints yields about 44% reduction in startup time. This improvement allows for either a longer period of on-spec production using the SMB unit, or a reduced processing time for a fixed amount of feed. The accelerated startup strategies with and without purity constraints had about the same startup time since the CSS conditions were satisfied within one SMB cycle time of each other. Based on the SMB model predictions, it was expected that there would be approximately 33% reduction in the startup time for both acceleration strategies before the experiments were performed. The nominal startup experiment took significantly longer to reach the CSS condition than predicted by the model. It appears that the model underestimates the nominal startup time of the real system, although the model is able to predict the CSS performance of the SMB. There is some model mismatch apparent in the experimental result shown in Figure 7.3 in Section 7.3.1 which may be compounded in the startup acceleration experiment due to inconsistent flow rates from the SMB

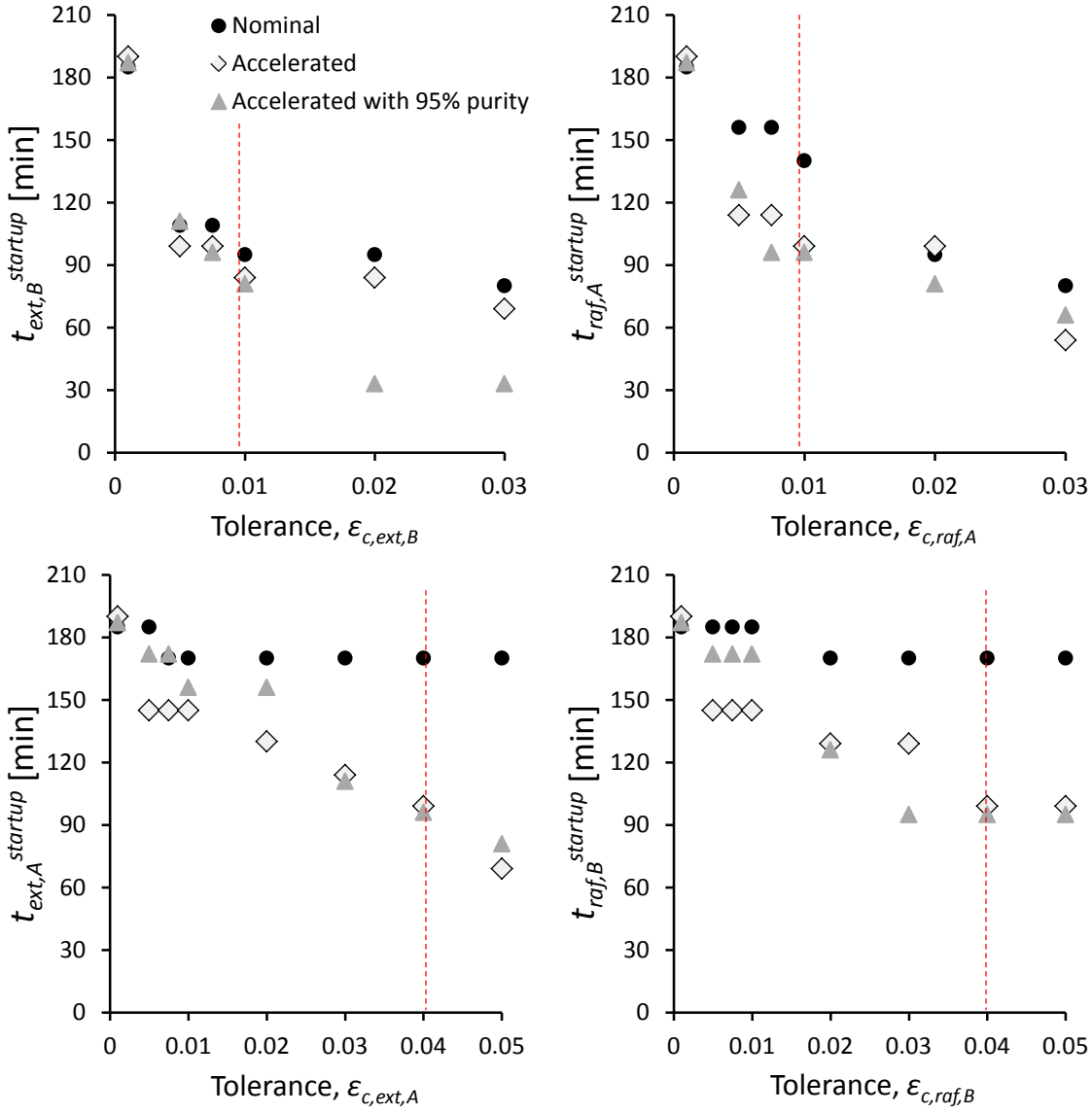

Figure 7.8: Comparison of experimental results measureing the time to reach CSS conditions in each profile, $t_{ext,i}$ and $t_{raf,i}$, for three startup strategies as a function of the CSS tolerance, $\epsilon_{c,ext,i}$ and $\epsilon_{c,raf,i}$, defined by Equation (7.7). Dotted lines indicate the selected tolerances for estimation of CSS conditions shown in Figures 7.4, 7.5, and 7.7

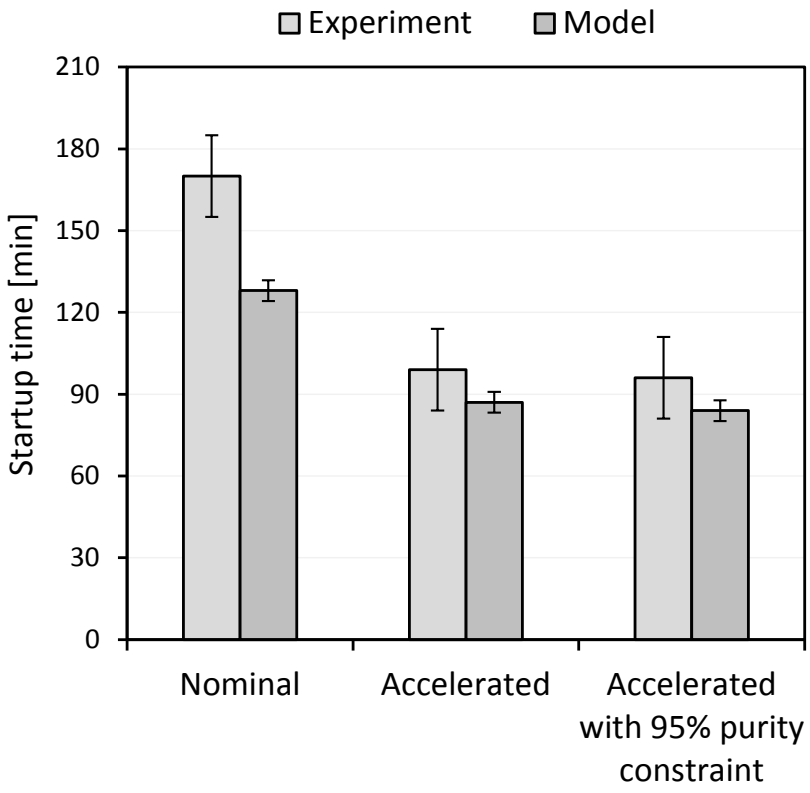

Figure 7.9: Comparison of startup times observed experimentally and predicted by the SMB model for different startup strategies. Error bars show plus-or-minus one SMB cycle time for experimental data and plus-or-minus one SMB step time for model prediction

pumps and unequal separation performance in the different SMB columns.

In Figure 7.9 there is a margin of error in the measurement of startup times equal to plus-or-minus 15.2 min (1 cycle). This error margin is due to the infrequent and discrete sampling strategy used in the SMB startup experiments, and the CSS conditions may be satisfied at some point between the samples. The margin of error for the model prediction of startup time is equal to plus-or-minus 3.8 min (1 step), There is less margin of error in the estimation of the startup time using the simulation of the experiment with the SMB model, because the model provides concentration data for each step of operation.

In Figure 7.10 the experimental average product concentrations are compared over

time for the three startup strategies. The average product concentrations are given by:

$$\text{Average extract concentration of } B = \frac{1}{t}\int_0^t c_B^{ext}\, dt \tag{7.8}$$

$$\text{Average raffinate concentration of } A = \frac{1}{t}\int_0^t c_A^{raf}\, dt$$

which are approximated using the trapezoidal rule with the experimental data points. Due to the accelerated startup strategy, the average product concentrations in the extract and raffinate streams are shown to be increased. The product concentrations increase rapidly in the first few cycles of operation due to average increase of throughput and decrease of desorbent consumption. The concentrations are about 20% greater in the accelerated startup, and about 15% greater is the accelerated startup with 95% purity constraint than in the nominal startup strategy after 100 min of operation. This can lead to significant cost savings in reduced processing time of fixed amount of feed, and reduced evaporation cost of solvent recovery from the products after the SMB processing.

In Figure 7.11, there is a comparison of the three startup strategies in terms of desorbent consumption over time using the piece-wise constant operating conditions. The desorbent consumption is defined as:

$$\text{Desorbent consumption} = \int_0^t F_{des}\, dt \tag{7.9}$$

where F_{des} is the desorbent flow rate. It should be noted from Figure 7.11 that both accelerated startup strategies require the same desorbent consumption in this case study. It may be that if there were more stages with frequent switching of operating conditions, the accelerated startup without purity constraints may save more desorbent than the purity constrained startup strategy. If the SMB is only operated for a short time, about 90 min, this may result in nearly 30% reduction

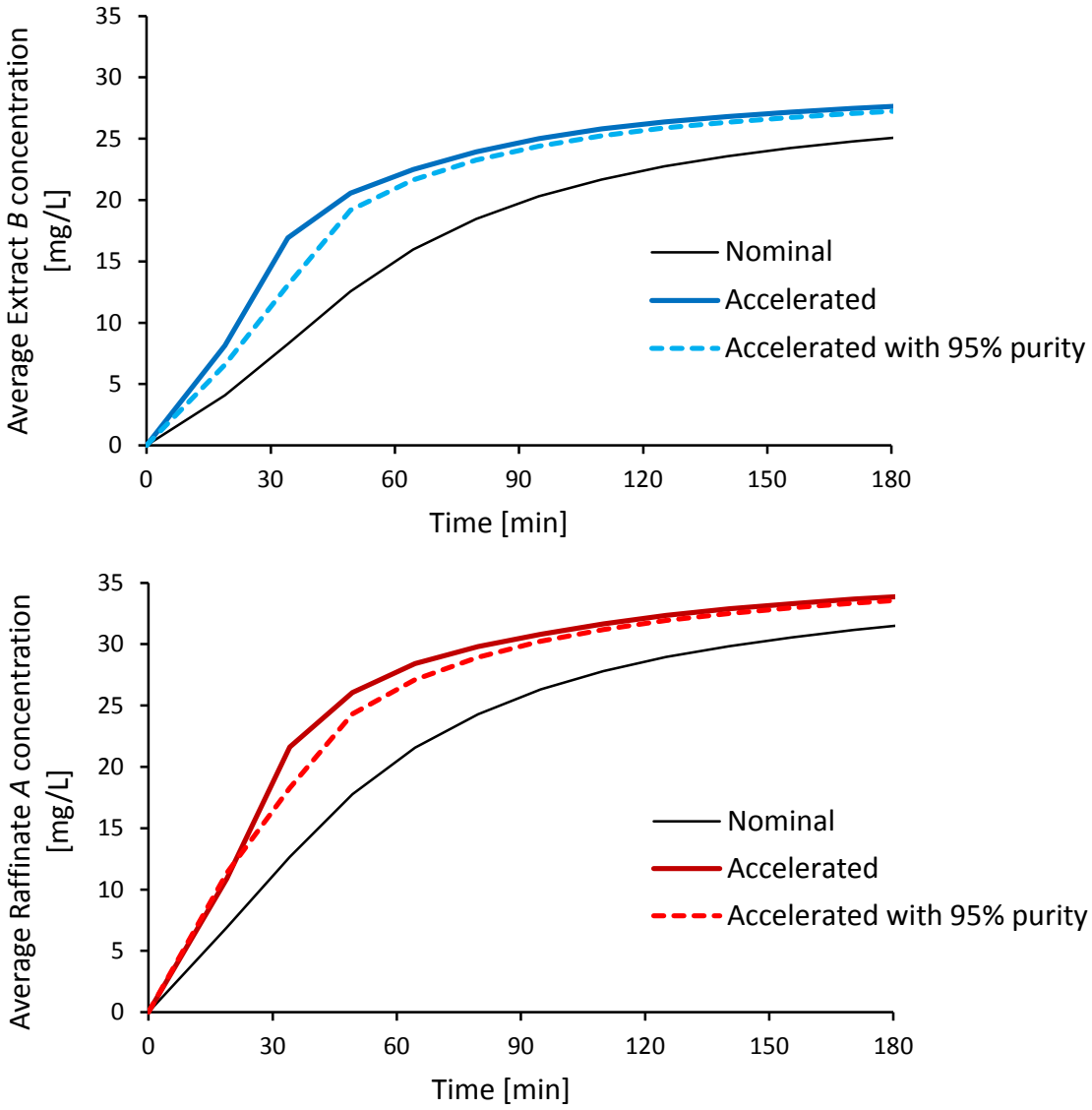

Figure 7.10: Comparison of average product concentrations over time for the three startup strategies. Component B is concentrated in the extract, and component A is concentrated in the raffinate

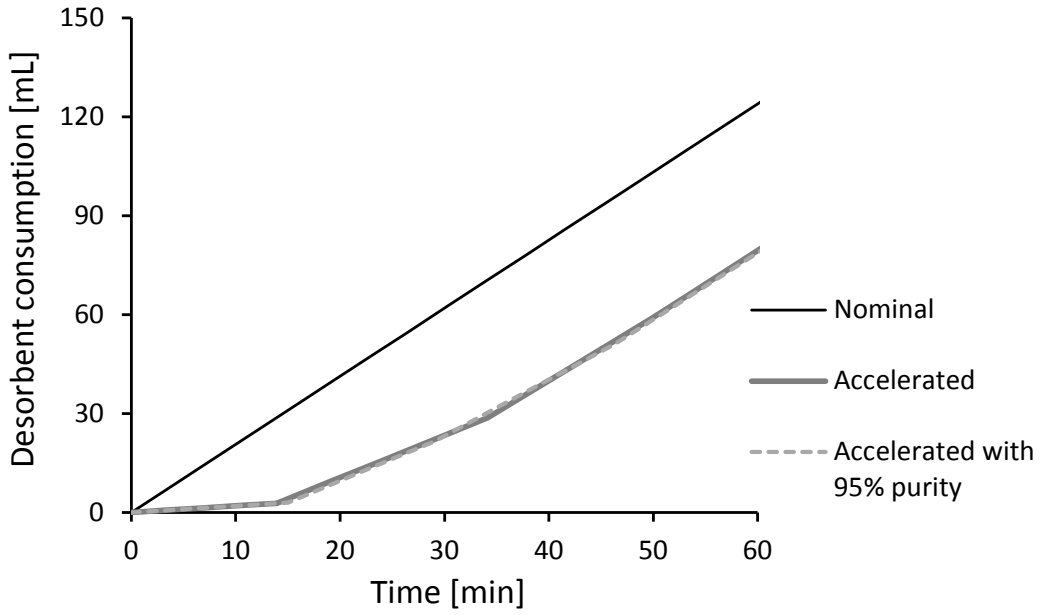

Figure 7.11: Comparison of desorbent consumption over time for different startup strategies. The two accelerated strategies have nearly the same desorbent consumption profile

in desorbent consumption. This can result in significant cost savings if an organic solvent is used in the mobile phase or there is a high turnover frequency with the SMB equipment.

In Figure 7.12, there is a comparison of the three startup strategies in terms of product purities accumulated during startup observed experimentally and predicted by the SMB model. The product purities were measured in the collected product tanks after 3 hrs of operation assuming none of the product is discarded. The target purities were 96% A in the raffinate, and 96% B in the extract product with a 1% safety margin. The accelerated startup strategy had no purity constraints in the optimization problem, and the extract purity was not horrible, but the target purity was not reached in the extract product after 3 hrs of startup operation. Therefore, if this accelerated startup strategy is used, the first cycle or two of product should be discarded in order to preserve the cumulative product purity. It may be unacceptable

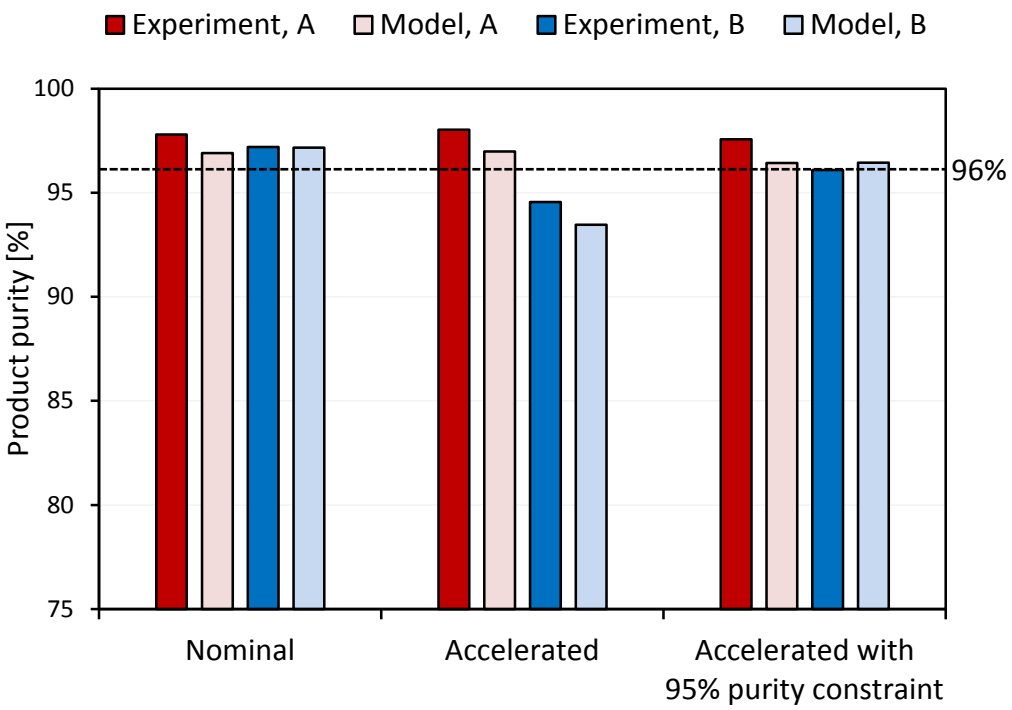

Figure 7.12: Comparison of product purities accumulated over 3 hrs of startup operation observed experimentally and predicted by the SMB model for different startup strategies. The target product purities were 96% A in raffinate, and 96% B in extract

to have to discard or reprocess the off-spec extract product for the first cycle or two of startup. On the other hand, startup acceleration with purity constraints does not have the same drawback, and high purity values were maintained over 3 hrs of operation. Therefore, even though the products collected in the first cycle or two are off-spec, after a few more cycles the purity is re-established in the product tank and no products need to be discarded during startup. In a nonlinear isotherm system, there may be violations in the product purities during startup even using nominal operation, as was reported in [56]. In this case study with a linear isotherm system, the nominal startup strategy maintains high purity values even during startup.

7.5 Conclusion

It has been shown experimentally that the startup time for a real SMB unit can be significantly reduced by solving model-based startup optimization problems using the SMB model developed from the PC method. The startup acceleration without constraints on purity was shown to be successful at reducing the startup time by about 42% although there was model mismatch in the first few cycles of operation, and there was significant contamination in the extract product. On the other hand, the startup acceleration strategy with 95% purity constraints was also successful at reducing the startup time by about 44%, and the model matched the experimental data quite well, and the product purities were both above 96% after 3 hrs of operation. Using a relatively simple startup acceleration strategy of three stages of different operating conditions can yield significant cost savings in terms of decreased processing time, increased average product concentrations, and decreased desorbent consumption. It may be possible to gain further marginal improvements in the startup acceleration if more stages are employed more frequently, i.e. every other step during startup. However, the implementation of such frequent switching of operating conditions would introduce more risk to the process.

CHAPTER 8

CONCLUSIONS AND FUTURE WORK

8.1 Conclusions

The results presented in this thesis have met the three main objectives stated in Chapter 2:

1. Provide framework for systematic decision-making between rival gas phase adsorption processes for the same separation problem

2. Streamline the process development methodology for SMB chromatography through simultaneous modeling and optimization

3. Demonstrate the optimization of transient operation of SMB processes for significant cost savings

In the investigation of SMB and PSA processes for the gaseous separation of enantiomers by multi-objective optimization, there is a systematic framework developed for making decisions about which process to use. Basically, there is a trade-off that exists in choosing the classical SMB or PSA operations. It has been found that the SMB process achieves high recovery which can be greater than 99%, while the recovery using 4-step PSA considered in this work remains relatively low. Nevertheless, the higher throughput of the PSA process can be a significant advantage for inexpensive feed mixtures. Even at reduced recovery, the productivity of the target component can be greater in PSA than the maximum productivity possible in SMB. Also, the PSA process features a low desorbent-to-feed ratio compared to SMB and this is also economically advantageous if the product concentration must be high or desorbent

cost cannot be neglected. The two processes were modeled using the same fundamental transport, kinetic, and thermodynamic models, with the same model parameters, and the same optimization method with the same constraints was used to compare the processes on a fair basis.

For the enantiomer separation of enflurane in particular, it is found that gas phase SMB is a good option to produce both *R*- and *S*-enflurane with high purity and recovery simultaneously. The same chiral stationary phase can be used to capture both enantiomers in a pure form that can be used for clinical trials to determine the efficacy of each enantiomer as a general anesthetic. If large scale production of a single-enantiomer is desired, the PSA may achieve greater productivity of a single-enantiomer from the racemic mixture.

The second objective is satisfied by the work on prediction-correction (PC) method presented in Chapters 5 and 6. The PC algorithm for SMB process development has been proposed and tested for both linear and nonlinear systems with the inclusion of a model selection step so that the SMB process is systematically modeled and optimized simultaneously. The PC algorithm was found to be efficient in numerous laboratory experiments with both linear and nonlinear isotherm systems. In two case studies of convergence, the algorithm was terminated in only two switches of the operating conditions while maintaining high purity constraints and maximizing the feed throughput. In other case studies of robustness the product purities were improved by about 30% in a single step for the linear and nonlinear systems when the initial model parameter estimates or initial isotherm model were poor. The PC algorithm is designed to proceed in an automatic and sequential manner until it terminates itself so that an SMB expert is not required to manually tune the SMB operating conditions. It should also be noted that this algorithm is designed to function with any choice of the isotherm model, with the possibility of updating the isotherm model systematically during the procedure. Overall, the PC method can be a reliable process

development strategy that may take only hours to arrive at the optimal operating conditions for a new separation problem. Meanwhile, the conventional methods for SMB process development, with more careful characterization of adsorption behavior using batch experiments, and manual tuning of the SMB unit, can take days and weeks.

The third objective is met because it is shown that the startup time for a real SMB unit can be significantly reduced by solving model-based startup optimization problems using the SMB model developed from the PC method. The SMB model parameters were obtained following the PC method, and the model-prediction is reliable enough to solve the stage-wise optimization problem and implement the piece-wise constant control profiles in the SMB. The startup acceleration without constraints on purity was shown to be successful at reducing the startup time by about 42% although there was model mismatch in the first few cycles of operation, and there was significant contamination in the extract product. On the other hand, the startup acceleration strategy with 95% purity constraints was also successful at reducing the startup time by about 44%, and the model matched the experimental data quite well, and the product purities were both above 96% after 3 hrs of operation. Using a relatively simple startup acceleration strategy of three stages with different operating conditions can yield significant cost savings in terms of decreased processing time, increased average product concentrations, and reduced desorbent consumption.

The startup acceleration results that are presented in Chapter 7 are conservative because the operating conditions were not switched more than three time during the startup operation, and the model prediction was not as reliable as it could be. The SMB model parameters used to solve the startup acceleration problems were obtained by performing the steps of the PC algorithm on a different system configuration. In particular, eight columns were used in the SMB for two iterations of the PC method, and then the estimated parameters were used to optimize a four column configuration

which is presented in this work. It may be possible to obtain more reduction in the SMB startup time with a more reliable set of model parameters, even using the same basic startup acceleration strategies.

Overall, this work shows that model-based optimization strategies can be successfully applied in practice to make systematic decisions regarding the separation problems that were studied. The optimization problems that were considered solve for cyclic steady state operating conditions, model parameter values through data-fitting, and optimal control profiles for transient operation. In comparing processes through multi-objective optimization, the trade-off between productivity and purity of products can be clearly seen. Thus, depending on the production goals, the favored process may be clearly determined by analyzing the optimization results. Therefore, as efforts are made to improve the prediction of physical phenomena through modeling, and the optimization tools and computation power are ever-improving, there will continue to be more application areas of model-based optimization for systematic decision-making in industry.

8.2 Future Work

After surveying the work done in this thesis, there are some open questions and opportunities for future research projects.

8.2.1 Separation of Gaseous Enantiomers Via Adsorption Processes

Some of the extensions of this work on the separation of gaseous enantiomers are already underway. In this project, which is discussed on Chapter 4, there will be experimental work where samples of enflurane racemate are obtained from a hospital in Magdeburg, Germany, and gas chromatographic separations are performed to provide enantiomerically pure anesthetics for some clinical trials. Yet the chiral stationary phase for this project is still under development.

There are other aspects of this project dealing with rival separation processes

that were limited in this thesis and may be explored further. Although there is a presentation of systematic decision-making procedures using model-based optimization in this work, certain decision variables are fixed in the formulation of the optimization problems. For example, there is no work performed here on the optimization of equipment size or mobile phase composition or operating temperature, etc. for SMB or PSA units. There is also no discussion of superstructure optimization for the processes in question; that is the number of columns, adjustments of flow rates and operating strategies, such as PowerFeed and ModiCon strategies for SMB, and pressure equalization steps for PSA, were not considered. Only the base-case system configurations and operating strategies which are typically used in the chemical industry are considered for the various separation problems. There are others who have solved superstructure optimization problems to discover the best column configurations and operation strategies for SMB, PSA, and other adsorption processes [45, 49, 61] but these have not been compared for the same gaseous separation problem. In addition to this, there may be further investigations of hybrid systems. For example, the hybrid SMB-PSA unit proposed by [51] may be investigated using multi-objective optimization to see any performance improvements for gaseous enantiomer separation. Furthermore, there may be interesting hybrid units to investigate in model-based optimization studies involving SMB-membrane and PSA-membrane processes.

8.2.2 SMB Process Development Using the PC Method

There are some additional experimental case studies where the PC method has been applied by others to develop optimal SMB operating conditions for a new mixture. For example, the PC method has been used to optimize an SMB unit for binary sugar separations, although using a different parameter estimation strategy [73]. In that work some SMB operating strategies were derived from the superstructure optimization of SMB units [45]. The PC method is also being applied to optimize an SMB

unit for ternary sugar separations, although with a different parameter estimation strategy. In that work some unique SMB operating strategies that are derived from superstructure optimization of SMB units for ternary separation are being used [7]. Ternary separations remain a significant challenge in separations technology.

There are some aspects of the PC method that deserve to be further explored. All of the separation problems considered in this work are binary systems. There is currently work underway to model and optimize SMB separations with ternary mixtures, however, these applications are not discussed in this thesis [7]. The methodology described in this thesis for process modeling and optimization is applicable to multi-component systems, and the results presented in this thesis perhaps may be generalized for multi-component systems. In addition, there may be other isotherm models, such as the Toth isotherm, or transport models, such as the general rate model, that can be used to fit experimental data from the SMB unit. The computational methods may be investigated further to minimize the computational effort for SMB optimization and parameter estimation in each iteration of the PC algorithm. Also, it may be desired to design a specific SMB experiment in the first iteration of the PC method that will maximize the usefulness of the concentration data for estimating model parameters using design of experiments.

8.2.3 Optimal Startup Operation for SMB

In the startup acceleration project, there are still some interesting open questions, such as applications for nonlinear isotherm systems and increased number of stages, that can be explored after the experimental proof of concept shown in this work. It may be shown that the nominal startup takes a significantly long time to reach the CSS conditions, and through model-based optimization, the startup may be dramatically shortened. Also, if more stages are employed in the early SMB cycles with more

frequent switching of the operating conditions, the startup may be further accelerated with additional cost savings on increased product concentrations and reduced desorbent consumption. There may also be other optimization problem formulations for optimal transient operation scenarios for SMB that can be further investigated. For example, in a scenario where there is a fixed amount of feed to be processed by an SMB unit, an alternative optimal control problem may be written as:

$$
\begin{aligned}
\min \quad & \phi_{SMB}(u(t)) &=\ & t_f && (8.1)\\
\text{s.t.} \quad & \int_0^{t_f} F_{feed}(t)\rho_{feed}\,dt &=\ & M_{feed} &&\\
& \text{Purity}_A^{raf} &\geq\ & \text{Purity}_{A,min}^{raf}, \quad \text{Purity}_B^{ext} \geq \text{Purity}_{B,min}^{raf} &&\\
& 0 \leq F_x &\leq\ & F_{max}, \quad x = 1,2,3,4 &&\\
& F_1 - F_2 &\geq\ & 0, \quad F_1 - F_4 \geq 0, &&\\
& F_3 - F_2 &\geq\ & 0, \quad F_3 - F_4 \geq 0 &&
\end{aligned}
$$

Equations (3.1) - (3.3), (3.6), (3.7), (3.8)

where $u(t)$ is the vector of SMB control variables that vary with time, ρ_{feed} is the density of the feed mixture and M_{feed} is the mass of feed mixture to be processed. In other words, the problem is to minimize the time to separate the feed mixture subject to some minimum product purity constraints. This problem may be used to find an optimal SMB operating strategy where the system does not reach any CSS conditions before the feed is all processed and the SMB unit can be shutdown.

In addition to this, the optimal shutdown strategy proposed by Li *et al.* [56] can be verified by some additional experimental work with the SMB unit.

APPENDIX A

DEFINITIONS OF PERFORMANCE MEASURES FOR SMB AND PSA

This appendix will show how the performance measures of throughput, productivity and desorbent-to-feed ratios are calculated in the comparison of SMB and PSA processes. Some sample calculations will also be shown for clarity.

A.1 Throughput

Feed throughput is defined as the mass of feed mixture supplied per unit time per unit volume of adsorbent in the SMB or PSA configuration. For the gas phase SMB unit the throughput is written as:

$$\text{Throughput}_{SMB} = \frac{P v_{s,feed} A_{col} \text{MW}_{ave}}{RT n_{col} V_{col} (1 - \epsilon_b)} \tag{A.1}$$

where P is the total pressure, $v_{s,feed}$ is the superficial velocity of the feed, A_{col} is the column cross-sectional area, MW_{ave} is the average molecular weight of the feed mixture, R is the gas constant, T is the temperature, n_{col} is the number of columns in the SMB unit, V_{col} is the column volume, and ϵ_b is the overall porosity of the packed bed. This equation was used to calculate the throughput values at each optimal solution of the Pareto plot shown in Figure 4.7 for the SMB unit. A sample calculation is performed by plugging the values given in Table A.1 into Equation (A.1). Using those values the throughput for SMB is found to be 5.0 g_{feed} day^{-1} cm^{-3} after applying the proper conversion factors.

For the PSA unit the throughput is written as:

$$\text{Throughput}_{PSA} = \frac{P_H v_{s,feed} A_{col} \text{MW}_{ave} \rho_{ads}}{RT V_{col} (1 - \epsilon_b)} \tag{A.2}$$

Table A.1: System parameters at SMB optimal point with 99% raffinate purity and 99% raffinate recovery for throughput calculation

System parameter	Value
P [bar]	4.5
$v_{s,feed}$ [m sec^{-1}]	0.020
A_{col} [m^2]	1.77×10^{-4}
MW$_{ave}$ [g mol^{-1}]	33.7
R [bar m^3 mol^{-1} K^{-1}]	8.31×10^{-5}
T [K]	306
n_{col}	4
V_{col} [m^3]	2.83×10^{-4}
ϵ_b	0.75

Table A.2: System parameters at PSA optimal point with 99% raffinate purity and 27.3% raffinate recovery for throughput calculation

System parameter	Value
P_H [bar]	4.5
$v_{s,feed}$ [m sec^{-1}]	0.022
A_{col} [m^2]	1.77×10^{-4}
MW$_{ave}$ [g mol^{-1}]	33.7
ρ_{ads}	0.74
R [bar m^3 mol^{-1} K^{-1}]	8.31×10^{-5}
T [K]	306
V_{col} [m^3]	2.83×10^{-4}
ϵ_b	0.75

where P_H is the high pressure during adsorption step, and ρ_{ads} is the ratio of time for adsorption, t_{ads}, to the time for a cycle, t_{cycle}. This equation was used to calculate the throughput values at each optimal solution of the Pareto plot shown in Figure 4.7 for the PSA unit. A sample calculation is performed by plugging the values given in Table A.2 into Equation (A.2). Using those values the throughput for PSA is found to be 16.6 g$_{feed}$ day^{-1} cm^{-3} after applying the proper conversion factors.

A.2 Productivity

Productivity is defined as the mass of target product produced per unit time given the SMB or PSA configuration. For the gas phase SMB unit the productivity of

component A, which is the target enantiomer, is written as:

$$\text{Productivity}_{SMB,A} = \text{Throughput}_{SMB} \times y_{A,feed} \frac{\text{MW}_A}{\text{MW}_{ave}} \times \text{Recovery}_A^{raf} \times n_{col} V_{col} (1 - \epsilon_b) \tag{A.3}$$

where Throughput_{SMB} is given by Equation (A.1), $y_{A,feed}$ is the mole fraction of component A in the feed, MW_A is the molecular weight of component A, Recovery_A^{raf} is given by Equation (4.14). Therefore, the productivity depends on both the feed throughput and the target recovery of the process. This equation was used to calculate the productivity values at each optimal solution of the Pareto plot shown in Figure 4.8 for the SMB unit. A sample calculation is performed by plugging the values given in Table A.3 into Equation (A.3). Using those values, the productivity for an SMB unit with 4 columns is found to be 218 g_A day^{-1} after applying the proper conversion factors.

For PSA the productivity of component A, is written as:

$$\text{Productivity}_{PSA,A} = \text{Throughput}_{PSA} \times y_{A,feed} \frac{\text{MW}_A}{\text{MW}_{ave}} \times \text{Recovery}_A^{raf} \times V_{col} (1 - \epsilon_b) \tag{A.4}$$

where Throughput_{PSA} is given by Equation (A.2), and Recovery_A^{raf} is given by Equation (4.16). This equation was used to calculate the productivity values at each optimal solution of the Pareto plot shown in Figure 4.8 for the PSA unit. A sample calculation is performed by plugging the values given in Table A.4 into Equation (A.4). Using those values, the productivity for a PSA unit with a column volume equivalent to the SMB system is found to be 167 g_A day^{-1} after applying the proper conversion factors.

Table A.3: System parameters at SMB optimal point with 99% raffinate purity and 99% raffinate recovery for productivity calculation

System parameter	Value
Throughput$_{SMB}$ [g$_{feed}$ day^{-1} cm^{-3}]	5.0
$y_{A,feed}$	0.018
MW$_A$ [g mol^{-1}]	184.5
MW$_{ave}$ [g mol^{-1}]	33.7
Recovery$_A^{raf}$ [n_{col}	4
V_{col} [m^3]	2.83×10^{-4}
ϵ_b	0.75

Table A.4: System parameters at PSA optimal point with 99% raffinate purity and 27.3% raffinate recovery for productivity calculation

System parameter	Value
Throughput$_{PSA}$ [g$_{feed}$ day^{-1} cm^{-3}]	16.6
$y_{A,feed}$	0.018
MW$_A$ [g mol^{-1}]	184.5
MW$_{ave}$ [g mol^{-1}]	33.7
Recovery$_A^{raf}$ [V_{col} [m^3]	1.13×10^{-3}
ϵ_b	0.75

A.3 Desorbent-to-Feed Ratio

The desorbent-to-feed ratio, or D/F ratio, is defined as the volume of desorbent supplied over the volume of feed supplied to the SMB or PSA systems. For the gas phase SMB unit the D/F ratio is simply written as:

$$\mathrm{D/F}_{SMB} = \frac{v_{s,des}}{v_{s,feed}} \tag{A.5}$$

where $v_{s,des}$ is the superficial gas velocity of the desorbent. The D/F ratios are calculated using all the optimal operating conditions for SMB in the Pareto plot shown in Figure 4.9. In fact, for all of the optimal SMB operating conditions, $v_{s,des}$ was nearly constant at 4.6 cm sec^{-1}.

For the PSA unit the D/F ratio is written as:

$$\mathrm{D/F}_{PSA} = \frac{P_{press} v_{s,press} \rho_{press} + P_L v_{s,purge} \rho_{purge}}{P_H v_{s,feed} \rho_{ads}} \tag{A.6}$$

where P_{press} is the average pressure during the pressurization step, which is the average of P_H and P_L, where P_L is the low pressure during the purge step, $v_{s,press}$ is the average superficial velocity of the desorbent supplied during the pressurization step, ρ_{press} is the ratio of t_{press} to t_{cycle}, $v_{s,purge}$ is the superficial velocity of the desorbent supplied during the purge step, and ρ_{purge} is the ration of t_{purge} to t_{cycle}. This equation was used to calculate the D/F values at each optimal solution of the Pareto plot shown in Figure 4.9 for the PSA unit. A sample calculation is performed by plugging the values given in Table A.5 into Equation (A.6). Using those values, the D/F ratio for a PSA unit is found to be 0.343, which is quite low compared to the SMB unit.

Table A.5: System parameters at PSA optimal point with 99% raffinate purity and 27.3% raffinate recovery for D/F ratio calculation

System parameter	Value
P_{press} [bar]	2.76
$v_{s,press}$ [m sec^{-1}]	0.021
ρ_{press}	0.029
P_L [bar]	1.01
$v_{s,purge}$ [m sec^{-1}]	0.107
ρ_{purge}	0.204
P_H [bar]	4.5
$v_{s,feed}$ [m sec^{-1}]	0.022
ρ_{press}	0.74

REFERENCES

[1] "Model builder guide," 2011. Published by Process Systems Enterprise Ltd., www.psenterprise.com.

[2] "Model validation guide," 2011. Published by Process Systems Enterprise Ltd., www.psenterprise.com.

[3] "Optimisation guide," 2011. Published by Process Systems Enterprise Ltd., www.psenterprise.com.

[4] Abel, S., Erdem, G., Amanullah, M., Morari, M., Mazzotti, M., and Morbidelli, M., "Optimizing control of simulated moving bedsexperimental implementation," *J. Chromatogr. A*, vol. 1092, no. 1, pp. 2–16, 2005.

[5] Aboul-Enein, H., Bojarski, J., Szymura-Oleksiak, J., and others, "The impact of chirality of the fluorinated volatile inhalation anaesthetics on their clinical applications," *Biomed. Chrom.*, vol. 14, no. 4, pp. 213–218, 2000.

[6] Aboul-Enein, H. and Wainer, I., *The impact of stereochemistry on drug development and use*, vol. 142. Wiley-Interscience, 1997.

[7] Agrawal, G. and Kawajiri, Y., "Comparison of various ternary simulated moving bed separation schemes by multi-objective optimization," *J. Chromatogr. A*, 2012.

[8] Akaike, H., "A new look at the statistical model identification," *Autom. Control IEEE*, vol. 19, no. 6, pp. 716–723, 1974.

[9] Altenhoner, U., Meurer, M., Strube, J., and Schmidt-Traub, H., "Parameter estimation for the simulation of liquid chromatography," *J. Chromatogr. A*, vol. 769, no. 1, pp. 59–69, 1997.

[10] Araújo, J., Rodrigues, R., and Mota, J., "Determination of competitive isotherms of enantiomers by a hybrid inverse method using overloaded band profiles and the periodic state of the simulated moving-bed process," *J. Chromatogr. A*, vol. 1189, no. 1, pp. 302–313, 2008.

[11] Bentley, J. and Kawajiri, Y., "Prediction-correction method for optimization of simulated moving bed chromatography," *AIChE J.*, 2012.

[12] Bentley, J., Huang, Q., Kawajiri, Y., Eic, M., and Seidel-Morgenstern, A., "Optimizing the separation of gaseous enantiomers by simulated moving bed and pressure swing adsorption," *Adsorption*, vol. 17, pp. 159–170, 2011.

[13] Bhaskar, V., Gupta, S., and Ray, A., "Applications of multiobjective optimization in chemical engineering," *Rev. Chem. Eng.*, vol. 16, no. 1, pp. 1–54, 2000.

[14] Biegler, L. T., Grossmann, I. E., and Westerberg, A. W., "A note on approximation techniques used for process optimization," *Comput. Chem. Eng.*, vol. 9, pp. 201–206, 1985.

[15] Biegler, L., *Nonlinear programming: concepts, algorithms, and applications to chemical processes*. SIAM, 2010.

[16] Biressi, G., Mazzotti, M., and Morbidelli, M., "Experimental investigation of the behavior of gas phase simulated moving beds," *J. Chromatogr. A*, vol. 957, no. 2, pp. 211–225, 2002.

[17] Biressi, G., Quattrini, F., Juza, M., Mazzotti, M., Schurig, V., and Morbidelli, M., "Gas chromatographic simulated moving bed separation of the enantiomers of the inhalation anesthetic enflurane," *Chem. Eng. Sci.*, vol. 55, no. 20, pp. 4537–4547, 2000.

[18] Broughton, D., "Continuous sorption process employing fixed bed," May 23 1961. US Patent 2,985,589.

[19] Cheng, L. and Wilson, S., "Process for separating propylene from propane," Sept. 25 2001. US Patent 6,293,999.

[20] Do, D., *Adsorption analysis: equilibria and kinetics*, vol. 2. World Scientific, 1998.

[21] Dünnebier, G., Fricke, J., and Klatt, K., "Optimal design and operation of simulated moving bed chromatographic reactors," *Ind. Eng. Chem. Res.*, vol. 39, no. 7, pp. 2290–2304, 2000.

[22] Dünnebier, G. and Klatt, K., "Modelling and simulation of nonlinear chromatographic separation processes: a comparison of different modelling approaches," *Chem. Eng. Sci.*, vol. 55, no. 2, pp. 373–380, 2000.

[23] Eger, E., Koblin, D., Laster, M., Schurig, V., Juza, M., Ionescu, P., Gong, D., and others, "Minimum alveolar anesthetic concentration values for the enantiomers of isoflurane differ minimally," *Anesth. Analg.*, vol. 85, no. 1, pp. 188–192, 1997.

[24] Engell, S. and Toumi, A., "Optimisation and control of chromatography," *Comput. Chem. Eng.*, vol. 29, no. 6, pp. 1243 – 1252, 2005.

[25] Erdem, G., Abel, S., Amanullah, M., Morari, M., Mazzotti, M., and Morbidelli, M., "Automatic control of simulated moving bedsexperimental verification," *Adsorption*, vol. 11, pp. 573–577, 2005.

[26] Feist, S. D., Hasabnis, Y., Pynnonen, B. W., and Frank, T. C., "Smb chromatorgaphy design using profile advancement factors, miniplant data, and rate-based process simulation," *AIChE J.*, vol. 55, pp. 2848–2860, 2009.

[27] Felinger, A., Cavazzini, A., and Guiochon, G., "Numerical determination of the competitive isotherm of enantiomers," *J. Chromatogr. A*, vol. 986, no. 2, pp. 207–225, 2003.

[28] Fourer, R., Gay, D., and Kernighan, B., "Ampl modeling language," *Mathematical Programming. Pacific Grove, CA: Thompson Learning*, 2003.

[29] Garton, K., Yuen, P., Meinwald, J., Thummel, K., and Kharasch, E., "Stereoselective metabolism of enflurane by human liver cytochrome p450 2e1," *Drug Metab. Dispos.*, vol. 23, no. 12, pp. 1426–1430, 1995.

[30] Golshan-Shirazi, S. and Guiochon, G., "Comparison of the various kinetic models of non-linear chromatography," *J. Chromatogr. A*, vol. 603, no. 1, pp. 1–11, 1992.

[31] Grosfils, V., Hanus, R., Wouwer, A. V., and Kinnaert, M., "Parametric uncertainties and influence of the dead volume representation in modelling simulated moving bed separation processes," *J. Chromatogr. A*, vol. 1217, pp. 7359–7371, 2010.

[32] Grosfils, V., Levrie, C., Kinnaert, M., and Wouwer, A. V., "A systematic approach to smb processes model identification from batch experiments," *Chem. Eng. Sci.*, vol. 62, pp. 3894–3908, 2007.

[33] Grossmann, C., Amanullah, M., Morari, M., Mazzotti, M., and Morbidelli, M., "Optimizing control of simulated moving bed separations of mixtures subject to the generalized langmuir isotherm," *Adsorption*, vol. 14, no. 2, pp. 423–432, 2008.

[34] Grossmann, C., Langel, C., Mazzotti, M., Morari, M., and Morbidelli, M., "Experimental implementation of automatic cycle to cycle-control to a nonlinear chiral simulated moving bed separation," *J. Chromatogr. A*, vol. 1217, no. 13, pp. 2013–2021, 2010.

[35] Grossmann, C., Erdem, G., Morari, M., Amanullah, M., Mazzotti, M., and Morbidelli, M., "'cycle to cycle' optimizing control of simulated moving beds," *AIChE J.*, vol. 54, pp. 194–208, 2008.

[36] Guiochon, G., Felinger, A., Shirazi, D. G., and Katti, A. M., *Fundamentals of Preparative and Nonlinear Chromatography*. San Diego: Academic Press, 2006.

[37] Hall, A., Lieb, W., and Franks, N., "Stereoselective and non-stereoselective actions of isoflurane on the gabaa receptor," *Br. J. Pharmacol.*, vol. 112, no. 3, pp. 906–910, 2012.

[38] Harris, B., Moody, E., Basile, A., and Skolnick, P., "Volatile anesthetics bidirectionally and stereospecifically modulate ligand binding to gaba receptors," *Eur. J. Pharmacol.: Molecular Pharmacology*, vol. 267, no. 3, pp. 269–274, 1994.

[39] Heuer, C., Küsters, E., Plattner, T., and Seidel-Morgenstern, A., "Design of the simulated moving bed process based on adsorption isotherm measurements using a perturbation method," *J. Chromatogr. A*, vol. 827, no. 2, pp. 175–191, 1998.

[40] Horvath, C. and Melander, W., "Liquid chromatography with hydrocarbonaceous bonded phases; theory and practice of reversed phase chromatography," *J. Chromatogr. Sci.*, vol. 15, no. 9, pp. 393–404, 1977.

[41] Huang, Q., Malekian, A., and Eić, M., "Optimization of psa process for producing enriched hydrogen from plasma reactor gas," *Sep. Purif. Technol.*, vol. 62, no. 1, pp. 22–31, 2008.

[42] James, A. and Martin, A., "Gas-liquid partition chromatography: the separation and micro-estimation of volatile fatty acids from formic acid to dodecanoic acid," *Biochem. J.*, vol. 50, no. 5, p. 679, 1952.

[43] Jiang, L., Biegler, L., and Fox, V., "Simulation and optimization of pressure-swing adsorption systems for air separation," *AIChE J.*, vol. 49, no. 5, pp. 1140–1157, 2003.

[44] Juza, M., Di Giovanni, O., Biressi, G., Schurig, V., Mazzotti, M., and Morbidelli, M., "Continuous enantiomer separation of the volatile inhalation anesthetic enflurane with a gas chromatographic simulated moving bed unit," *J. Chromatogr. A*, vol. 813, no. 2, pp. 333–347, 1998.

[45] Kawajiri, Y. and Biegler, L., "Nonlinear programming superstructure for optimal dynamic operations of simulated moving bed processes," *Ind. Eng. Chem. Res.*, vol. 45, no. 25, pp. 8503–8513, 2006.

[46] Kawajiri, Y. and Biegler, L. T., "Optimization strategies for simulated moving bed and powerfeed processes," *AIChE J.*, vol. 52, pp. 1343–1350, 2006.

[47] Kawajiri, Y. and Biegler, L. T., "Comparison of configurations of a four-column simulated moving bed process by multi-objective optimization," *Adsorption*, vol. 14, pp. 433–442, 2008.

[48] Klatt, K.-U., Hanisch, F., Dunnebier, G., and Engell, S., "Model-based optimization and control of chromatographic processes," *Comput. Chem. Engng.*, vol. 24, pp. 1119–1126, 2000.

[49] Ko, D., Siriwardane, R., and Biegler, L., "Optimization of a pressure-swing adsorption process using zeolite 13x for co2 sequestration," *Ind. Eng. Chem. Res.*

[50] König, W., Krebber, R., and Mischnick, P., "Cyclodextrins as chiral stationary phases in capillary gas chromatography. part v: Octakis (3-o-butyryl-2, 6-di-o-pentyl)-γ-cyclodextrin," *J. High Res. Chromatog.*, vol. 12, no. 11, pp. 732–738, 2005.

[51] Kostroski, K. and Wankat, P., "Separation of dilute binary gases by simulated-moving bed with pressure-swing assist: Smb/psa processes," *Ind. Eng. Chem. Res.*, vol. 47, no. 9, pp. 3138–3149, 2008.

[52] Küpper, A., Wirsching, L., Diehl, M., Schloder, J. P., Bock, H. G., and Engell, S., "Online identification of adsorption isotherm in smb processes via efficient moving horizon state and parameter estimation," *Comput. Chem. Eng.*, vol. 34, pp. 1969–1983, 2010.

[53] LaCava, A. and McKeigue, K., "Continuous pressure difference driven adsorption process," Jan. 30 1996. US Patent 5,487,775.

[54] Langel, C., Grossmann, C., Jermann, S., Mazzotti, M., Morari, M., and Morbidelli, M., "Experimental optimizing control of the simulated moving bed separation of trogers base enantiomers," *Ind. Eng. Chem. Res.*, vol. 49, no. 23, pp. 11996–12003, 2010.

[55] Lehoucq, S., Verheve, D., Wouwer, A. V., and Cavoy, E., "Smb enantioseparation: Process development, modeling, and operating conditions," *AIChE J.*, vol. 46, pp. 247–256, 2000.

[56] Li, S., Kawajiri, Y., Raisch, J., and Seidel-Morgenstern, A., "Optimization of startup and shutdown operation of simulated moving bed chromatographic processes," *J. Chromatogr. A*, vol. 1218, pp. 3876–3889, 2011.

[57] Lisec, O., Hugo, P., and Seidel-Morgenstern, A., "Frontal analysis method to determine competitive adsorption isotherms," *J. Chromatogr. A*, vol. 908, no. 1, pp. 19–34, 2001.

[58] Mazzotti, M., Storti, G., and Morbidelli, M., "Optimal operation of simulated moving bed units for nonlinear chromatographic separations," *J. Chromatogr. A*, vol. 769, pp. 3–24, 1997.

[59] Meinwald, J., Thompson, W., Pearson, D., König, W., Runge, T., and Francke, W., "Inhalational anesthetics stereochemistry: optical resolution of halothane, enflurane, and isoflurane," *ChemInform*, vol. 22, no. 20, 1991.

[60] Migliorini, C., Mazzotti, M., and Morbidelli, M., "Simulated moving bed units with extra-column dead volume," *AIChE J.*, vol. 45, pp. 1411–1421, 1999.

[61] Mota, J., Esteves, I., and Eusébio, M., "Synchronous and asynchronous smb processes for gas separation," *AIChE J.*, vol. 53, no. 5, pp. 1192–1203, 2007.

[62] Nilchan, S. and Pantelides, C. C., "On the optimization of periodic adsorption processes," *Adsorption*, vol. 4, pp. 113–147, 1998.

[63] Perrut, M., "Advances in supercritical fluid chromatographic processes," *J. Chromatogr. A*, vol. 658, no. 2, pp. 293–313, 1994.

[64] Rajendran, A., Paredes, G., and Mazzotti, M., "Simulated moving bed chromatography for the separation of enantiomers," *Journal of Chromatography A*, vol. 1216, no. 4, pp. 709 – 738, 2009.

[65] Rao, D., Sivakumar, S., Mandal, S., Kota, S., and Ramaprasad, B., "Novel simulated moving-bed adsorber for the fractionation of gas mixtures," *J. Chromatogr. A*, vol. 1069, no. 1, pp. 141–151, 2005.

[66] Ruthven, D., *Principles of adsorption and adsorption processes*. Wiley New York, 1984.

[67] Ruthven, D., Farooq, S., and Knaebel, K., *Pressure swing adsorption*, vol. 288. VCH publishers New York, 1994.

[68] Ruthven, D. M. and Ching, C. B., "Counter-current and simulated counter-current adsorption separation processes," *Chem. Eng. Sci.*, vol. 44, pp. 1011–1038, 1989.

[69] Sá Gomes, P., Lamia, N., and Rodrigues, A., "Design of a gas phase simulated moving bed for propane/propylene separation," *Chem. Eng. Sci.*, vol. 64, no. 6, pp. 1336–1357, 2009.

[70] Schiesser, W. E., *The numerical method of lines: integration of partial differential equations*. San Diego, CA: Academic Press, 1991.

[71] Schmidt-Traub, H., *Preparative Chromatography: Of Fine Chemicals and Pharmaceutical Agents*. Weinheim: Wiley VCH, 2005.

[72] Seidel-Morgenstern, A., "Experimental determination of single solute and competitive adsorption isotherms," *J. Chromatogr. A*, vol. 1037, no. 1, pp. 255–272, 2004.

[73] Sreedhar, B. and Kawajiri, Y., "Optimal binary separation schemes using simulated moving bed superstructure." Preparative and Process Chromatography Symposium, July 17, 2012, Boston, MA.

[74] Storti, G., Baciocchi, R., Mazzotti, M., and Morbidelli, M., "Design of optimal operating conditions of simulated moving bed adsorptive separation units," *Ind. Eng. Chem. Res.*, vol. 34, no. 1, pp. 288–301, 1995.

[75] Storti, G., Mazzotti, M., Furlan, L., Morbidelli, M., and Carrà, S., "Performance of a six-port simulated moving-bed pilot plant for vapor-phase adsorption separations," *Sep. Sci. Technol.*, vol. 27, no. 14, pp. 1889–1916, 1992.

[76] Storti, G., Mazzotti, M., Morbidelli, M., and Carrà, S., "Robust design of binary countercurrent adsorption separation processes," *AIChE J.*, vol. 39, no. 3, pp. 471–492, 2004.

[77] Strube, J., Altenhoner, U., Meurer, M., Schmidt-Traub, H., and Schulte, M., "Dynamic simulation of simulated moving-bed chromatographic processes for the optimization of chiral separations," *J. Chromatogr. A*, vol. 769, no. 1, pp. 81–92, 1997.

[78] Strube, J. and Schmidt-Traub, H., "Dynamic simulation of simulated-moving-bed chromatographic processes," *Comput. Chem. Eng.*, vol. 22, no. 9, pp. 1309–1317, 1998.

[79] Subramani, H., Hidajat, K., and Ray, A., "Optimization of reactive smb and varicol systems," *Comput. Chem. Eng.*, vol. 27, no. 12, pp. 1883–1901, 2003.

[80] Toumi, A., Hanisch, F., and Engell, S., "Optimal operation of continuous chromatographic processes: Mathematical optimization of the varicol process," *Ind. Eng. Chem. Res.*, vol. 41, no. 17, pp. 4328–4337, 2002.

[81] Tswett, M., "Physikalisch-chemische studien über das chlorophyll," *Berichte der Deutschen Botanischen Gesellschaft*, vol. 24, pp. 316–323, 1906.

[82] Vira, C. and Haimes, Y., *Multiobjective decision making: theory and methodology*. No. 8, North-Holland, 1983.

[83] Wagner, J., "Selective adsorption process," Mar. 4 1969. US Patent 3,430,418.

[84] Weiskopf, R. B., Nau, C., and Strichartz, G. R., "Drug chirality in anesthesia," *Anesthesiology*, vol. 97, pp. 497–502, 2002.

[85] Xie, Y., Mun, S.-Y., and Wang, N.-H. L., "Startup and shutdown strategies of simulated moving bed for insulin purification," *Ind. Eng. Chem. Res.*, vol. 42, no. 7, pp. 1414–1425, 2003.

[86] Yashima, E., "Polysaccharide-based chiral stationary phases for high-performance liquid chromatographic enantioseparation," *J. Chromatogr. A*, vol. 906, no. 1, pp. 105–125, 2001.

[87] Zhang, Z., Hidajat, K., Ray, A., and Morbidelli, M., "Multiobjective optimization of smb and varicol process for chiral separation," *AIChE J.*, vol. 48, no. 12, pp. 2800–2816, 2004.

[88] Zhang, Z., Mazzotti, M., and Morbidelli, M., "Multiobjective optimization of simulated moving bed and varicol processes using a genetic algorithm," *J. Chromatogr. A*, vol. 989, pp. 95 – 108, 2003.